Characterization and stability investigation of water dispersible colloids (WDCs) in natural soils

Canlan Jiang

Member of the Helmholtz Association

Schriften des Forschungszentrums Jülich
Reihe Energie & Umwelt / Energy & Environment Band / Volume 181

Forschungszentrum Jülich GmbH
Institute of Bio- and Geosciences (IBG)
Agrosphere (IBG-3)

Characterization and stability investigation of water dispersible colloids (WDCs) in natural soils

Canlan Jiang

Schriften des Forschungszentrums Jülich
Reihe Energie & Umwelt / Energy & Environment Band / Volume 181

ISSN 1866-1793 ISBN 978-3-89336-887-7

Bibliographic information published by the Deutsche Nationalbibliothek.
The Deutsche Nationalbibliothek lists this publication in the Deutsche Nationalbibliografie; detailed bibliographic data are available in the Internet at http://dnb.d-nb.de.

Publisher and Distributor:	Forschungszentrum Jülich GmbH Zentralbibliothek 52425 Jülich Tel: +49 2461 61-5368 Fax: +49 2461 61-6103 Email: zb-publikation@fz-juelich.de www.fz-juelich.de/zb
Cover Design:	Grafische Medien, Forschungszentrum Jülich GmbH
Printer:	Grafische Medien, Forschungszentrum Jülich GmbH

Schriften des Forschungszentrums Jülich
Reihe Energie & Umwelt / Energy & Environment, Band / Volume 181

D 82 (Diss., RWTH Aachen University, 2013)

ISSN 1866-1793
ISBN 978-3-89336-887-7

Acknowledgements

The work was carried out at the Agrosphere Institute (IBG-3) in Forschungszentrum Juelich. I would like to thank the institute for supporting my research and the Chinese Scholarship Council (CSC) for financial support for my PhD in Germany.

I would like to express my sincere gratitude to my supervisor, Prof. Dr. Erwin Klumpp. His insightful comments and constructive criticisms were inspiring and he helped me to learn how to design the topics and consider the possibilities and how to write the scientific papers, which would be also invaluable to my career in the future. My deeply appreciate is also given to my direct supervisor, Dr. Jean-Marie Séquaris. He helped me to make progress and get over the handicaps over the entire PhD program. I learnt how to think and solve problems with his encouragement and guidance for this work. The patience and support from both of them helped me and their interest in science increased my motivation.

I would also like to give my sincere thanks to Prof. Dr. Harry Vereecken for reading my reports and discussions about my work. I am also grateful to Prof. Dr. Andreas Schäffer for reviewing my thesis. Sincere thanks to Prof. Dr. Wulf Amelung for his kind help and encouragement during the last year of my PhD. I also want to thank Prof. Dr. Attila Bota and András Wacha of Hungarian Academy of Sciences, for their valuable ideas and support with SAXS measurement and I really cherish the time with a lot of laugh when I was in Budapest with them. I am grateful to Dr. Stefan Pätzold and PD Dr. Welp from Bonn University for the distribution analysis of particle size and the mineral XRD analysis. I am thankful to Dr. Stephan Küppers for the soil chemical analysis in my work. My PhD program would not been possible to finish without the help from them.

Thanks to my colleagues who have helped me in experimental work. I want to express my deep appreciation to Claudia Walraf for her help in all aspects. I also appreciate the help of Ursula Paffen for the TOC measurement, of Hannelore Lippert, Sabrina Kohnen and Jennifer Bachhausen on soil and solution characterization, of Bochem, Hans Peter for the SEM pictures and of Thomas Schuster on the computer maintenance.

I would also like to thank all my colleagues and friends for their support beyond the scientific aspects. In particular, I would like to thank, Rudong who always listen to me and show me the positive aspects in the difficulties. I want to give a special thanks to Andrea, Qingmei, Sebastian, Gaby, and Anja, for their encouragement and help all the time, Jing, Chengliang, Yan, Daniela, Xiaoqian, Miaoyue for their warm-hearted help along the way and sharing the time in the past three years.

Last but not the least, I want to thank my parents for their love and encouragement. Without their love I could not fluently complete my PhD work. I seriously want to thank my brother and his family, my relatives and all my dear friends in China for their understanding and support.

Abstract

In this work, surface properties, colloidal behaviours and mobilization processes of easily dispersed soil colloids or water dispersible colloids (WDCs) from three TERENO silt loam soils (arable, grassland and forest soils) have been investigated.

Firstly, the colloidal behavior of soil mineral colloids (quartz and illite) was investigated in Na, Ca and mixed Na-Ca systems with photon correlation spectroscopy (PCS) and microeletrophoretic method, respectively. The critical coagulation concentrations (*CCCs*) were determined for Na^+ and Ca^{2+} solutions containing anions of a different nature (Cl^-, SO_4^{2-} and ubiquitous soil organic anions formate and oxalate) at pH 5.5 and pH 8.5. In the Na-system, a higher stability for colloidal illite and quartz particles suspensions in the presence of oxalate anions confirmed surface complexation at an acidic pH. In the Ca-system, slight *CCC* variations in illite suspensions in the presence of Cl^-, SO_4^{2-}, formate and oxalate supported attractive ion-ion correlation forces between equally highly charged clay mineral colloids. It was shown that the *CCCs* of mixed Na-Ca systems can be calculated using the *CCCs* for colloidal illite and quartz particles in pure Na and Ca systems at pH 5.5 and pH 8.5.

Secondly, the distribution of different metal oxides forms and OC fractions as well as their contributions to the surface and pore properties of topsoils from the three TERENO test sites were compared. In the CO_2 gas sorption, the additional CO_2 binding follows the series < 2 µm (WDC) < 2-20 µm < bulk soil samples. It indicates a stronger CO_2 binding to the major non-associated OC fraction (POM). In N_2 gas sorption, a lowering of µpore $vol._{70}$ was measured in comparison with µpore $vol._{400}$, which confirms a hindrance of the N_2 sorption kinetics due to a blocking effect of OC associated to the mineral surface in micropores. In the case of the metal oxide, there is a satisfactory linear correlation between the released $SSA_{CB\text{-}DCB\ 400}$ and the extracted $Fe_{DCB\text{-}CB}$ content with DCB. The surface contribution of amorphous metal oxide in bulk soils SSA is higher than in WDC which also supports a distribution of metal oxide outside the particle size fraction, < 2 µm. In WDC, SSA of 217-420 m^2g^{-1} is found for the total extracted metal oxide particles with sizes of 4-8 nm. The pore structure of WDC has been investigated with the SAXS. Guinier plots of WDC, before and after removal of nanoparticles with DCB, indicate a contraction of the WDC mesopore structure in the presence of metal oxide nanoparticles

Thirdly, soil fraction method which has included 6 hours of shaking and 12 hours of sedimentation processes was conducted under different temperatures (7°C, 15°C, 23°C and 35°C). A decrease of WDC amount against the temperature after the soil fractionation was generally measured where the effects of the temperature on the WDC mobilization process (shaking step) and sedimentation steps must be distinguished. It was demonstrated that a rapid WDC sedimentation at higher temperature due to decrease of water viscosity must be taken into account for the interpretation of the effective effect of the temperature on the WDC mobilization step. In the case of dispersed colloidal particles as WDC, the increase of temperature in the sedimentation step decreases not only the detected released WDC mass but also shifts the distribution of WDC to lower particle size with a corresponding higher SSA. It can be also shown that the increase of temperature accelerates the aggregation kinetic of WDC in the presence of salt in the electrolyte phase. A decrease of *CCC* can be measured with PCS, which also explains a decrease of the WDC colloidal stability at a higher temperature.

Fourthly, the effect of the temperature on the WDC mobilization during the shaking step has been precised. The effects of temperature (7°C, 23°C and 35°C) on the release kinetics in deionized water of water-dispersible colloids (WDCs) from three TERENO topsoils were investigated (soil/water: 1/2) by a rotating shaking method. The cumulative released WDC fraction $F(t)$ versus square root of shaking time implies diffusion-controlled kinetics. Mobilization kinetics modeling, based on diffusive transport of WDC (< 2 μm) through boundary layer of immobile water at the surfaces of clay aggregates in macropore mainly formed by silt and sand fractions was thus applied. Strong dependences of $F(t)$ on total organic carbon (TOC) content and pH were observed, which imply a strong dependence of the water layer thickness (l_t) on the soil texture. This can be confirmed from results of the water volume (V_{water}) in the sediment of soaked soils at 7°C, 23°C and 35°C. A linear correlation can be established between V_{water} and l_t values. Temperature-sensitive soil texture variations also determine the temperature effect on WDC diffusion-controlled transport.

List of contents

List of contents

List of figures

List of figures

List of tables

Abbreviations

WDC	Water dispersible colloids
NOM	Natural organic matter
SAR	Sodium adsorption ratio
DLVO theory	Deryagin-Landau-Verwey-Overbeek theory
LMW	Low molecular weight
SOC	Soil organic carbon
OC	Organic carbon
SSA	Specific surface area
DCB	Dithionite-citrate-bicarbonate
WAXS	Wide angle X-ray scattering
SAXS	Small angle X-ray scattering
CCC	Critical coagulation concentration
PCS	Photon correlation spectroscopy
HHF relation	Hogg, Healy and Fuerstenau relation
PZC	Point of zero charge
TN	Total nitrogen
ICP-OES	Inductively coupled plasma optical emission spectroscopy
DR	Dubinin-Radushkevich

Symbols

ζ	Zeta potential	mV
Rg	Radius of gyration	Å
I_q	Scattered intensity	cm^{-1}
D_f	Fractal dimension	—
D_m	Mass fractal dimension	—
2θ	Scattering angle	^{o}
V_s	Sedimentation volume	cm^3
D	Diffusion coefficient	m^2 s^{-1}
k_B	Boltzmann constant	1.38×10^{-23} m^2 kg s^{-2} K^{-1}
T	Absolute temperature	K
η	Viscosity of solvent	Pa·s
r	Radius of the spherical particle	nm
F_g	Force of the gravity	J
ρ	Density	Kg m^3
g	Acceleration due to the gravity	9.8 m s^{-2}
F	Faraday constant	9.65 10^4 C mol^{-1}
ψ	Stern potential	v
I	Ionic strength	(mol L^{-1})
k_a	Aggregation rate constant	-
r_h	Hydrodynamic radiu	nm
C	Concentrations	Mm
f	Molar fraction	-
K	Debye-Hückel parameter	m^{-1}
ε	Permittivity	C^{2}J^{-1}m^{-1}
R_p	Average pore radius	-
V_p	The total pore volume	(cm^3 g^{-1})
$f(ka)$	Henry's function	-
$A_{Hamaker}$	Hamaker constants	J
F	Cumulative fraction	-
kT	Thermal energy	J
R	Gas constant	8.31 J K^{-1} mol^{-1}
Er	Angular kinetic energy	J
l_t	Plane sheet of thickness	m

Note: -, non-unit

Chapter 1

Introduction

1.1 The water dispersible colloids (WDCs)

WDCs are soil particles < 2 μm in soil clay fractions that can be easily dispersed in soil water. They mainly include aluminosilicates and metal oxide particles which can be released from soil aggregate structures. The charged WDC particles have high surface area and can migrate at long distance. They contribute to soil erosion and possible transport of organic matter and pollutants in the subsurface environment (McGechan and Lewis, 2002). They can act as carriers for contaminant, which are adsorbed on their surface and thereby enhance the spreading of pollutants in subsurface system which otherwise are surmised to be immobile (Czigány et al., 2005; Grolimund et al., 1996; Sen et al., 2004).The release and transport of WDCs in soils are affected by the hydrodynamic water flow and the solution chemistry.

1.2 Solution chemistry effect on the WDC stability

Solution chemical conditions are crucial factors for the concentration and stability of mobile WDC such as presence of natural organic matter (NOM), varying pH, electrolyte concentration and the sodium adsorption ratio (SAR) and they have been widely documented (Grolimund and Borkovec, 2005; Kaplan et al., 1997; Kaplan et al., 1993; Kjaergaard et al., 2004c; Kretzschmar et al., 1999; Majzik and Tombácz, 2007a; Séquaris, 2010). These factors control the equilibrium between repulsive electrostatic forces and van der Waals attractive forces between particles, which govern the stability of WDC dispersions according to the Deryagin-Landau-Verwey-Overbeek (DLVO) theory (Overbeek, 1980). Based on physico-chemical parameters such as particle size, surface electro-kinetic potential (zeta potential, ζ) and the material Hamaker constant (A), DLVO theory can satisfactorily describe interactions between particles (Séquaris, 2010; Zhou et al., 2009).

It has been demonstrated that under soil electrolyte conditions, the mobilization of WDC depends on the relative saturation of the medium with major available cations (Ca-system and Na-system) (Grolimund et al., 1998). However, the modelling of WDC mobilization in mixed Na-Ca systems, which are more related to soil conditions, has not been investigated as thoroughly (Grolimund et al., 2001). A large distribution of mineral and organic anions also exists in soil, which necessitates a comparative investigation of anionic ligand effects on WDC dispersion phenomena (Grolimund et al., 2001; Grolimund, 2007). It has been shown that the adsorption extent of anions at the surface of metal oxyhydroxide mineral components depends on their chemical reactivity. Thus, outer-sphere and inner-sphere complexations with metal cations of surface metal oxyhydroxide characterize the electrostatic and chemical adsorption of anions, respectively. Chloride anions mainly interact as an outer-sphere surface complex while SO_4^{2-} and low molecular weight (LMW) organic acids are known to form both outer- and inner-sphere surface complexes depending on the nature of anions, the surface metal oxyhydroxide and pH (Axe and Persson, 2001; Johnson et al., 2004; Wijnja and Schulthess, 2000). In most soils, SO_4^{2-} thus competes for the same adsorption sites with LMW anions from plant roots and microorganisms (Martinez et al., 1998). Among them, NOM in the form of oxalic and formic acids is largely distributed and ubiquitous in forest and agricultural soils (Fox and Comerford, 1990; Strobel, 2001). In the long term, the surface modification of metal oxyhydroxide by organic acids results in the release kinetics of metal cations in solution by complexation as is the case with oxalic acid (Axe and Persson, 2001; Bennett, 1991; Furrer and Stumm, 1986; Johnson et al., 2004). However, in the short term, a surface coating causes variations in the colloidal behavior of WDC depending on the pH, cation nature and concentration (Frenkel et al., 1992; Johnson et al., 2005; Oades, 1984). It must be noted that the interactions of LMW organic acids with minerals based on ligand exchange and Ca^{2+} bridging / Ca^{2+}-LMW organic acid precipitation have been recognized as an important pathway of organic matter stabilization against microbial degradation in soils (Jones, 1998; Majzik and Tombácz, 2007a; Majzik and Tombácz, 2007b).

1.3 Organic carbon and metal oxides effects on soil WDC and soil fraction

1.3.1 Effect of soil organic carbon on soil structure

Soil aggregation is strongly depended on the soil organic carbon (SOC) which acts as a binding agent and as a nucleus in the formation of aggregates (Six et al., 2000a; Tisdall and Oades, 1982). The organic matter stored in the soils is one of the largest reservoirs of the organic carbon (OC) at the global scale (Schlesinger, 1995). Better sequestration of organic matter in soils can be a solution for slowdown the carbon cycle which need more information on the interaction mechanisms and kinetics between organic matter and soil mineral matrix

(Sollins et al., 2007). The ability of mineral particles to protect SOM from biological attack was demonstrated by many scientists (Baldock and Skjemstad, 2000; Jones and Edwards, 1998; Kalbitz et al., 2005). It is widely assumed that the protected effect of clay mineral on SOM can influence strongly on the turnover of the SOM (Parfitt et al., 1997; Tipping et al., 2012). Parameters including mineral surface activity, solution chemistry and the bonding mechanism are the crucial for the stability of mineral-associated soil and OM (Mikutta et al., 2007). Christensen (Christensen, 2001) pointed out that 50%-75% of SOM exists within clay-size organo-mineral particles. A positive effect of fine mineral particles on OC in soil can be found (Burke et al., 1989; Mayer and Xing, 2001). The specific surface areas (SSA) both of soil particles and SOM are crucial parameters for sorption mechanisms of organic contaminants (Mayer and Xing, 2001) that organic matter can be bound to mineral surface via variety of mechanisms (Feng et al., 2005; Schlautman and Morgan, 1994). The interaction of water and organic matter (OM) in pores is also important for the capacity of long-term C sequestration and water retention in soils (Zhuang et al., 2008).

1.3.2 Effect of metal oxides on soil structure

Soil structures affect the soil ability to support plant and animal life and have important influence on environmental processes such as soil carbon (C) sequestration and water filtration. Soil structure depends on the stability of aggregates which are formed as a result of flocculation, cementation, and arrangement of soil particles (Bronick and Lal, 2005; Duiker et al., 2003; Six et al., 2000b). Due to the chemical reactivity of their surfaces, metal oxide particles are important for sorption of OM in soils. They are stronger adsorbents of NOM compared to aluminosilicate clays. SOM aggregation properties are thus associated with covalent binding to mineral surfaces where Al and Fe hydrous oxides play important roles (Kögel-Knabner et al., 2008; Mikutta et al., 2006). The heterogeneous microstructures formed by metal oxide nanoparticles and large plate like particles of clay minerals can favor clay-associated OC pool sequestration (Kaiser and Guggenberger, 2000; Wagai and Mayer, 2007). In the absence of OM, the attraction between positively charged Al and Fe hydrous oxides and negatively charged clay surfaces also favors aggregation and contributes to the building of the porous structure in the soil mineral matrix. Indeed, Igwe et al. (Igwe et al., 1995; Igwe et al., 2009) have found in some tropical soils that the organic matter contents in soils were too low for contributing to the formation of microaggregates and that Fe and Al oxides played the most important roles in clay aggregation processes. Mbagwu and Schwertman (Mbagwu and Schwertmann, 2006) have found in some soils of Nigeria that Al oxides were more important than Fe oxides as aggregating agents. In some oxisols and inceptisols from Brazil and Cameroon, Pinheiro-Dick and Schwertmann (Pinheiro-Dick and Schwertmann, 1996) have also found that it was the oxalate extracted amorphous oxides that was mainly responsible for the formation of aggregates. Duiker et al. (Duiker et al., 2003) studied some United States soils and demonstrated the importance of amorphous Fe hydroxides in stabilizing aggregates. The extent of their contributions equals or exceeds that of organic carbon.

Metal oxides in relatively low mass fractions are largely distributed in German soils (Eusterhues et al., 2005; Kaiser and Guggenberger, 2003; Pronk et al., 2011). Various forms of iron oxides occur in soils (Cornell and Schwertmann, 1996). Iron oxides in crystalline form such as goethite (α-FeOOH) and in poorly crystalline or amorphous forms such as hydrous oxide ferrihydrite are the most abundant, (Childs, 1992; Gaboriaud and Ehrhardt, 2003; Roden and Zachara, 1996). In the case of aluminium oxide, the amorphous form such as hydrous oxide gibbsite is the most common (Gilkes et al., 2006; Rosenqvist et al., 2003). These metal oxides can be selectively extracted by differential dissolution. The dithionite-citrate-bicarbonate treatment (Kiem and Kögel-Knabner, 2002b; Mehra and Jackson, 1960) completely dissolves all metal oxide forms (M_{DCB}). For selective dissolution of amorphous forms, an ammonium oxalate treatment (Kiem and Kögel-Knabner, 2002b; Schwertmann, 1964) is generally used ($M_{oxalate}$).

1.3.3 Using N_2 adsorption and SAXS techniques on surface area and pore structure characterization

Surface area and pore structure are important properties in protection of OM through interaction with the mineral matrix of soils. The surface area is controlled by the content of clay and by the nature of the minerals present in the clay fraction (Saggar et al., 1996). N_2 gas sorption technique is a standard method for the measurement of specific surface area (SSA) of soil. This method has been also used to variously probe the OC/mineral surface interactions by characterizing the contributions of OM and metal oxides effects on the soil porous structure (de Jonge and Mittelmeijer-Hazeleger, 1996; Eusterhues et al., 2005; Hiemstra et al., 2010a; Kaiser and Guggenberger, 2003; Mayer and Xing, 2001). Pore space, size and amount exist in soil can influence SOC and its turnover; conversely, SOC and soil texture can influence porosity (Thomsen et al., 1999). There is a wide range of pore sizes existing in soils between and within aggregates (Dalal and Bridge, 1996). According to IUPAC nomenclature

(Pierotti and Rouquerol, 1985), pores <2 nm are regarded as micropores, those of 2-50 nm are mesopores and >50 nm are macropores, respectively. The pore can be defined as open pores when they communicate with the external surface and are accessible to molecules or ions from the surrounding. Conversely, the closed pore are not interconnected by "channels" but are closed as individual voids in the mineral matrix (Radlinski et al., 2004). It should be noted that only the open micropores are detected by BET-N_2 gas sorption technique (Mayer et al., 2004; Pronk et al., 2011). Small-angle X-ray scattering (SAXS) technique is used for the internal and external structural characterization of solid and fluid materials in the nanometer (nm) range. It probes inhomogeneity of the electron density on a length scale of typically 1-100 nm (Guinier and Fournet, 1955), thus yielding complementary structural information to XRD (WAXS - wide angle X-ray scattering) data. From the measured scattered intensity $I(q)$ as a function of the scattering angle 2θ (Guinier and Fournet, 1955), the Guinier's law allows the determination of a radius of gyration (R_g). In the case of suspension of clay particles, R_g can be related to the clay particle thickness (Shang et al., 2001; Saunders et al., 1999). The SAXS method gives information on both closed and open pores whose sizes are in the range from micropores (<2 nm) to macropores (>50 nm). In this case, R_g can be associated to mean pore diameter in the case of porous solid samples. Application of SAXS for characterizing meso- and macroporous solid materials has been demonstrated with silica gel and other porous substances (Schmidt, 1991; Schmidt et al., 1991). SAXS has been applied to systematic studies of surface and pore structure of clay minerals (Pernyeszi and Dékány, 2003). SAXS data have demonstrated that the arrangement of aluminosilicate particles that form the mesopore in soil and sediment samples remains largely unaffected after the removal of OM by muffling at 375°C (Mayer et al., 2004). A fractal dimension, D is also provided from a power law of $I(q)$ which expresses the compactness of the aggregated clusters (Chevallier et al., 2010; Cohaut et al., 2000). Borkovec et al found that the fractal character of rough surface of soil grains can be characterized by the SAXS method (Borkovec et al., 1993).

There is sufficient information of metal oxides effects on soil SSA and pores by BET method, However, few studies have used SAXS methods. Kaiser & Guggenberger found in their study that SSA of soils is highly correlated to the amounts of Fe oxyhydroxides (Kaiser and Guggenberger, 2003). amorphous Fe (hydr)oxides have a much larger and more reactive surface area than crystalline Fe (hydr)oxides and they also facilitate more the aggregation (Schahabi and Schwertmann, 1970). K. Eusterhues et al (Eusterhues et al., 2005) show in a study of two German acid forest soils that after dissolution of Fe oxides only very few samples still contain micropores. The soluble minerals in DCB extract were identified as the main microporous phases of the soil. Furthermore , using N_2 gas sorption method, Filimonova et al (Filimonova et al., 2006) reported that removal of iron oxides by the DCB treatment has decreased SSA by up to 50%, and that the micropores were completely vanished in two German Luvisol and Gleysol soils. After the removal of iron and aluminium metal form sepiolites with acid treatment, Dékány et al found with SAXS method an increase of the porosity in mineral characterized by a decrease of the mass fractal dimension, D_m (Dékány et al., 1999). Both gas adsorption and SAXS are, to a certain extent, insufficient for characterization of the porous structures. It is thus meaningful to combine the two techniques to gain an overview on the porosity and surface characteristics of samples.

1.4 Temperature effect on WDC release and soil erosion

Previous studies suggest that soil temperature and soil moisture will affect aggregation processes and biological activity (Lavee et al., 1996; Sarig and Steinberger, 1993). Soil erosion, the term used to describe the washing or blowing away of the upper part of the soil cover, is a major environmental and agricultural problem worldwide (Pimentel et al., 1995). Due to the strong effect on the storage capacity of terrestrial carbon (Hancock et al., 2010) in soil, soil erosion has a significant impact on soil carbon cycling (Polyakov and Lal, 2004; Van Oost et al., 2005). The importance of the clay fraction in the soil carbon sequestration and soil structure stability has been widely documented (Kögel-Knabner et al., 2008; Tisdall and Oades, 1982).The factors influencing the soil erosion are extremely complex where geology, precipitation, temperature and biology are interrelated. There is clearly significant potential for climate change to increase the soil erosion by water (Nearing et al., 2005). The increasing amounts and intensities of rainfall will lead to greater rates of erosion unless protection measures are taken (Nearing et al., 2004). The release of easily dispersed soil particles < 2 µm from the soil clay fraction, assigned to the water-dispersible colloid (WDC) fraction, has a statistically significant relationship with the water soil erodibility (Brubaker et al., 1992; Miller and Baharuddin, 1986; Shainberg et al., 1992). The release of WDC from topsoil is generally based on mechanical and chemical processes which affect the stability of soil aggregates (Bissonnais, 1996) . Indeed, a combination of hydrodynamic parameters (intensive rain, splash erosion, infiltration water rate) and chemical dispersion conditions such as the presence of organic matter, increasing pH, decreasing ionic strength and increasing sodium adsorption ratio (SAR), are crucial factors that can affect the release and stability of mobile

WDCs (Frenkel et al., 1978; Jarvis et al., 1999; Kaplan et al., 1996; Kjaergaard et al., 2004a; Kjaergaard et al., 2004b; Seta and Karathanasis, 1996). As a result of the influences of the various parameters mentioned above, the definition and quantification of key mechanisms affecting the WDC release processes in soil porous media is rather complex. Attempts to model WDC release have been made by formulating a two-step mechanism whereby the dispersion of WDC in soil aggregates is followed by a transport step of the mobilized WDC. Under soil conditions, the interacting surfaces of major mineral colloids and grains are negatively charged, which implies that aggregation or deposition processes of WDC are only possible under charge screening conditions where the critical energy potential conditions for the release process can be modelled by the Derjaguin-Landau-Verwey-Overbeek (DLVO) theory (Overbeek, 1980) by changing the soil electrolyte conditions. In the absence of an energy barrier, under conditions of low ionic strength solution, a fast first step in the release process of WDC from the aggregate surface can be considered. The WDC diffusion across a boundary immobile water layer to the mobile phase is thus the rate-limiting second step (Ryan and Gschwend, 1994; Ryan and Elimelech, 1996). Indeed, under steady water infiltration, results with saturated soil columns have indicated that WDC mobilization appears to be limited by a diffusion-controlled step (Jacobsen et al., 1998; Jacobsen et al., 1997; Lægdsmand et al., 1999; Laegdsmand et al., 2007). A low rate of water infiltration maintains a diffusion gradient within a stagnant water layer at the surface of WDC aggregates.

1.5 Objectives and significance

The first objective of this study is to investigate the stability of illite and quartz colloids dispersion under various solution chemistry conditions in order to approach the environmental behaviour of soil colloids. Na^+ (monovalent) and Ca^{2+} (divalent) salts of simplest largely distributed soil organic anions, formate (monocarboxylate form, CHO^{2-}) and oxalate (dicarboxylate form, $C_2O_4^{2-}$)were considered. The results were compared to the Na^+ and Ca^{2+} salts with major Cl^- (monovalent) and SO_4^{2-} (divalent) anions. The critical coagulation concentration (CCC) was systematically measured in Na-, Ca- and Na-Ca systems at pH 5.5 and 8.5. The combination of PCS and microelectrophoretic (ζ-potential) methods allowed us to determine parameters, which control the stability of illite and quartz dispersions according to the DLVO theory (Novich and Ring, 1984; Overbeek, 1980). The coagulation property of low soluble calcium oxalate was investigated with oxalate-modified illite in the presence of $CaCl_2$. In mixed Na-Ca systems, the results were tested and modelled in order to detail the effects of NOM compounds such as oxalate and pH on the stability of WDC under soil conditions. The results contribute to approach the environmental behaviour of soil colloids under various solution chemistry conditions.

Secondly, different soil particle size fractions from three topsoils were systematically analysed. The goal is to evaluate the organic carbon and metal oxide effects on the mineral surface area and pore structure. Organic carbon and metal oxide were removed from samples and the results were compared with the “blank” samples. Possible interactions between organic carbon and soil minerals were detected with N_2 and CO_2 gas adsorption methods. Potential structural changes of soil particles due to metal oxide $_{DCB}$ and metal oxide$_{oxalate}$ were tested with the both gas sorption and SAXS methods which further has been confirmed with photon correlation spectroscopy (PCS). The knowledge of the results contributes to the understanding of the carbon sequestration and contaminant mobility in soil.

Thirdly, for approaching natural soil erosion process, the temperature effect on a soil fractionation procedure was investigated. The object was to analyse the temperature effect on the distribution of soil fraction masses and properties, especially in the case of the WDC fraction. First, considered the effect of the temperature on the whole soil fractionation procedure was considered, which includes the WDC release during the shaking step and the sedimentation step. Under environment conditions, these two temperature-driven steps as the WDC release from soil aggregates and WDC sedimentation mainly affect the WDC mobility. In a second part was differentiated, the temperature effects on the sedimentation steps. The experimental parameters for measuring the WDC release kinetics in batch experiments were discussed.

Finally, in order to assess the environmental behavior of WDCs, the factors controlling WDC release in soil structure have to be investigated. Quantitative models capable of capturing the main features of these processes merit further study and need to be validated with soil samples (Jarvis et al., 1999; Laegdsmand et al., 2007). In this work, the release kinetics of potentially mobile WDCs from three TERENO soil test sites in deionized water were investigated, under batch experiments saturated conditions. At first, the colloidal stability behavior of WDC in Na- and Ca-systems was characterized by measuring the critical coagulation concentrations (CCC) of cation, which define the ionic solution conditions for the rapid detachment step of WDC by modelling the net-interaction energy potential between colloids and mineral grains. Under steady mechanical shaking conditions simulating the erosive dispersion and infiltration of low-ionic strength rainwater, WDC mobilization was then monitored at 7°C, 23°C and 35°C. The influence of the soil texture on the release kinetics was investigated by measuring the specific surface area (SSA) of soil samples and the corresponding sedimentation volume (V_s) of soil suspensions. The results are used to scale the extent of WDC release kinetics along with the temperature where the diffusion-controlled step was modelled by transport through immobile water layers at soil aggregates surface.

As a whole, the objectives of this study are summarized as:

1) Effects of inorganic and organic anions on the stability of WDCs (illite and sand colloid) in Na-, Ca- and mixed Na-Ca systems.
2) Characterization of organic carbon and metal oxides in soil WDCs in three topsoils and their particle size fractions with gas sorption (N_2 and CO_2) and SAXS methods.
3) Temperature effects on soil physical fractionation, sedimentation and aggregation behaviours of WDCs from three topsoil samples.
4) Diffusion-controlled mobilization of WDCs from three topsoils in batch experiments.

Chapter 2

Theory

2.1 Fundamentals of colloid interaction and stability

2.1.1 Diffusion and sedimentation of colloids

Dispersed colloids in solution are engaged in ceaseless irregular movement in constant random motion. This is Brownian movement which results directly from the thermal motion of the molecules of the liquid in which they are suspended. Due to the Brownian motion, diffusion of the colloid particles can happened, the colloid can move from the region of the dispersion with higher concentration to region with lower concentration (Gregory, 2005). Colloid can diffuse as fast as ordinary molecules. The brownian motion assume that a particle will move a certain distance in a given time. In a time *t*, the mean dislocation *S* is calculated:

$$S = \sqrt{2Dt} \qquad \text{Eq. (2.1.1)}$$

where *D* is the diffusion coefficient of the particle. The diffusion coefficient of a spherical particle, is given by the Stokes-Einstein equation:

$$D = \frac{k_B T}{6\pi\eta r} \qquad \text{Eq. (2.1.2)}$$

where k_B is the Boltzmann constant and *T* is the absolute temperature. η is the viscosity of solvent, *r* is the radius of the spherical particle.

Colloid particles are also subjected to the terrestrial gravitational attraction field and settle. This settle motion against fluid drag in solution which is depended on the particle velocity. The particle settle velocity will accelerate until the drag force and the gravitational force will be balanced. The particle will moved at a constant terminal velocity (Nickel, 1979). This behavior, in the case of dilute suspensions of low particle size, satisfactorily responds to the sedimentation rate (Stokes' law) of particle

$$V = \frac{h}{t} = \frac{(\rho-\rho_0)g}{18\eta}d^2 = \frac{\beta}{\eta} \qquad \text{Eq. (2.1.3)}$$

with v the sedimentation rate, h the fall height, t the falling time for the fall height (h); ρ, ρ_0 are the particle and water density; g, the gravitation constant; η, the water viscosity and d, particle diameter. Falling time t can be simply calculated.

where β is a constant value, which characterizes the WDC particle. It can be assumed that the WDC sedimented mass varies according to a general relation,

$$WDC_{sed\,T} = Actv = Ac\beta t/\eta \qquad \text{Eq. (2.1.4)}$$

with A, vessel geometry parameter (bottom surface), c, dispersed WDC concentration and $vt = h = \beta t / \eta$. (Eq. (2.1.3)).

2.1.2 DLVO theory

The DLVO theory describe the sum of van der Waals attractive and electrical double layer repulsive forces that exist between particles as they approach each other for the colloid stability. There is an energy barrier resulting from the repulsive force prevents two particles coming into contact and adhering together. If the particles have sufficient energy to overcome this energy barrier, the attractive force will pull them to adhere strongly and irreversibly together and the particle will held in a primary minimum where the repulsive force is limit and the attract force will be infinite largest. In some situations, with lower energy barrier existing, there is a possibility of a “secondary minimum”. A much weaker and potentially reversible adhesion between particles exists (Gregory, 2005).

2.1.2.1 Modelling the total interaction energy between soil WDC with the DLVO theory

For modelling the repulsive electrostatic double-layer interaction energy between two charged spheres when the surface potentials of each remain constant during the interaction (Hogg et al., 1966), the Hogg, Healy and Fuerstenau (HHF) relation can be used.

$$\Phi_E = \left(\frac{\pi\varepsilon\,\varepsilon_0 r_1 r_2}{r_1+r_2}\right)(2\psi_1\psi_2)ln\frac{1+\exp(-kH_E)}{1-\exp(-kH_E)} + ({\psi_1}^2 + {\psi_2}^2)\ln(1-\exp(-2kH_E)) \qquad \text{Eq. (2.1.5)}$$

In this equation, r is particle radius and ψ is the Stern potential of two interacting spherical particles, which can be measured as $d_z/2$ and ζ potential, respectively. The effective separation (H_E) for the interacting electrostatic forces is given by

$$H_E = H - 2s \qquad \text{Eq. (2.1.6)}$$

where H (m) is the particle interdistance and s is the Stern layer thickness.

A correction for the effective separation distance was made by considering that the size of the hydrated counterion Ca^{2+} is equal to the thickness of the Stern layer (s). A value of 0.5 nm was chosen which can be estimated from half the interdistance between plates of Ca-montmorillonite quasi-crystals in water with a (d_{001}) basal spacing of 1.9 nm after subtracting the alumino-silicate plate thickness of 0.95 nm (Norrish, 1954). The energy of attraction Φ_A is given by the complete Hamaker expression (Gregory, 2006).

$$\Phi_A = -\frac{A}{12}\left[\frac{1}{X^2+2X} + \frac{1}{X^2+2X+1} + 2ln\frac{X^2+2X}{X^2+2X+1}\right] \qquad (2.1.7)$$

where x = $H/2r$. The total interaction energy Φ_T (J) of the coagulation under varying ionic strength conditions is given by

$$\Phi_T = \Phi_E + \Phi_A \qquad (2.1.8)$$

where Eq. (2.1.8) is calculated from the sum of Eq. (2.1.5) and Eq. (2.1.7).

The Debye- Hückel κ (m^{-1}) value is given by

$$k = \sqrt{\frac{2F^2}{\varepsilon_r \varepsilon_{0RT}} I} \qquad (2.1.9)$$

with I, ionic strength, F, Faraday constant, R, Boltzmann constant and T, temperature. The following parameters were used to calculate the total interaction energy Φ_T: T = 293 °K; Faraday constant: $F = 9.65\ 10^4$ C mol^{-1}; Permittivity of the water: $\varepsilon = \varepsilon_r \varepsilon_0 = 7\ 10^{-10}$ $C^2 J^{-1} m^{-1}$; Thermal energy: $kT = 4\ 10^{-21}$ J; Gas constant: R = 8.31 J K^{-1} mol^{-1}; Stern layer: $s = 5 \times 10^{-10}$ m; Particle interdistance: H (m); particle radius: r (m); Stern potential: ψ (V) is given by the ζ potential (V), ionic strength: I (mol l^{-1}); effective Hamaker constant: A (J). The potential-energy diagrams are characterized by the presence of an energy maximum (Φ_{max}), which acts as a repulsive energy barrier.

2.2 Determination of aggregation kinetics and critical coagulation concentration (CCC)

2.2.1 CCC determined with photon correlation spectroscopy (PCS)

The critical coagulation concentration (CCC) of colloid points to the minimum concentration of electrolyte for fast aggregation of colloid (Hiemenz, 1986) which is one of the most important parameter for considering colloid stability. The photon correlation spectroscopy (PCS) measurements can be made at a scattering angle to measure the aggregation kinetics and calculate the CCC of colloidal soil materials at a certain temperature. This method gives more reliable results than batch turbidity (Chorom and Rengasamy, 1995; Czigány et al., 2005) and flocculation test (Hesterberg and Page, 1990) methods. The monomodal cumulant method (in this work that of the Nano-ZS apparatus software was used) can be used to analyse the correlation function. The rate of aggregation depends primarily on the number of colloids (N_0) and the aggregation rate constant (k_a). This rate can be measured in a short time by considering a second-order kinetic reaction where single colloidal particles are exclusively aggregated into doublets while the initial number of particles does not vary sensitively. With these initial concentrations, it can be achieved that the rate is given by the time dependence of the increase in colloidal particle size (d_z) in a short time (t). This can be investigated by PCS in the case of the coagulation of colloids. The initial change in the measured hydrodynamic radius (r_h) of the coagulating suspension is given by

$$\frac{1}{r_h(0)}\left(\frac{dr_h}{dt}\right)_{t\to o} = \theta N_0 k_a \qquad (2.2.1)$$

where $r_h(0)$ is the mean hydrodynamic radius of the singlet at $t = 0$,Θ is an instrument constant depending on the scattering angle and properties of the particles and N_0 is the number of particles in suspension (Grolimund et al., 2001; Holthoff et al., 1996). For the smallest $\mathrm{r_h}$ variations in a short time, Eq. (2.2.1) can be replaced by

$$\frac{dlnr_h}{dt} = \theta N_0 k_a \qquad (2.2.2)$$

The slope of Eq. (2.2.2) is obtained by a linear fitting of the experimental results in the case of slow aggregation and by a third-order polynomial fitting in the case of fast aggregation. An important experimental criterion for the reliability of the fit is the extrapolated initial hydrodynamic radius of the non-aggregated or single colloidal particle (Holthoff et al., 1996).

After transformation according to Eq. (2.2.2), where r_h is replaced by $d_z/2$ (PCS), the stability ratio of the dispersion W can be calculated (Novich and Ring, 1984). This W ratio is defined by the ratio of the rate constant for the diffusion-controlled rapid coagulation ($k_{a,fast}$) to the slow or reaction limited coagulation (k_a). For suspensions with the same particle concentration, the W values are given directly by the ratio of the slopes (Grolimund et al., 2001) according to

$$W = \frac{\left(\frac{dlnr_h}{dt}\right)_{fast}}{\frac{dlnr_h}{dt}} = \frac{k_{a,fast}}{k_a} \qquad \text{Eq. (2.2.3)}$$

In this work, under *CCC* of Ca^{2+} or Na^+, the repulsive electrical forces were screened and the rapid aggregation kinetics ($k_{a,\ fast}$) was assumed to be close to a pure diffusion controlled coagulation only governed by the attractive van der Waals interactions according to the DLVO theory (Overbeek, 1980). The stability ratios W of illite and quartz colloid dispersions were plotted against the Ca^{2+} and Na^+ concentrations (C_s). The extrapolation of the linear variation of log W against log C_s was used to determine *CCC* according to the empirical relation,

$$W = (C_S\ /\ CCC)^{\ -\beta} \qquad \text{Eq. (2.2.4)}$$

where $W = 1$ or log $W = 0$ when C_s = *CCC* (see Fig 2.2.1). The *CCC* thus characterizes the transition between a salt independent fast rate of aggregation at a high electrolyte concentration and slow aggregation rates, which strongly decrease with a decreasing salt concentration.

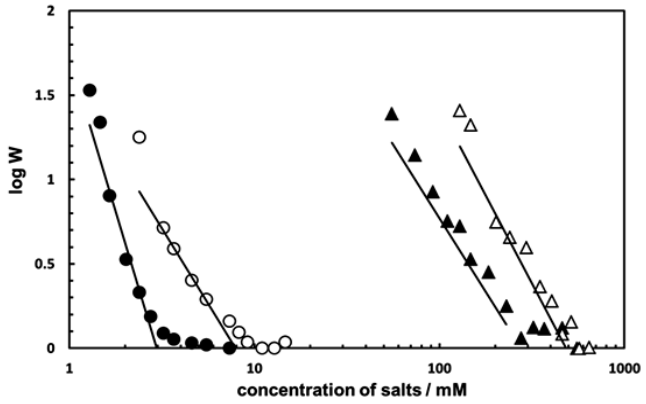

Fig. 2.2.1: Effects of Na^+ and Ca^{2+} concentration on the stability ratio (W) of illite and quartz colloids at pH 8.5. ●, illite, CaCl2; ○, quartz, CaCl2; ▲, illite, NaCl; △, quartz, NaCl.

2.2.2 Modelling *CCC* in mixed Na-Ca systems

The empirically established relation in mixed Na-Ca systems (Grolimund and Borkovec, 2006; Grolimund et al., 2001) can be used,

$$\frac{1}{CCC_{(Na+Ca)}} = \frac{1}{CCC_{Na}} f + \frac{1}{CCC_{Na}} (1-f) \qquad \text{Eq. (2.2.5)}$$

where f is the molar fraction of Na^+, CCC_{Na} and CCC_{Ca} are the CCC for pure Na- and Ca-systems, respectively. The molar fraction f is given by

$$f = \frac{1}{(1+X)} \qquad \text{Eq. (2.2.6)}$$

where X is the molar ratio of calcium to sodium, X = $[Ca^{2+}]$ / $[Na^+]$. The soil sodium adsorption ratio (SAR) in mixed Na-Ca systems can be defined as

$$SAR = \frac{|Na^+|}{\left\{\frac{[Ca^{2+}]}{2}\right\}^{0.5}} \qquad \text{Eq. (2.2.7)}$$

2.2.3 Scaling an effective attraction energy Hamaker constant: *A* (J)

The Hamaker constant, A, (in Joules) can be roughly defined as a material property that represents the strength of van der Waals interactions between macroscopic bodies. The DLVO model can be used to compare the effectiveness of the attraction energy (A), during the coagulation process. Typical values of A are in the range of 10^{-19} - 10^{-20} J. In a first approximation the Eiler and Korff relation (Eilers and Korff, 1940; Overbeek, 1980) having the dimension of energy can be used

$$A_{scaled} = \frac{\zeta_{CCC}^2}{K_{CCC}} \qquad \text{Eq. (2.2.8)}$$

where ζ_{CCC} is the zeta potential at CCC and the Debye-Hückel parameter K_{CCC} can be calculated from the ionic strength (I_{CCC}) at the *CCC*.

$$K_{CCC}^2 = \frac{2000F^2}{\varepsilon RT} I_{CCC} \qquad \text{Eq. (2.2.9)}$$

with the universal gas constant, R, the absolute temperature T, Faraday′s constant, F, and the permittivity, ε.

For water at 20°C, the parameter K_{CCC} is related to I_{CCC} by the following relation,

$$K_{ccc} = 3.28 \times 10^9 \, I_{ccc}{}^{0.5} \ (\mathrm{m}^{-1}) \qquad \text{Eq. (2.2.10)}$$

Using the A_{scaled} values, the effective A of the WDC across water can be estimated under different salt and pH conditions. I_{CCC} values can be calculated with the chemical equilibrium model *Visual Minteq 3.0* (Gustafsson, 2011) which enables the concentration of ionic species to be determined from inorganic and organic salts at different pHs.

It must be noted that the effective Hamaker constant (A) of two identical particles across water is given by

$$A = \left(\sqrt{A_P} - \sqrt{A_w}\right)^2 \qquad \text{Eq. (2.2.11)}$$

where A_{p} and A_{w} are the non-retarded Hamaker constants of particle and water interacting across a vacuum (Israelachvili, 1992) . In the case of two different particles (p_1 and p_2), a combining relation is used to calculate the effective Hamaker constant (A) across water,

$$A = \left(\sqrt{A_{P1}} - \sqrt{A_w}\right)\left(\sqrt{A_{P2}} - \sqrt{A_w}\right) \qquad \text{Eq. (2.2.12)}$$

2.3 Background of applied methods

2.3.1 Gas adsorption method

The specific surface area (SSA) is defined as the total surface area of a material per unit of mass.The specific surface area and the total pore volume can be determined by the N_2 adsorption technique. This method is widely used on understanding the pore structure of soil and to gain the ideas of the distribution and the contribution of the OM and the metal oxides effect in pores (Mayer et al., 2004; Pronk et al., 2011). It must be remarked that open pores are only detected by gas adsorption methods.

In the case of pore of cylindrical geometry, an average pore radius (R_p) can be also calculated from the N_2 sorption results with the following equation

$$R_p = 2\frac{V_p}{SSA} \qquad \text{Eq. (2.3.1)}$$

where the ratio of the total pore volume (V_p) and the BET surface area (SSA) is considered. A direct dependence with 1/SSA exists thus for modelling cylindrical pore. It has been demonstrated that the sorption kinetics of gas N_2 and CO_2 can be used to variously probe the OC/mineral surface interactions in soil (de Jonge and Mittelmeijer-Hazeleger, 1996; Eusterhues et al., 2005) and the low temperature of N_2 sorption measurement (77K) impedes rapid kinetics of gas molecules through OC/mineral surface (Kaiser and Guggenberger, 2003). It results into a relative blocking effect which can be used to measure the accessibility to underlying mineral surfaces. In the case of CO_2, a much higher temperature of measurement (273K) enhances the kinetics in porous systems where not only existing micropores at mineral surface but also OC bulk structure are rapidly saturated.

2.3.2 Photon correlation spectroscopy (PCS)

2.3.2.1 Size measurement

PCS is a light-scattering technique which is widely used for studying the dispersed colloids, macromolecules and polymers. Due to the Brownian motion, small particles move quickly and large particles move more slowly and the relationship between the size and its speed of a particle can be related with the Stokes-Einstein equation (Eq. (2.1.2)). The particle size measured is the diameter of the sphere that diffuses at the same speed as the particle being measured. With the diffusion coefficient (*D*), the hydrodynamic diameter can be calculated by using:

$$dz = \frac{kT}{f} = \frac{kT}{3\pi\eta D} \qquad \text{Eq. (2.3.2)}$$

dz : hydrodynamic diameter. *k* : Boltzmann constant. *f* : particle frictional coefficient. η: solvent viscosity. *T* : absolute temperature. *D*: diffusion coefficient.

2.3.2.2 Zeta- potential

The charge distributed at the particle surface affects the ions distribution in the surrounding interfacial region that the concentration of ions charged with opposite charge compared to the particle will be increased in the field of closing to the surface of particle. The liquid layer surrounding the particle exists as two parts; an inner Stern layer and a diffuse layer. In diffuse layer, there is a notional boundary inside and when a particle moves, ions within this boundary move with it, but any ions beyond the boundary will not move with the particle. This boundary is called the surface of hydrodynamic shear or slipping plane. The potential that exists at this boundary is known as the Zeta potential (Gregory, 2005).

The movement velocity of a particle in an electric field is commonly referred to as its electrophoretic mobility. The zeta potential (ζ) can be used to characterize electrokinetic properties of colloids by:

$$U = \frac{\zeta 2\varepsilon f(ka)}{3\eta} \qquad \text{Eq. (2.3.3)}$$

where: *U* is the microelectrophoretic mobility; η is the viscosity of the medium; ε is the dielectric constant. *f(ka)* is come from Henry's function and either 1.5 or 1.0 are used as approximations for the *f(ka)* determination. If the diffuse layer is very thin compared to the particle size, *f(ka)* in this case is 1.5, which is referred Smoluchowski approximation (Gregory, 2005). Therefore calculation of zeta potential from the mobility can be made as:

$$\zeta = U\eta / \varepsilon \qquad \text{Eq. (2.3.4)}$$

where ε is the permittivity ($\varepsilon = \varepsilon_r\varepsilon_0$) and η is the viscosity of the medium used to transform the microelectrophoretic mobility (U) into ζ-potential, which is justified according to the relative size of the colloidal particles (radius r = $d_z/2$) and their electrochemical double layers (K^{-1}, the Debye-Hückel length).

2.3.3 Small angle X-ray scattering (SAXS)

Small-angle X-ray scattering (SAXS) is a technique that is used for the structural characterization of solid and fluid materials in the nanometer (nm) range. It probes inhomogeneity of the electron density on a length scale of typically 1-100 nm (Guinier and Fournet, 1955), thus yielding complementary structural information to XRD (WAXS - wide angle X-ray scattering) data. It is applicable to crystalline and amorphous materials alike.

The Guinier plot allows the determination of the radius of gyration (R_g) from the measured scattered intensity $I(q)$ as a function of the scattering angle 2θ. The scattered intensity can be plotted as a function of the scattering vector, $q = 4\pi \sin\theta/\lambda$ with the wavelength λ of the X-ray, to give information on R_g. R_g can simply be calculated using the Guinier approximation as follows:

$$I\,(q) = Gexp\left(\frac{-q^2R_g^2}{3}\right) \qquad \text{Eq. (2.3.5)}$$

R_g is given in the region of smallest angles without any prior assumption on the shape and internal structure of the particles under investigation. For homogeneous particles, R_g is only related to the geometrical parameters of simple triaxial bodies (Mittelbach, 1964). A general validity rule for the Guinier approximation is given by $qR_g \leq 1$ for sphere but can be expanded to $qR_g < 3$ in the case of ellipsoids of revolution (Glatter and May, 2006).

In the case of suspension of clay particle as illite, R_g has been related to the clay particle layer thickness (Shang et al., 2001). In the case of solid sample, R_g can be associated to surface heterogeneities such pore and holes cavities (Glatter and Kratky, 1982). R_g results have been thus used to analyse the pore structure in solid particles (Dubinin et al., 1964; Fukuyama et al., 2001).

The logarithmic form of the power-law scattering relation gives the exponent *k,* whose magnitude has been discussed in term of fractal dimension in the case of porous systems (Bale and Schmidt, 1984; Schmidt, 1991). The power-law scattering of SAXS results in a large range of q, where qR_g>> 1 has been also considered in Eq. (2.3.6).

$$I(q) = \frac{P}{q^k} \qquad \text{Eq. (2.3.6)}$$

Indeed, power-low scattering exponent ≤ 3 are typical for mass fractals which are often aggregates of sub-units (Höhr et al., 1988; Schmidt, 1991).

Chapter 3

Materials and methods

3.1 Materials

3.1.1 Illite and quartz sand

Colloidal fractions of crushed quartz F32 from Quarzwerke GmbH (Frechen, Germany) and illite from Cs-Ker Illite Bt (Bekecs, Hungary) were obtained after a fractionation procedure based on sedimentation and centrifugation steps (Séquaris, 2010). The SEM images are shown in Fig. 3.1.1.

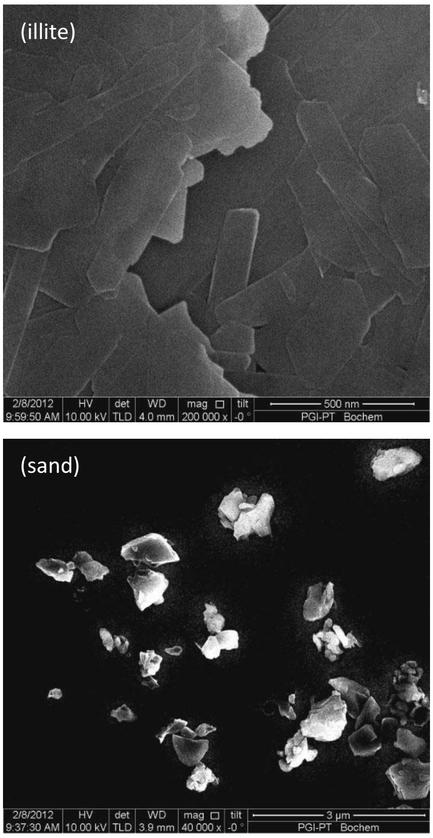

Fig. 3.1.1 Illite and quartz colloids structure scanned by SEM.

Illite and quartz particles are ubiquitous minerals which are found in soil clay fractions. Under soil electrolyte conditions, they carry an overall negative charge which makes them potentially stable WDCs. However, the heterogeneous chemical composition of the illite phyllosilicate structure at edge sites and basal planes contrasts with the more homogeneous chemical composition of quartz surfaces. The peculiar properties of illite surfaces are characterized by pH-dependent titrating aluminol (> AlOH) and silanol (> SiOH) groups at edge sites. The aluminol group of octahedral sheets has an apparent pk_{a} 6-8 at a low ionic strength (< 10 mM) (Delhorme et al., 2010), which varies from positive to negative values along the pH under soil electrolyte conditions. A net negative charge is also formed under alkaline conditions due to the dissociation of the > SiOH group from the tetrahedral sheets. On the other hand, the particle basal plane is characterized by a permanent negative charge mainly resulting from isomorphous substitutions of silicium (Si^{IV}) by aluminum atoms (Al^{III}). These anisotropic surface properties induce various models of particle aggregations between the edge surface and basal planes. The formation of a card-house structure under acidic conditions is favored where contacts between the positively charged edges and negatively charged basal planes are established (Gu and Doner, 1992; Lagaly, 2006; O'brien, 1971; Yan et al., 2011). At a basic pH, an overwhelming negative charge characterizes the illite surface as in the case of quartz particles point of zero charge (PZC) 2-4 (Fuerstenau, 1970) where silanol groups (pk_{a} 7-8) are predominantly anionic (Bennett, 1991; Delhorme et al., 2010).

3.1.2 Soil samples

Topsoil samples (0-10 cm) from three TERENO test sites were collected in July 2010. The test sites were located at Selhausen (50°52’08”N; 6°26’59’’E; arable soil, luvisol), Rollesbroich (50°37’18”N; 6°18’15’’E; grassland soil, cambisol) and Wüstebach (50°30’15”N; 6°18’15’’E; forest soil, gleyosol) in Germany. The samples were air-dried. Stones and large pieces of plant materials were removed by hand. The soil samples were coarsely ground and sieved through two sieves (mesh width 5 mm and 2 mm). The mean grain size distribution, soil pH, total organic carbon (TOC) , total nitrogen (TN) and particulate organic carbon (POC) in bulk soil samples (< 2mm) are listed in Table 3.1.1.

Table 3.1.1 The characteristics of soil studied

Soil samples	pH [a]	TOC /g kg^{-1b}	T N/g kg^{-1}	POC /gkg^{-1}	Clay /%	Silt/%	Sand/%
Selhausen	7.07	10.0 ± 0.2	1.07 ± 0.05	2.2 ± 0.2	19	65.6	15.7
Rollesbroich	5.82	40.4 ± 1.7	4.62 ± 0.09	9.1 ± 1.7	20	59.2	20.8
Wüstebach	4.25	83.1 ± 2.5	6.10 ± 0.40	17.2 ± 2.5	21	60.2	18.5

[a] soil / water = 1 / 2.5 ; [b] values are average of three different experiments ± standard deviation

3.1.3 Chemicals

$CaCl_2$, $CaSO_4$, Ca-formate $Ca(CHOO)_2$, NaCl, Na_2SO_4 and Na-oxalate ($Na_2C_2O_4$) (certified ACS reagent) were purchased from Merck (Germany). Water purified through Millipore filters was used in all experiments.

3.2 Methods

3.2.1 Soil particle size fractionation

Soil samples were fractionated according to the method of Séquaris & Lewandowski (2003) (Séquaris and Lewandowski, 2003).

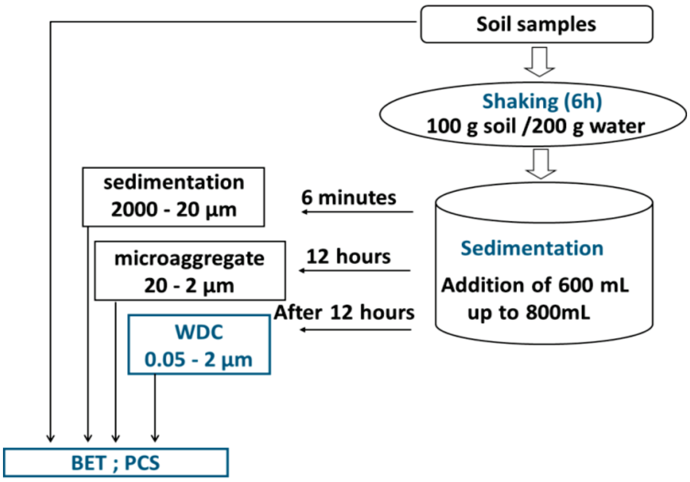

Fig.3.2.1Schematic of the soil physical fractionation method.

.

One hundred g of air-dried soil was added to a one litre Duran bottle (Schott, Germany) containing 0.2 litre of Millipore deionized water and shaken using a thermostated incubator (170 rpm) for 6 h. Six hundred ml of distilled water was then added, and the suspension was mixed and allowed to settle. Three soil phases containing varying soil-aggregate sizes were collected by a pipette method based on Stokes' law: soil aggregate fraction > 20 µm after 6 min, soil aggregate fraction from 2 µm to 20 µm after 12 h, and a separate phase containing non-settling colloidal aggregates after a 12 h sedimentation period at 23°C was designated water-dispersible colloids (WDCs). A solid size fraction from 0.05 µm to 2 µm was obtained by high-speed centrifugation (10,000g; 90 min) of the colloidal dispersion without any filtration. The remaining aqueous upper phase was the electrolyte phase and was operationally defined as containing the dissolved organic carbon (DOC). The mineralogical composition of the WDCs obtained from XRD analyses is given in Table 3.2.1.The SEM picture for three soils are listed in Fig. 3.2.2.

Table 3.2.1 Characteristics of WDCs from the soils studied

WDC	TOC gkg^{-1}	TN gkg^{-1}	SSA_{min} m^2g^{-1} [a]	minerals in WDC[b]
Selh	21 ± 1	2.9 ± 0.1	87	I^A, C/V^B, K^C
Roll	67 ± 1	6.6 ± 0.1	66	I^A, K^B, C/V^C
Wüst	71 ± 1	8.0 ± 0.1	88	I^A, C/V^B, K^C

[a] mineral SSA after OC removal [b] XRD mineral analysis: I, illite; S/V, chlorite and/ or vermicullite; K, kaolinite; A = abundant; B = present; C = little

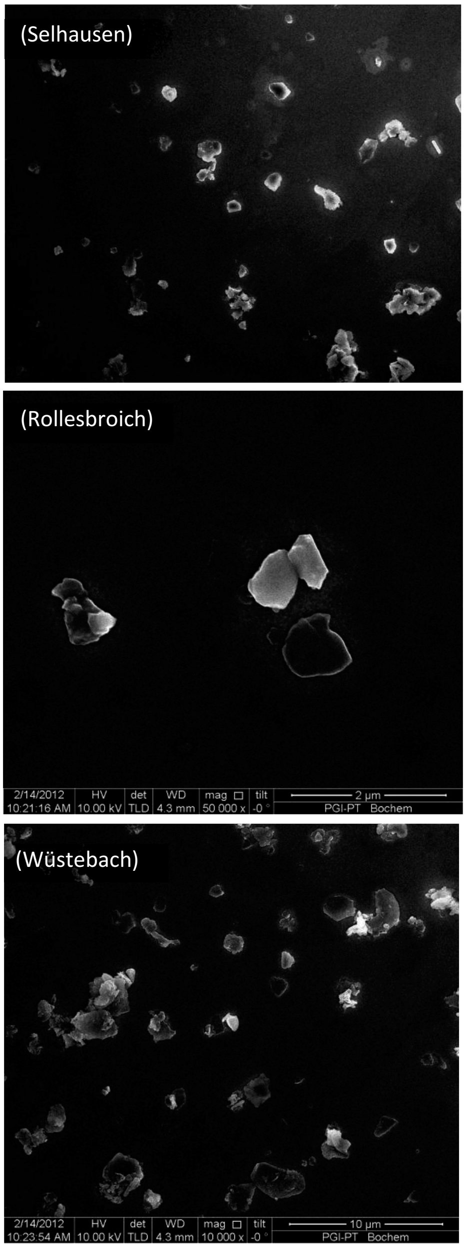

Fig.3.2.2 SEM images of WDCs from the soils studied.

3.2.2 Characterization of water-dispersible colloids (WDCs)

The photon correlation spectroscopy (PCS) measurements were performed using a Malvern Nano-ZS apparatus. Measurements were made at the scattering angle of 173° to measure the aggregation kinetics and calculate the critical coagulation concentration (CCC) of colloidal soil materials at 20°C. The monomodal cumulant method of the Nano-ZS apparatus software was used to analyse the correlation function. An averaged translational diffusion constant was thus obtained and used to calculate an equivalent spherical hydrodynamic diameter (z-average diameter, d_z) for the particles. The suspension concentration was 0.4 g L^{-1}. For the electrokinetic investigation, a Malvern Nano-ZS apparatus was used to measure the microelectrophoretic mobility (u) at 20°C. The suspension concentration was 0.4 g L^{-1}. An Expandable Ion Analyser EA 940 from Orion Research pH measurements was used for pH measurements.

3.2.3 Zeta potential measurement

For zeta potential measurements, 800 μL illite dispersion was added to 9200 μL $CaCl_2$ solution. After a waiting time of 2 hours, the dispersion was filled into a folded microelectrophoretic capillary cell.

3.2.4 CCC measurement

In order to investigate the CCC in different electrolyte at pH 5.5 and 8.5, a salt solution with certain concentration was prepared as an example stock solution and diluted to different concentrations. All of this diluted solution was adjusted to pH 8.5 or pH 5.5 before the measurements began. For illite and sand colloids, 5 g L^{-1} colloid dispersion was vigorously shaken with a magnetic stirring machine for 12 h in a 25 mL volumetric flask and the pH was then adjusted to 8.5 or pH 5.5. For soil colloid, 5 g L^{-1} of freeze-dried WDC was vigorously shaken for12 h after an ultrasonication of 4 min. The dispersion was sonicated for another 10 minutes before the measurements. 80 μL illite dispersion was added to 920 μL chemical solution at different concentration in disposable polystyrene cuvettes. After 1 sec., the PCS measurement was started and the particle size variations were measured every 33 sec.

3.2.5 Gas adsorption experiment

The specific surface area (SSA, m^2 g^{-1}) and microporosity (V_{micro}, cm^3 g^{-1}) were analysed by N_2 adsorption at 77K and by CO_2 adsorption at 273K with an AUTOSORB^{-1} (Quanta chrome) apparatus. The specific surface area was calculated by the multi-point BET method (N_2 gas sorption) and the microporosity (N_2 and CO_2 gas sorption) was calculated according to the Dubinin-Radushkevich (DR) equation. The linear form of the DR equation was also used to calculate micropore surface area based on a CO_2 molecules monolayer in micropore (Lowell et al., 2004). Three replicate measurements were generally performed. The bulk soil samples were degassed for 16 h at 70°C using N_2 as carrier gas before SSA determination. The organic matter of WDC soil samples was removed by thermal oxidation (400°C, 12h) in order to measure the *SSA* of the mineral phase (SSA_{mineral}) (Séquaris et al., 2010) The WDC samples were thus degassed for 2 h at 200°C using N_2 as the carrier gas before SSA determination. .

3.2.6 SAXS measurement

The SAXS measurements were performed on a modified compact Kratky-type instrument using line collimated Cu K_α radiation (wavelength 1.542 Å): A one-dimensional position sensitive proportional detector (MBraun PSD50) was used to record the scattering curves from samples situated at 21 cm apart from the detector. A thin layer of freeze-dried WDC samples was fixed between two sheets of Mylar foils and placed in the X-ray beam. After a typical exposure of 1000 seconds, the abscissa of the scattering curves was calibrated according to a measurement of silver behenate (Binnemans et al., 2004).

3.2.7 POM fractionation

Wet sieving soil particle size fractionation was performed in triplicates after chemical dispersion according to Cambardella and Elliot (Cambardella and Elliott, 1992) and Séquaris et al. (Séquaris et al., 2010). Ten g soil (< 2 mm) was shaken overnight on a flat-bed shaker with 0.05 litre of fresh Na hexametaphosphate (5 g l^{-1}) solution. The dispersed soil samples were passed sequentially through a 250 µm (Retsch GmbH, Haan, Germany), 53 µm and 20 µm sieve (Fritsch GmbH, Idar-Oberstein, Germany) and rinsed thoroughly with water until the rinsate was clear. The material remaining on the sieves (250-2000 µm, 53-250 µm, 20-53 µm) was freeze dried and weighed. The TOC contents were measured. The OC content of the particle-size fraction that passed the 20 µm sieve was calculated by the difference from the TOC of the bulk soil sample. It is considered that the soil particle size fraction 0-20 µm passing through the 20 µm sieve contains the mineral-associated and water-soluble C, while the soil particle size fraction 20-2000 µm remaining on the 20 µm, 53 µm and 200 µm sieves contains the particulate organic matter (POM) (Bornemann et al., 2011).

3.2.8 Dithionite-citrate-bicarbonate (DCB) extraction method

The Fe and Al oxides were extracted from soil particle size fractions in triplicate with the dithionite-citrate-bicarbonate (DCB) method (Mehra and Jackson, 1960). Two hundred mg of soil WDC was dispersed in a centrifugation tube containing 40 mL of the DCB stock solution (Kiem and Kögel-Knabner, 2002b). DCB stock solution was prepared from a mixture of 600 mL sodium citrate (0.3 M) and 0.15 L sodium hydrogencarbonate (1 M), to which 15 g of sodium dithionite was added. After shaking for 16 h at room temperature, the soil dispersion was centrifuged at 8000 rpm for 30 minutes and the supernatant was saved. The centrifugate was dispersed in 32 mL magnesium sulfate (0.05 M) and centrifuged a second time. The two supernatant phases were combined and the Fe_{DCB} and Al_{DCB} contents were analysed by an ICP-OES Thermo Elemental (TJA) Iris Intrepid spectrometer. Average values were obtained from three replicate measurements. Based on an operational approach, it can be assumed that the DCB method metals extract (M_{DCB}) includes both crystalline and poorly crystalline forms of Fe and Al oxides. In order to distinguish possible citrate-bicarbonate and magnesium effects from dissolution effects due to dithionite (Barberis et al., 1991), the soil samples were treated without the dithionite reagent (CB treatment) and were used as reference. Fe (Fe_{CB}) and Al (Al_{CB}) can be assigned to soluble forms of metal complexes. The residue of DCB and CB treatment after the centrifugation method was collected and freeze dried. The OC content has been removed by thermal oxidation of one part of the soil samples at 400°C, 16h (CB_{400} and DCB_{400}). This can remove 99% of the total OM originally in the soil sample.

3.2.9 Determination of oxalate-extractable Fe and Al

The concentration of $Fe_{oxalate}$ (Fe_o) and $Al_{oxalate}$ (Al_o) in non-crystalline compounds and in organo-metal complexes can be extracted from soils in triplicate with ammonium oxalate measures (Kleber et al., 2005; Masiello et al., 2004; Mikutta et al., 2005). 200 mg of soil samples (bulk soil sample, macroaggregates and WDC) was dispersed in a centrifugation tube containing 40 mL of an acidic oxalate solution (0.2 M, pH around 3) and was shaken for 2 hours in the dark. The 0.2 M oxalate solution was prepared with 0.113 M ammonium oxalate and 0.087 M oxalic acid (Kiem and Kögel-Knabner, 2002b). The soil dispersion was centrifuged at 8000 rpm for 30 minutes and the Fe_o and Al_o contents in the supernatant were analysed by an ICP-OES Thermo Elemental (TJA) Iris Intrepid spectrometer. Average values were obtained from three replicate measurements.

3.2.10 Organic-carbon metal oxides and electrolyte analysis

TOC was determined with a LECO RC-612 carbon analyser after correcting the total carbon from the inorganic carbon content. Total nitrogen (TN) contents were analysed with a C/N analyser (Vario EL cube; Elementar, Hanau, Germany). Ca and Na in the electrolyte phase were determined by using inductively coupled plasma optical emission spectrometry (ICP-OES). The pH of the colloidal dispersion and electrolyte solution was adjusted at pH 5.5 and 8.5 by adding HCl and NaOH solutions. The pH measurements were made with an expandable ion analyser EA 940 from Orion Research.

Chapter 4

Results and discussion

4.1 Effects of inorganic and organic anions on the stability of illite and quartz soil colloids in Na-, Ca- and mixed Na-Ca systems[1]

In this chapter, the colloidal behavior of soil mineral colloids (quartz and illite) in Na, Ca and mixed Na-Ca systems was systematically investigated. The critical coagulation concentrations (CCCs) were determined for Na^+ and Ca^{2+} solutions containing anions of a different nature (Cl^-, SO_4^{2-} and ubiquitous soil organic anions formate and oxalate) at pH 5.5 and pH 8.5. CCC of low soluble Ca^{2+}-oxalate was tested with oxalate-modified illite in $CaCl_2$. Attraction energy between colloids was experimentally scaled at CCC from zeta potential and aggregation kinetics measurements. CCC in pure Na- and Ca-systems was used to predict CCC in mixed Na-Ca systems.

4.1.1 Effect of cation nature, pH and mineral composition on the coagulation kinetics of illite and quartz colloids

The critical coagulation concentration (CCC) was systematically measured with photon correlation spectroscopy (PCS) by following the variation of the z-averaged diameter (d_z) of illite and quartz colloidal particles by increasing the salt concentration (Novich and Ring, 1984) in Na-, Ca- and Na-Ca systems. The monomodal cumulant method of the Nano-ZS apparatus software was used to analyse the correlation functions (see Chapter 2.2.1).

In Fig. 4.1.1, the effect of Na^+ and Ca^{2+} concentration on the particle diameter (d_z) variations of illite particles at pH 5.5 and pH 8.5 are plotted after an incubation time of 1000 sec. These snapshots of the aggregation kinetics already indicate sensitive d_z variations at the lower pH of 5.5 and in the presence of Ca^{2+}.

---

[1] This result has been already published: Jiang, C.-L., J.-M. Séquaris, H. Vereecken, and E. Klumpp. 2012. Effects of inorganic and organic anions on the stability of illite and quartz soil colloids in Na-, Ca- and mixed Na–Ca systems. Colloids and Surfaces A: Physicochemical and Engineering Aspects 415:134-141.

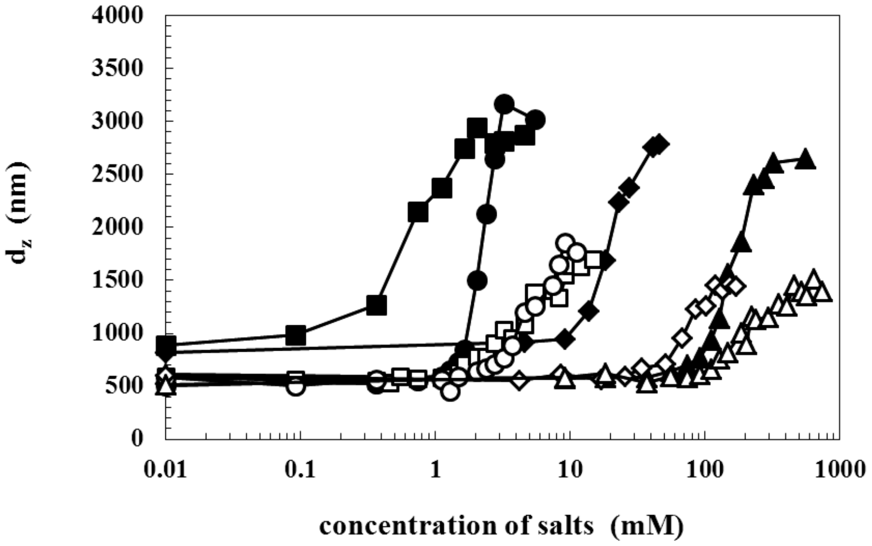

Fig. 4.1.1 Effects of cations (monovalent: Na^+; divalent: Ca^{2+}) and pH on the aggregation (d_z) of illite and quartz colloids (incubation time, 1000 sec). illite: ◆, NaCl at pH 5.5; ▲, NaCl at pH 8.5; ■, $CaCl_2$ at pH 5.5; ●, $CaCl_2$ at pH 8.5. quartz: ◇, NaCl at pH 5.5; △, NaCl at pH 8.5;□, $CaCl_2$ at pH 5.5; ○, $CaCl_2$ at pH 8.5.

In a general way, Table 4.1.1 shows that the *CCCs* of salts ($CaSO_4$, Ca $(HCOO)_2$, $CaCl_2$, Na_2SO_4 and NaCl) are higher at pH 8.5 than pH 5.5. $CCC_{\text{pH 8.5}}/CCC_{\text{pH 5.5}}$ ratios of about 8 and 2 were found for Na- and Ca-systems, respectively.

Increase of the coagulation at lower salt concentration at acidic pH can be related to charge modification of the edge surfaces due to a surface-specific proton interaction, which favors the card-house aggregate structure between positively charged edge sites and negatively charged basal planes. When the pH approaches or exceeds the pK_a 6-8 of aluminol and pk_a 7-8 of silanol functions (Delhorme et al., 2010) at the edge site, the increasing overall negative charge along the pH favors the electrostatic repulsion between colloids, so that a greater electrolyte concentration is required to achieve the aggregation at pH 8.5. At basic pH, the positive edge surface disappears and coagulation mainly occurs between negatively charged basal planes (Lagaly, 2006).

Table 4.1.1 Colloidal parameters of illite and quartz particles

soil materials	salt	pH	*CCC*, mM	ζ_{CCC} , mV	$CCC_{pH\ 8.5}/CCC_{pH\ 5.5}$
illite	NaCl	5.5	34 ± 3	-(54 ± 11)	7.7 ± 1.3
		8.5	261 ± 22	$\sim$-40 [a]	
	Na_2SO_4	5.5	42 ± 2	-(51 ± 11)	7.7 ± 0.7
		8.5	323 ± 16	$\sim$-40 [a]	
	$Na_2C_2O_4$	5.5	431 ± 19	$\sim$30 [a]	0.8 ± 0.1
		8.5	356 ± 17	$\sim$-40 [a]	
	$CaCl_2$	5.5	1.3 ± 0.2	-(20 ± 5)	2.2 ± 0.5
		8.5	2.8 ± 0.2	-(23 ± 4)	
	$Ca(HCOO)_2$	5.5	1.2 ± 0.2	-(18 ± 4)	2.4 ± 0.7
		8.5	2.9 ± 0.3	-(23 ± 4)	
	$CaSO_4$	5.5	1.4 ± 0.2	-(21 ± 4)	1.9 ± 0.4
		8.5	2.6 ± 0.2	-(24 ± 6)	
quartz	NaCl	5.5	137 ± 24	-(33 ± 17)	3.5 ± 0.8
		8.5	472 ± 40	$\sim$-20 [a]	
	Na_2SO_4	5.5	147 ± 30	-(33 ± 13)	4.0 ± 1.0
		8.5	551 ± 70	$\sim$-20 [a]	
	$Na_2C_2O_4$	5.5	250 ± 15	$\sim$-30 [a]	1.7 ± 0.2
		8.5	417 ± 20	$\sim$-20 [a]	
	$CaCl_2$	5.5	7 ± 1.1	-(22 ± 5)	1.3 ± 0.3
		8.5	9.3 ± 0.3	-(20 ± 6)	
	$Ca(HCOO)_2$	5.5	7.1 ± 0.2	-(23 ± 5)	1.4 ± 0.4
		8.5	10 ± 1.3	-(21 ± 5)	
	$CaSO_4$	5.5	10 ± 0.7	-(26 ± 5)	1.2 ± 0.4
		8.5	12 ± 3	-(22 ± 5)	

[a] values are only indicative due to the large absolute error

A strong dependence of *CCC* on the counterion charge in Table 4.1.1 was confirmed by the *CCC* decrease from Na- to Ca-systems in the presence of chloride and sulfate anions. Average CCC_{Na} / CCC_{Ca} ratios in Table 4.1.2 of about 30 and 110 at pH 5.5 and pH 8.5, were calculated with Na- and Ca-systems, respectively. A lowering of ζ –potential absolute value is observed at *CCC* with ζ_{CCC} varying around -20 mV and -50 mV with Ca^{2+} and Na^{+} cations, respectively (see Fig 4.1.2). A less negative ζ_{CCC} in the presence of divalent Ca^{2+} is due to a more effective charge screening and possible specific interactions with the illite surface (Polubesova and Nir, 1999).

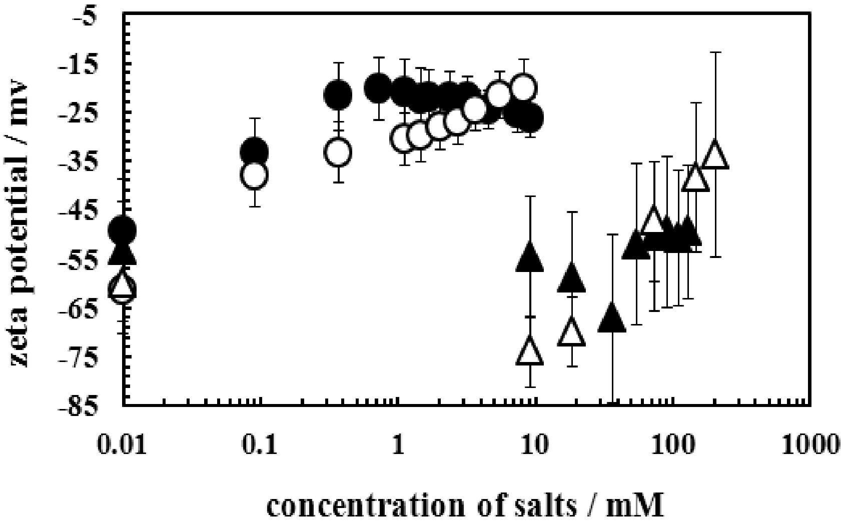

Fig. 4.1.2 Effect of Na^+ and Ca^{2+} concentration on the ζ-potential of illite and quartz colloids at pH 8.5. ●, illite, $CaCl_2$; ○, quartz, $CaCl_2$; ▲, illite, NaCl; △, quartz, NaCl.

For comparison, the colloidal stability behavior of quartz particles, another soil clay WDC material with a more homogeneous chemical structure (SiO_x) was also investigated. In Fig. 4.1.1, the effects of Na^+ and Ca^{2+} concentrations on the particle diameter (d_z) variations of quartz particles at pH 5.5 and 8.5 are plotted after an incubation time of 1000 sec for illustration. Sensitive effects of Ca^{2+} on d_z variations were also observed at lower concentration than in Na-systems. However, both Na^+ and Ca^{2+} concentration ranges for particle aggregation were systematically higher than in the case of illite particles, which will be discussed later. A much lower d_z value of about 1.5 µm also characterized the quartz aggregates in comparison with a d_z value of about 2.5 µm for the illite aggregates. Illite plate-like structures are capable of forming larger porous aggregates (Oster et al., 1980). In the presence of $CaCl_2$, $Ca(CHOO)_2$, $CaSO_4$, Na_2SO_4 and NaCl, a sensitive pH effect on *CCC* for quartz particles were only found in Na-systems. $CCC_{\text{pH 8.5}} / CCC_{\text{pH 5.5}}$ ratios of about 4 were found (Table 4.1.1). A shift to higher *CCC* values at pH 8.5 can be explained by the major negative ionization of silanol groups (pK_a 7-8). A sensitive decrease of *CCC* is also observed from Na- to Ca-systems. Higher CCC_{Na} / CCC_{Ca} ratio values of about 50 observed at pH 8.5 compared to about 20 at pH 5.5, in Table 4.1.2, indicate a similar pH sensitive dependence as in the case of illite particles.

Table 4.1.2 Comparison of CCC ratios of NaCl to $CaCl_2$, Na_2SO_4 to $CaSO_4$ and $Na_2C_2O_4$ to NaCl with illite and quartz particles at pH 5.5 and 8.5

soil materials	pH 5.5	pH 8.5
	CCC_{NaCl} / CCC_{CaCl2}	
illite	26 ± 6	93 ± 15
sand-quartz	20 ± 7	51 ± 6
	CCC_{Na2SO4}/ CCC_{CaSO4}	
illite	30 ± 6	124 ± 6
sand-quartz	15 ± 3	46 ± 17
	CCC_{Na2SO4}/ CCC_{CaSO4}	
illite	12.7 ± 1.7	1.4 ± 0.2
sand-quartz	1.8 ± 0.4	0.9 ± 0.1

Higher *CCC* ranges of Na^+ and Ca^{2+} were systematically measured at both pHs in the case of quartz particles in comparison with illite particles, which merit further explanations. In order to compare the effects of the mineral composition, alkaline conditions at pH 8.5 were chosen, as they ensure an initial dispersion of the single particles of both soil materials with net negative charges. Average CCC_{Na} / CCC_{Ca} ratios of about 93 and 51 or 124 and 46 were calculated for illite and quartz particles in a suspension containing Cl^- or SO_4^{2-} anions respectively. It must be remarked that the *CCCs* of quartz minerals at pH 8.5 obeys the Schulze -Hardy rule where *CCC* is proportional to the inverse sixth-power of the cation valence, (CCC_M^+ / CCC_M^{2+} = 64). The DLVO model can be used to compare the effectiveness of the attraction energy (*A*), during the coagulation process (See chapter 2.2.3 and Eq.2.2.8). In Table 4.1.3, the rate of aggregation $\theta N_0 k_{a,\ fast}$ and ζ^2_{CCC}/K or A_{scaled} calculated respectively (Chapter 2.2.3), are shown for illite and quartz particles in the Ca-system in the presence of Cl^-, formate and SO_4^{2-} anions.

Table 4.1.3 Comparison of aggregation kinetics parameters of illite and quartz particles in Ca^{2+}-system at pH 8.5

Salt	Soil materials	I_{CCC}, M [a]	A_{scaled} V^2m	$\theta N_0 k_a$, min^{-1}
$CaCl_2$	illite	8.3×10^{-3}	$(1.6\pm0.6) \times 10^{-12}$	1.0×10^{-2}
	sand-quartz	2.4×10^{-2}	$(0.7\pm0.4) \times 10^{-12}$	3.9×10^{-3}
$Ca(HCOO)_2$	illite	9.2×10^{-3}	$(1.7 \pm0.6) \times 10^{-12}$	0.8×10^{-2}
	sand-quartz	2.6×10^{-2}	$(0.8 \pm0.6) \times 10^{-12}$	2.4×10^{-3}
Ca SO_4	illite	7.8×10^{-3}	$(2.0 \pm1.0) \times 10^{-12}$	0.9×10^{-2}
	sand-quartz	2.6×10^{-2}	$(0.8 \pm0.6) \times 10^{-12}$	2.3×10^{-3}

[a] calculated Iccc with Visual Minteq (Gustafsson, 2011).

A similar critical ζ_{CCC} of about –20 mV characterizes both particles at pH 8.5. It was shown that A_{scaled} values of illite particles were a factor of about 2.3 higher than of the value for quartz particles. In the same way, the highest $\theta N_0 k_{a,\ fast}$ values were also measured for the illite particles. Considering for both mineral particles, the same mass concentration in suspension, close hydrodynamic particle size d_z (see below), solid density (~ 2.6 g cm^{-3}) and refractive index (~1.5555), $k_{a,\ fast}$ ratios of about 3.1 can be directly derived from the $\theta N_0 k_{a,\ fast}$ ratios of illite to quartz results, which also implies a more rapid coagulation of illite particles. Thus, the results obtained from the two experimental methods at *CCC* confirm stronger attraction energy between illite particles based on van der Waals forces. Indeed, higher Hamaker constants ($A_{Hamaker}$) for clay minerals materials ($A_{Hamaker}$, 2.5-4.5 × 10^{-20} J) than for quartz ($A_{Hamaker}$, 1.7-1.8 X 10^{-20} J) are generally reported in the literature (Séquaris, 2010) .

4.1.2 Effect of anion nature on the coagulation kinetics of illite and quartz colloids

In the case of Na-systems, the effects of chloride, sulfate and oxalate anions on the *CCCs* of illite and quartz particles are compared in Table 4.1.1. In the case of illite particles, a sensitive effect of oxalate can be observed along the series $CCC_{NaCl} < CCC_{Na2SO4} << CCC_{Na2C2O4}$ at both pHs. In the case of quartz particles, a $CCC_{Na2C2O4}$ higher than CCC_{NaCl} and CCC_{Na2SO4} was only measured at pH 5.5. A higher stability of illite colloids in the presence of oxalate is also illustrated in Fig. 4.1.3 by a large shift to higher Na concentrations of the particle d_z increase in comparison with NaCl solution.

In the case of illite, higher *CCC* values at both pHs in the presence of oxalate are an indication of a sensitive modification of the surface. An increase in the surface charge, which stabilizes the illite suspension by electrostatic repulsion, is generally admitted (Frenkel et al., 1992; Oades, 1984). High $CCC_{Na2C2O4} / CCC_{NaCl}$ ratios of about 13 and 3.5 at pH 5.5 and pH 8.5, respectively (Table 4.1.2) support a chemical surface modification by a surface complexation of oxalate, which contrasts with the electrostatic sorption of Cl^-. Protonated > MOH_2^+ surface groups enhance the inner-sphere adsorption of oxalate at an acidic pH (Kubicki et al., 1999), where the negative divalent anions contributed to the negativation of the edge surface charge. At more neutral and basic pH, >MOH and >MO^- surface species weakened or hindered, the adsorption of oxalate anions respectively. This was clearly shown in the case of quartz particles, where *CCC* in the presence of oxalate only increased at pH 5.5 (Table 4.1.1) when a $CCC_{Na2C2O4} / CCC_{NaCl}$ ratio of about 2 was calculated (Table 4.1.2).

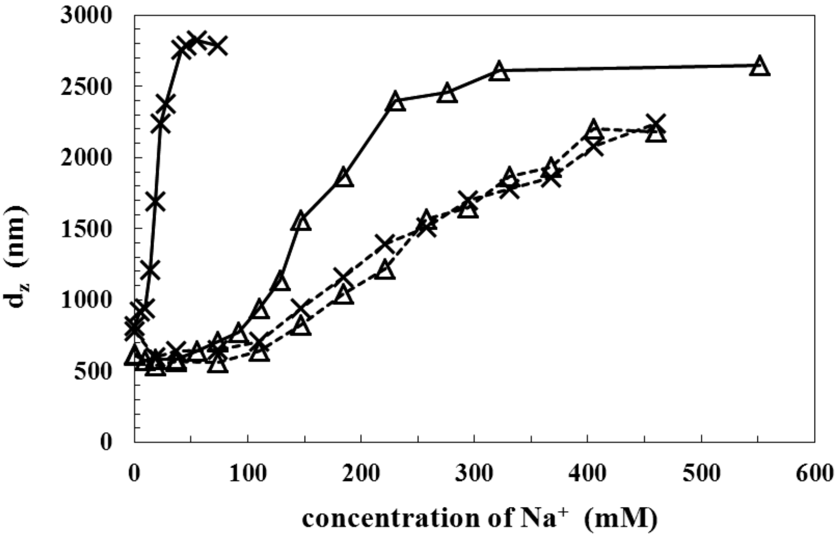

Fig. 4.1.3 Effects of anions (—–, chloride; ----, oxalate) and pH on the aggregation (*d*$_z$) of illite colloids in the Na-system (incubation time, 1000 sec). ×, pH 5.5; △, pH 8.5.

This may indicate some surface reaction (Bennett, 1991). On the other hand, at pH 8.5, a CCC_{Na2C2O4} / CCC_{NaCl} ratio of about 1 (Table 4.1.2) indicates that the oxalate anion does not specifically react with a quartz surface (Kubicki et al., 1999) covered by a high density of negatively ionized silanol species SiO^-.

The results show that a negativation of the surface charge due to interacting dicarboxylate or basic pH are factors that favor the dispersion of illite in single particles. In the presence of $Na_2C_2O_4$ or at pH 8.5, similar d_z of about (630 ± 25) nm and (650 ± 30) nm, respectively, were measured. These values are much lower than d_z in acidic pH. Indeed, at low Na^+ concentrations, hydrodynamic diameters d_z of about (840 ± 40) nm were measured for illite particles at pH 5.5. In comparison, d_z values of about (580 ± 30) nm for quartz particles are not sensitively affected by the pH or oxalate presence, which would characterize a single particle form.

In the case of Ca-systems, the effects of monovalent anions Cl^-, formate and divalent anion SO_4^{2-} on the aggregation of illite are compared in Fig. 4.1.4.

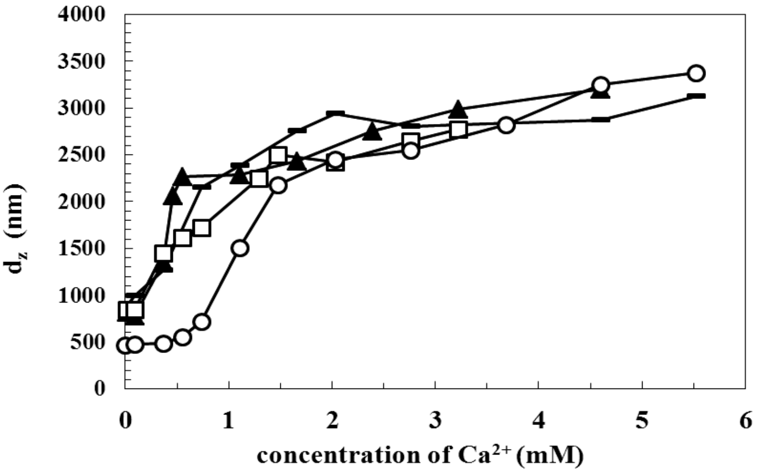

Fig. 4.1.4 Effects of anions (chloride, formate, sulfate and oxalate) on the aggregation (d_z) of illite colloids in the Ca-system (incubation time, 1000 sec) at pH 5.5.■, calcium chloride; ▲, calcium formate; □, calcium sulfate; ○, oxalate-modified illite and calcium chloride (see also Text).

The snapshots of the coagulation extent at 1000 sec in relation to the Ca^{2+} concentration only show slight effects of the anion nature on the particle diameter. In the same way, the calculated *CCC* values of Ca^{2+} in the presence of three anions in Table 4.1.1 are close. In the case of oxalate, the low solubility of the calcium oxalate (CaC_2O_4) salt (less than 6.7 mg/L or 0.052 mM) renders a direct comparison difficult. In order to evaluate the potential effect of oxalate under the same Ca^{2+} concentration range as the other anions Cl^-, SO_4^{2-} and formate, illite particles were first conditioned with $Na_2C_2O_4$. The oxalate surface reaction was followed (dispersion effect) by a decrease in pristine illite particle size d_z (dispersion effect) in Fig. 4.1.5.

A $Na_2C_2O_4$ concentration of 9.2 mM was chosen for the illite particle (5 g/L) conditioning. Sorption results of comparable strongly reactive oxyanions as arsenate and phosphate on illite (Violante and Pigna, 2002) indicate that illite particles have a maximum sorption capacity of about 0.010 mM g^{-1} illite. A sorption can be readily attained during the conditioning step where an excess concentration of oxalate per g illite was fixed at 1.8 mM $Na_2C_2O_4$ g^{-1} illite.

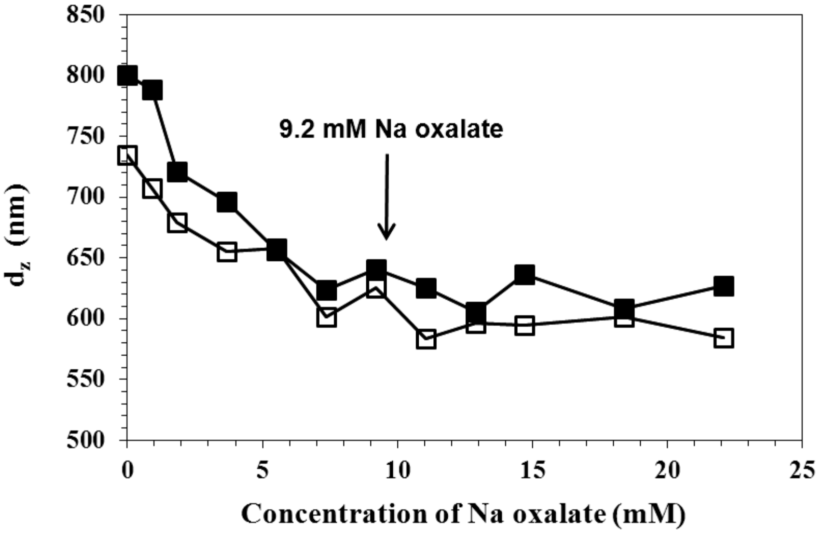

Fig. 4.1.5 Effects of Na-oxalate and pH on the particle size (d_z) of the illite suspension (incubation time, 1000 sec): ■, Na oxalate at pH 5.5; □, Na oxalate at pH 8.5.

Under these sorption conditions, it was shown that the particle d_z reaches a minimum value in this $Na_2C_2O_4$ concentration range, which can be taken as a criterion for an extended modification of illite surface. Thus, in the oxalate-modified illite particles preparation, 125 mg illite was suspended in 25 mL Na oxalate (9.2 mM) solution and mixed. After 12 hours of stirring, the suspension (5 g L^{-1}) was centrifuged at 20,000 rpm for 30 min. The Na-oxalate solution phase (about 24.5 mL) was removed and the solid phase was dispersed in 24.5 mL Millipore water. The final concentration of oxalate in the oxalate-modified suspension (5 g L^{-1}) was 0.2 mM before PCS and zeta potential measurements (see chapter 3.2.3, 3.2.4). For comparison, PCS and zeta potential measurements of oxalate-modified suspension in the presence of a final concentration of 4.6 mM oxalate were investigated.

After the conditioning step, the aggregation kinetics of oxalate-modified illite suspension was investigated with $CaCl_2$ at pH 5.5 and pH 8.5. The irreversible character of the oxalate modification was confirmed by a sensitive decrease in d_z (480 nm) and an increase in the negative ζ-potential (-29 mV) at 10^{-1} mM $CaCl_2$ compared to the pristine illite particles (d_z = 990 nm and ζ-potential = -25 mV). In Fig. 4.1.4, the coagulation results are shown at 1000 sec and compared to other results with $CaCl_2$, Ca formate, $CaSO_4$ and pristine illite. A slight shift to higher Ca concentrations was observed in the case of oxalate-modified illite, which was also calculated in the corresponding CCC_{Ca} value of about 1.5 mM in Table 4.1.4. A possible effect due to the complexation of added Ca^{2+} (calcium oxalate, log K = 3.19, (Gustafsson, 2011) with the remaining $Na_2C_2O_4$ traces (0.02 mM) was negligible according to the chemical equilibrium model *Visual Minteq* 3.0 (Gustafsson, 2011), which indicates that the distribution of free Ca^{2+} species at CCC_{Ca} is about 99%. On the other hand, measuring the CCC_{Ca} of the oxalate-modified illite suspensions (0.4 g L^{-1}) in the presence of 4.6 mM $Na_2C_2O_4$ indicates a sensitive shift to higher values (CCC_{Ca} of 3.6 mM in Table 4.1.4) due to the complexing properties of free oxalate in solution. Indeed, the calculation of the corresponding concentration of free Ca^{2+} species ($CCC_{\mathrm{free\ Ca}}$) with *Visual Minteq* 3.0 confirmed a value of about 1.5 mM. In this case, the distributions of free Ca^{2+} and Ca-oxalate forms were about 43% and 57%, respectively. For comparison, $CCC_{\mathrm{free\ Ca}}$ for pristine illite suspension under similar Na^+ salt concentrations (9.2 mM) where the oxalate anion was replaced by a Cl^- ion was only 1 mM in the mixed Na-Ca system, which confirms the higher stability of the oxalate-modified illite suspensions.

Table 4.1.4 Colloidal parameters of oxalate-modified illite particles

pH	$Na_2C_2O_4$	CCC_{Ca}, mM	$CCC_{\mathrm{free\ Ca}}$, mM [a]	ζ_{CCC}, mV
5.5	0.02 mM	1.5 ± 0.1	1.5 ± 0.1	-(21 ± 4)
5.5	4.60 mM	3.6 ± 0.2	1.5 ± 0.2	-(47 ± 7)
8.5	0.02 mM	3.2 ± 0.3	3.2 ± 0.1	-(24 ± 4)

[a] calculated $CCC_{\mathrm{free\ Ca}}$ with Visual Minteq (Gustafsson, 2011).

It should be noted that the *CCC* results in the Ca-system are in a narrow concentration range between 1.2 mM Ca^{2+} and 1.5 mM Ca^{2+} at pH 5.5 and between 2.8 mM Ca^{2+} and 3.2 mM Ca^{2+} at pH 8.5. This indicates a relatively weak dependence of *CCC* on the interfacial behavior of anions (Tables 4.1.1 and 4.1.4). This was exemplified at pH 5.5 by comparing of *CCC* in the Na- and Ca-systems in the case of oxalate and chloride anions. In the Na-system, a $CCC_{\mathrm{oxalate}}/CCC_{\mathrm{chloride}}$ ratio of a factor about 13 was calculated while in the Ca-system and mixed Na-Ca system, $CCC_{\mathrm{oxalate}}/CCC_{\mathrm{chloride}}$ varied from 1.2 to 1.5. One reason lies in the divalent nature of Ca^{2+}, which favors interactions between permanently negatively charged plates of illite (Lagaly, 2006), where edge sites are modified by a specific sorption of anion are not directly involved. It was demonstrated that attractive ion-ion correlation forces exist between equally highly charged clay mineral colloids (Kjellander et al., 1988; Quirk, 1994) in addition to the van der Waals forces. They are more effective in the presence of divalent cations at short distances than for monovalent cations. It can be assumed that these forces in Ca-system prevail over interfacial dispersion effects due to anions such as oxalate in the Na-system.

4.1.3 Coagulation of illite and quartz colloids in mixed Na-Ca systems

Under soil solutions conditions, with a slightly acidic or basic pH, the simultaneous presence of exchangeable Na^+ and Ca^{2+} and the surface coating of mineral particles by NOM influence the release and deposition of WDC (Grolimund, 2007). This results in a complex fate behavior of WDC where knowledge about the colloidal properties is determinant.

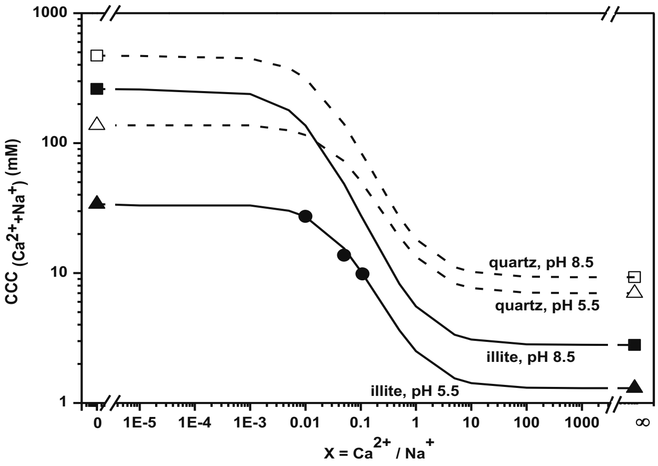

Fig. 4.1.6 Effect of the molar ratio of calcium to sodium, *X*, on the critical coagulation concentration for the total concentration of all cations $CCC_{\text{Na + Ca}}$ in the case of illite and quartz colloids in a mixed Na-Ca system at pH 5.5 and pH 8.5 in the presence of chloride anion. CCC measured in pure Ca- and Na- systems:▲, illite at pH 5.5; ■, illite at pH 8.5; △, quartz at pH 5.5; □, sand–quartz at pH 8.5. (—; ----,) prediction curves calculated with Eq.2.2.5 and measured *CCC* in pure Ca-system and Na-system ●, tested $CCC_{\text{Na + Ca}}$ in mixed Na-Ca systems.

The present results in pure Na- and Ca-systems allow us to assess the colloidal stability of illite and quartz colloids dispersion in mixed Na-Ca systems by using relation (9) Eq. 2.2.5 and the results in Table 4.1.1 and Table 4.1.4. In Fig. 4.1.6, the *CCC* for the total concentration of all cation in solutions $CCC_{\text{Na + Ca}}$ in relation to the molar ratio of calcium to sodium, $X = [Ca^{2+}] / [Na^{+}]$ have been reported in the case of illite and quartz colloids at pH 5.5 and pH 8.5 in the presence of Cl^{-} anions.

The validity of the established Eq.2.2.5 taken from Grolimund et al. (Grolimund et al., 2001; Grolimund, 2007) was satisfactorily confirmed by measuring the aggregation kinetics of illite suspension at fixed *X* values of 0.01 and 0.05 in the presence of NaCl and $CaCl_2$ at pH 5.5 (Table 4.1.5). The results give an overview of the electrolyte *X* conditions, which promote the coagulation of the two different mineral colloids at pH 5.5 and pH 8.5.

Table 4.1.5 CCC_{Ca+Na} of illite and oxalate-modified illite in mixed Na-Ca systems at pH 5.5

	X [a] =0.01	X = 0.05	X =0.108	X =0.163
pristine illite	27±1	14±1	10 ±1	-
oxalate-modified illite	95±4	32 ± 4	-	10 ±1

[a] $X = [Ca^{2+}] / [Na^{+}]$

As already discussed, a shift of $CCC_{\mathrm{Na+Ca}}$ to higher values characterizes the higher stability of the quartz suspension under the same pH conditions as for the illite suspension. A transition between dominating monovalent cation in solution at low *X* values and dominating divalent cation in solution at high *X* values was observed from $X = 0.01$ to $X = 10$. This corresponds to molar fractions of Na^{+} from $f = 0.99$ to 0.09 or to corresponding SAR values from 10 to 0.32 $meq^{0.5}$ (chapter 2.2.2 and Eq. (2.2.7)). High $CCC_{\mathrm{Na+Ca}}$ values associated with the dispersion effects of illite or quartz colloids can be directly related to an increased electrostatic interaction due to the surface ionization at an alkaline pH and/or to the relative increase of the electrochemical double layer thickness due to the Na^{+} surface contribution at low *X* values.

In Fig. 4.1.7, the modelling results are shown for the illite suspension in the presence of divalent sulfate and oxalate anions at both pH 5.5 and pH 8.5. Additional results from Table 4.1.4 have been also added after considering the corresponding *X* values. The validity of the Eq. (2.2.5) was also satisfactorily confirmed by measuring the aggregation kinetics of the oxalate-modified illite suspension at fixed *X* values of 0.01 and 0.05 in the presence of NaCl and $CaCl_2$ at pH 5.5 (Table 4.1.5).

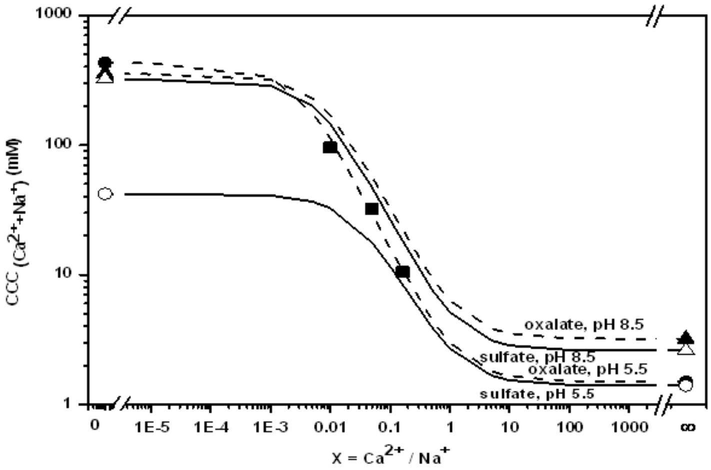

Fig. 4.1.7 Effect of the molar ratio of calcium to sodium, *X*, on the critical coagulation concentration for the total concentration of all cations CCC_{Na+Ca} in the case of pristine illite colloids and oxalate-modified illite in a mixed Na Ca system at pH 5.5 and pH 8.5 in the presence of sulfate and chloride anions, respectively. *CCC* measured in pure Ca- and Na- systems:○, pristine illite at pH 5.5; ●, oxalate-modified illite at pH 5.5;△, pristine illite at pH 8.5; ▲, oxalate-modified illite at pH 8.5. (—; ----,) prediction curves calculated with Eq.2.2.5 and measured *CCC* in pure Ca-system and Na-system; ■, tested CCC_{Na+Ca} in mixed Na-Ca systems.

The highest dispersion of the illite suspension due to oxalate modification was clearly demonstrated by the highest CCC_{Na+Ca} values at both pH 5.5 and pH 8.5 along the *X* values. At pH 5.5 and low *X* values, in particular, the oxalate surface modification levels the pH effects on the coagulation process. This effect is obtained with a simple LMW bifunctional organic acid, which can be considered as representative for complex multifunctional acidic structures of NOM in soil solution. The systematic results in Fig. 4.1.7 allow the soil electrolyte conditions to be determined for the stabilization of WDC suspension with NOM. A soil process, which favors the transport of sequestered OM as well as adsorbed chemical contaminants (Bin et al., 2011; Kaplan et al., 1993) by WDC.

4.1.4 Conclusion

The combination of PCS and zeta-potential methods allowed following the aggregation kinetics of potential WDC, illite and quartz particles in solution under various chemical conditions. The importance of the pH, nature and concentration of electrolyte ions on the stability of colloidal dispersions can be analysed by measuring the *CCC*. The main role played by the cation valence in decreasing the stability of the colloidal particles at lower concentrations of Ca^{2+} was confirmed. A higher stability of the dispersion of colloidal quartz particles than for illite particles was related to lower van der Waals interaction forces, which were scaled by the Eilers and Korff relation, ζ_{CCC}^2 / K and the fast aggregation rate with $\Phi k_{a, fast}$. The variations of *CCC* with the pH and the anion nature demonstrated the sensitivity of the edge site to illite particles in the aggregate formation. A high dispersibility of WDC particles was detected in the Na-system after interaction with oxalate anions. This is related to the capacity of bifunctional carboxylic acid to interact through inner-sphere complexes with surface Al and Si. In the Ca-system, the strong coagulation power of calcium prevailed over the surface effects of anions, which supports attractive ion-ion correlation forces between equally highly charged illite colloids. However, the distribution of its coagulating free Ca^{2+} species in suspension can be limited by the complexation capacity of the anion as in the case of oxalate. The results in mixed Na-Ca systems are of great interest for the interpretation of coagulation/deposition processes under soil chemical conditions. It was shown that the CCCs of mixed Na-Ca systems can be calculated using the *CCCs* for colloidal illite and quartz particles in pure Na and Ca systems. Dispersion effects due to adsorbed oxalate as a representative of ubiquitous polyvalent LMW organic acids in NOM could be here analysed as a function of the molar ratios of calcium to sodium in solution.

4.2 Characterization of organic carbon and metal oxides in soil WDC and soil fractions

In this chapter, the specific surface area (SSA) and micro pore (µpore) structure of < 2 µm WDC, 2-20 µm particle size fractions and bulk soil samples (< 2 mm) were studied before and after OC and metal oxides extraction with N_2 and CO_2 gas sorption and SAXS methods. For metal oxides, dithionite-citrate-bicarbonate (DCB) extracted metal oxides were compared with oxalate extracted ones which can look into different functions of various metal oxides types. Three topsoil samples (0-10 cm) from three TERENO test sites were collected (Chapter 3.1.2) and the soil samples were fractionated (Chapter 3.2.1). Soil pH and the mean grain size distribution are reported in Table 3.1.1.

4.2.1 Organic matter content in soil fractions and bulk soil samples

4.2.1.1 Distribution of TOC in soil WDC and soil fraction

In Table 4.2.1, the TOC contents of particle size fractions (< 2 µm (WDC), 2-20 µm, 20-2000 µm) and < 2 mm soil samples are reported. The TOC content increases along the series: Selhausen < Rollesbroich < Wüstebach. In the case of Wüstebach soil, it must be remarked that the highest TOC content of the 20-2000 µm particle size fraction in comparison with 2-20 µm and WDC particle size fractions is an indication for a relative high distribution of free OC in large soil aggregates samples.

Table 4.2.1 Mass distributions of different particle size fractions and corresponding TOC contents in the three topsoils

	Selh		Roll		Wüst	
Soil fraction	Mass g kg^{-1}	TOC g kg^{-1}	Mass g kg^{-1}	TOC g kg^{-1}	Mass g kg^{-1}	TOC g kg^{-1}
< 2µm	81±2	21.7±0.07	41±2	67.74±1.11	41±1	71.25±0.10
2-20 µm	276±2	21.47±0.48	379±16	45.51±4.88	501±12	58.67±1.95
20-2000 µm	635±8	7.31±0.70	543±11	39.63±4.72	433±16	93.94±10.82
bulk	1000	10.03±0.22	1000	40.37±1.69	1000	83.08±2.50

4.2.1.2 Application of gas adsorption to measure the effect of OC content in the microstructure of particle size fractions and bulk soil samples

Soil aggregate porous structure is formed by the arrangement of mineral porous surface and OC structure which can be probed by the sorption of gas. Depending on the temperature, it has been demonstrated that the sorption kinetics of gas N_2 and CO_2 can be used to variously probe the OC/mineral surface interactions in soil (de Jonge and Mittelmeijer-Hazeleger, 1996; Eusterhues et al., 2005). In order to test the effect of OC, the sorption of gas was compared on soil samples before and after removal of OC. Thus, pristine soil samples were dried at 70°C while free-OC samples were obtained after a thermal oxidation at 400°C (12 h). The variations of micropore measured from N_2 and CO_2 gas sorption (see Chapter 3.2.5) for particle size fractions and bulk soil samples are reported in table 4.2.2.

Table 4.2.2 Micropore properties of WDC and soil fractions before and after OC removal measured with gas adsorption method

		TOC	$V_{micropore-CO2}$ cm^3 g^{-1}		$V_{micropore-CO2}$ variation	$V_{micropore-N2}$ cm^3 g^{-1}		$V_{micropore-N2}$ variation
		g kg^{-1}	70°C	400°C	%	70°C	400°C	%
<2 mm	Selh	10	5.11E-03	4.14E-03	23.33	4.29E-03	5.61E-03	-23.57
	Roll	40	7.42E-03	5.09E-03	45.82	2.69E-03	6.21E-03	-56.70
	Wüst	83	1.45E-02	8.51E-03	69.92	4.16E-03	9.52E-03	-56.32
2-20 µm	Selh	21	1.27E-02	1.11E-02	15.02	9.08E-03	1.49E-02	-39.22
	Roll	46	1.16E-02	8.94E-03	30.09	3.86E-03	9.91E-03	-61.00
	Wüst	59	1.65E-02	1.09E-02	52.12	6.33E-03	1.29E-02	-50.98
< 2µm	Selh	21	2.15E-02	1.90E-02	12.99	2.07E-02	2.95E-02	-29.90
	Roll	67	2.05E-02	1.83E-02	12.14	1.08E-02	2.32E-02	-53.51
	Wüst	71	2.53E-02	2.32E-02	9.10	1.38E-02	2.95E-02	-53.26

In Fig. 4.2.2, calculated µpore $vol._{70}$ results of soil samples with the Dubinin-Radushkevich (DR) method are plotted against TOC. In reference, the corresponding µpore $vol._{400}$ results of the mineral content are also shown. In the case of bulk soil samples and particle size fraction 2-20 µm, the higher gas sorption results with the particle size (< 2 µm, WDC) than those with bulk soil samples and particle size fraction 2-20 µm demonstrate the major contribution of clay and metal oxide fractions to the surface properties of soils. It can also be seen that relative variations of µpore volumes in soil samples before (70) and after (400) OC removal strongly depend on the type of gas sorption measurement.

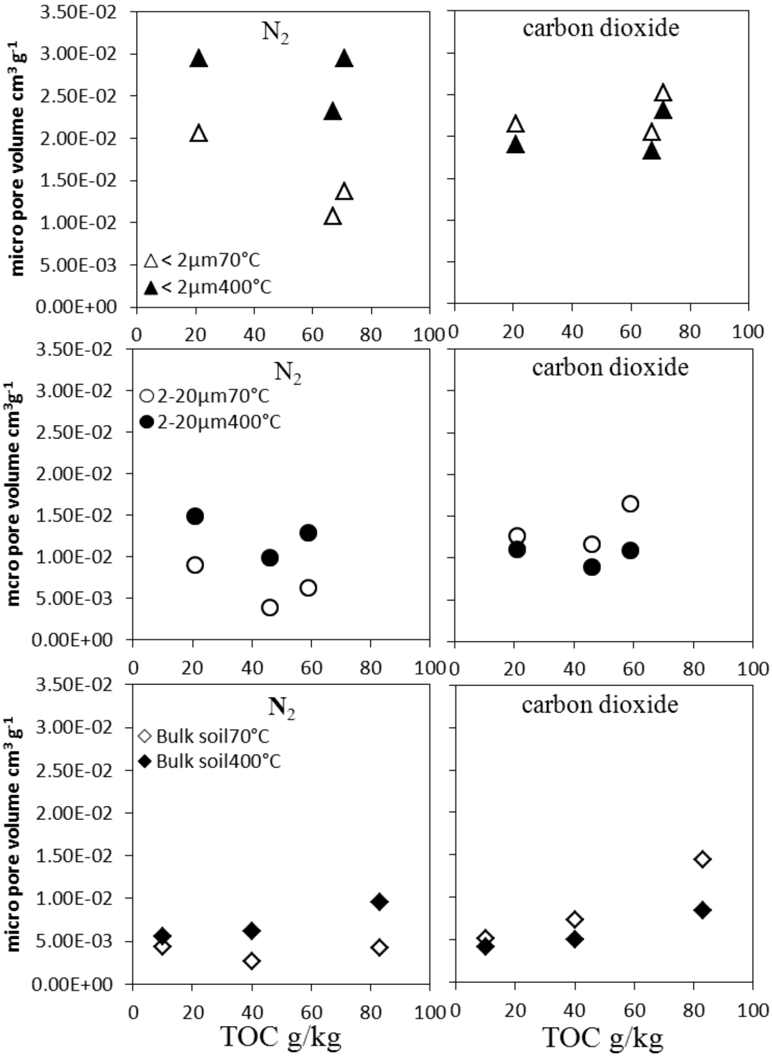

Fig. 4.2.1 Micropore volumes of bulk soil samples and particle size fractions < 2 µm (WDC), 2-20 µm samples from the three soils measured with N_2 and CO_2 gas sorption method.◆, bulk soil samples 70°C; ■, bulk soil samples 400°C; —, WDC 70°C; ✕, WDC 400°C.

In the case of N_2, a systematic lowering µpore vol.$_{70}$ was measured which confirms a blocking effect of OC on the N_2 sorption kinetics. The filling of strongly bound OC to mineral micropore impedes the accessibility to the mineral surface. This effect correlates to the OC content of particle size fractions and bulk soil samples. In the case of CO_2, a contrast sorption behavior was detected. First, there is no decrease of the CO_2 sorption in the presence of OC as shown by the systematic higher values of µpore vol.$_{70}$ results than µpore vol.$_{400}$. An additional adsorption of CO_2 at mineral surface due to organic matter can be clearly shown. A strong dependence of the CO_2 sorption to the OC content is observed in the case of particle size fraction 2-20 µm and bulk soil samples. In the case of particle size fraction < 2 µm (WDC), a CO_2 transport to the mineral surface through sorbed OC layer remains unaffected but the dependence of the µpore vol.$_{70}$ results on the OC concentration is less evidenced. These results were rationalized by using the Eq. (4.2.1). The variations of N_2 and CO_2 gas sorption for particle size fractions and bulk soil samples (Table 4.2.2) have been reported against the TOC content in Fig. 4.2.2.

$$variation = \frac{\mu pore_{70} - \mu pore_{400}}{\mu pore_{400}} \qquad \text{Eq. (4.2.1)}$$

In the case of CO_2 sorption, the increase of additional CO_2 binding, expressed in percentage, in function of OC content depends on the WDC fraction (Table 4.2.2). A relative large increase is observed along the series: particle size fractions (< 2 µm (WDC)) < (2-20 µm) < (bulk soil samples) which can be related to the growing distribution of non-associated OC. Indeed, an increase of the particular organic matter (POM) distribution in TOC of bulk soil samples along the series Selhausen < Rollesbroich < Wüstebach was measured. POC > 20 µm of 2.2 OC g kg^{-1}, 9.1 OC g kg^{-1} and 17.2 OC g kg^{-1}were measured after fractionation by wet-sieving in Selhausen, Rollesbroich and Wüstebach bulk soil samples. It can be thus concluded to a stronger CO_2 binding to particular organic matter than to mineral-associated OC.

In the case of N_2 sorption, a similar decrease of accessibility was measured for particle size fractions (< 2 µm (WDC)), (2-20 µm) and (bulk soil samples) in each soils (Table 4.2.2), which confirms the main role played by the particle size fraction < 2 µm (soil clay fraction) in the OC sorption. Maximal accessibility decreases due to an OC blocking effect of about 55% were measured with Rollesbroich and Wüstebach particle size fractions < 2 µm (WDC), 2-20 µm and bulk soil samples, in a concentration range ≥ 40 g OC kg^{-1} (Fig. 4.2.2). In the case of the three bulk topsoils containing a similar clay content (~ 20% in the three bulk soil samples, Table 3.1.1), a maximal blocking effect of micropore due to an OC sorption or sequestration up to 40 g OC kg^{-1} can be hypothesized.

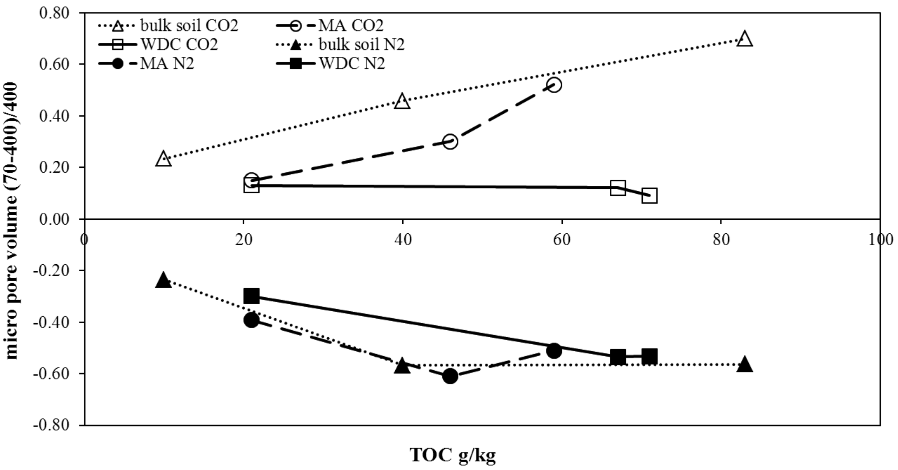

Fig. 4.2.2 The variations of N_2 and CO_2 gas sorption in different soil fractions of three soils. ◆, bulk soil sample with CO_2; ■, WDC with CO_2; ▲, bulk soil sample with N_2; ×, WDC with N_2.

However, the variations of accessibility of N_2 to the mineral surface due to blocking effect of OC between the three bulk soils and corresponding particle sizes depend not only on the OC content but also of the available SSA on mineral. This can be rationalized by considering the ratios OC/SSA$_{400}$ or OC/µpore vol.$_{400}$ as parameters for the potential extent association between OC and mineral surfaces, which allows a direct comparison between three bulk soils and corresponding particle sizes. It results into a general curve which supports a critical OC/SSA$_{400}$ or OC/µpore vol.$_{400}$ values for reaching a maximal blocking effect of N_2 sorption . In Fig. 4.2.3-a and Fig. 4.2.3-b , critical OC/SSA$_{400}$ or OC/µpore vol.$_{400}$ values of about 8 g TOC cm^{-2} and 2 g TOC cm^{3} can be extrapolated from the intersections of the two curves branches. These characteristic values independent on the soil type and particle sizes can be used for estimating the maximal extent of OC at the mineral surface or sequestrated stable OC. Thus, it can be assumed that, in the case of Selhausen agricultural bulk soil, the potential maximal OC sequestration is not reached, which is not the case for the Rollesbroich and Wüstebach soils where an OC saturation of the mineral surface can be admitted.

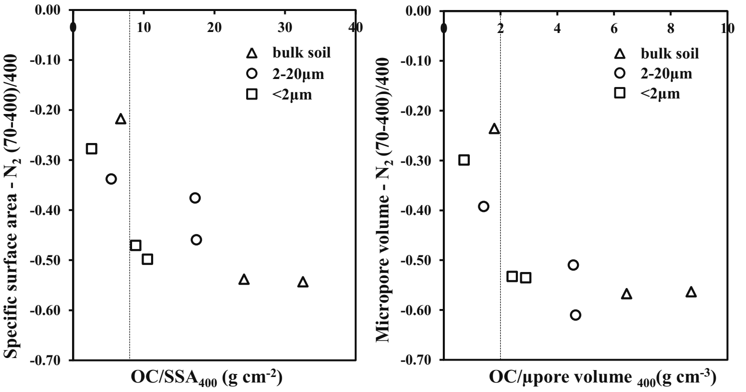

Figure 4.2.3-1

Figure 4.2.3-2

Fig. 4.2.3 a) The correlation between SSA $_{(70\text{-}400)/400}$ (increased mineral SSA) and OC/SSA$_{400}$ (gram OC per cm^{-2} mineral surface), b) The correlation between µpore volume$_{(70\text{-}400)/400}$ (increased mineral µpore volume) and OC/ µpore volume$_{400}$ (gram OC per cm^{-3} mineral volume) in different soil fractions of three soils. △, bulk soil; ○, 2-20µm; □, <2µm.

The results of the sorption analysis of soil samples with N_2 and CO_2 for the speciation of OC forms can be thus resumed as following. The OC strongly associated to mineral surfaces can be indirectly probed by N_2 gas while the presence of free OC is directly probed by CO_2 gas.

In the case of N_2 gas sorption, the classical BET method allows to measuring the accessibility of mineral specific surface area (SSA) on a more rapid way. Indeed, it must be remarked that measured SSA with BET and DR methods give similar SSA results (see table 4.2.3) which support the microporous nature of the mineral surface.

Table 4.2.3 Specific surface area (SSA) of soil fractions and bulk soil sample before and after OC removal

fraction	Selhausen			Rollesbroich			Wüstebach		
	SSA 400°C	SSA 70°C	SSA/DR 400°C	SSA 400°C	SSA 70°C	SSA/DR 400°C	SSA 400°C	SSA 70°C	SSA/DR 400°C
< 2µm (WDC)	86.56	56.72	0.97	66.14	26.77	0.98	86.34	41.72	0.97
2-20 µm	40.08	28.04	0.93	27.78	10.65	0.95	36.10	17.26	0.94
20-2000 µm	7.48	5.66	-	16.82	7.07	-	26.56	8.46	-
bulk	17.30	12.85	0.94	20.12	8.67	0.95	28.60	11.09	0.95

$$(\mathrm{SSA}_{\mathrm{OC-block}})\ \% = \frac{(\mathrm{SSA}_{400°\mathrm{C}} - \mathrm{SSA}_{70°\mathrm{C}})}{\mathrm{SSA}_{400°\mathrm{C}}}\ \% \qquad \text{Eq. (4.2.2)}$$

In Fig. 4.2.4, the blocking effects of OC on the N_2 accessibility to mineral particle size fractions (< 2 µm (WDC)), (2-20 µm) and (bulk soil sample) are also reported with a similar equation (Eq.4.2.2) and lead thus to similar conclusions that in Fig. 4.2.2.

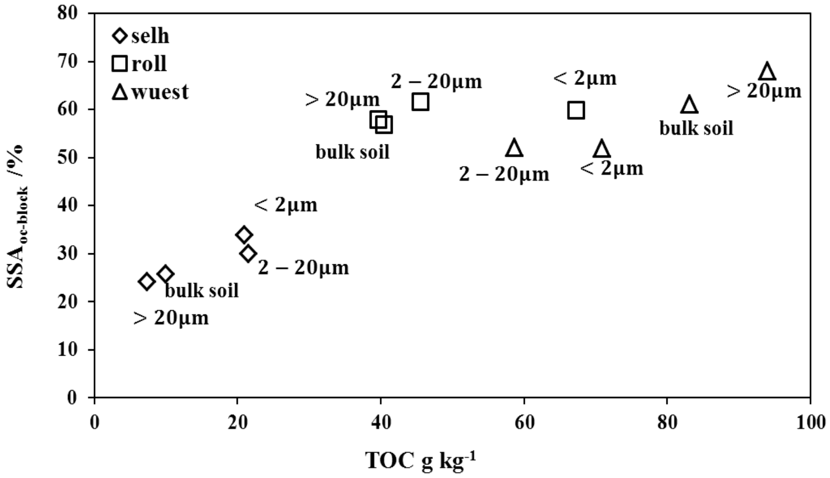

Fig. 4.2.4 The relationship between TOC content and SSA$_{\mathrm{OC-block}}$% in different soil fractions of three soils. ◇, Selh; □, Roll; △,Wüst.

4.2.2 Metal oxide content and surface properties of particle size fractions and bulk soil samples

4.2.2.1 Distribution of different metal oxides in soil fractions and bulk soils

In order to characterize the metal oxide content of particle size fractions and bulk soil samples, two chemical extraction methods have been used. Using the DCB method, extractable M_{DCB} contents are related to both crystalline and amorphous forms of metal oxides (Cornell and Schwertmann, 1996; Kiem and Kögel-Knabner, 2002a) after subtracting the corresponding M_{CB} extracts (Material and methods) or M_{DCB-CB} in Table 4.2.4-1. The content of M_{DCB-CB} decreases along the series (< 2 µm or WDC) > (2-20 µm) > (< 2 mm or bulk soil sample). The mass distributions of Fe, Al, and Si in M_{DCB-CB} are in the range of 88%-91%, 7%-11% and 0.5%-3.8%, respectively. The corresponding molar distributions of Fe, Al and Si in M_{DCB-CB} are in the range of 79%-84%, 13%-20% and 1-7%, respectively, which confirm the main contribution of Fe in the total metal oxide content from particle size fractions and bulk soil samples.

Table 4.2.4-1 Distribution of DCB-extracted metal oxides in the soil fractions

Soil	Fraction	M_{DCB} mg g^{-1}			$Me_{DCB\text{-}CB}$ mg g^{-1}		
		Al	Fe	Si	Al	Fe	Si
Selh	<2 mm	1.07±0.04	11.75±0.48	0.56±0.01	0.89±0.05	11.44±0.48	0.33±0.12
	2-20 µm	2.24±0.06	22.34±1.17	1.19±0.03	1.90±0.06	21.72±1.17	0.94±0.37
	< 2 µm	3.93±0.05	39.47±0.71	1.64±0.03	3.36±0.06	38.56±0.72	1.26±0.05
Roll	<2 mm	3.31±0.10	16.68±0.64	0.33±0.04	1.68±0.10	14.33±0.64	0.13±0.04
	2-20 µm	4.64±0.20	21.35±0.79	0.36±0.02	2.34±0.20	18.73±0.79	0.18±0.03
	< 2 µm	11.73±3.38	56.54±15.10	0.75±0.15	5.04±3.38	41.80±15.1	0.23±0.15
Wüst	<2 mm	5.71±0.22	26.26±1.66	0.79±0.02	1.87±0.21	18.77±1.67	-0.1±0.02
	2-20 µm	6.28±0.28	29.19±1.95	0.54±0.03	2.47±0.41	20.64±2.02	0.05±0.03
	< 2 µm	9.37±1.87	45.12±8.55	0.67±0.14	4.91±1.87	39.89±8.55	0.31±0.16

Using the oxalate method, $Al_{oxalate}$, $Fe_{oxalate}$ and $Si_{oxalate}$ contents are reported in Table 4.2.4-2. The negligible contents of corresponding metals under shaking conditions in water, M_{blank}, are also reported. In comparison to DCB results, lower $Al_{oxalate}$, $Fe_{oxalate}$ and $Si_{oxalate}$ contents in particle size fractions and bulk soils are operationally related to amorphous forms of metal oxides. The content of $M_{oxalate}$ decreases along the series (< 2 µm or WDC) > (2-20 µm) > (< 2 mm or bulk soil sample). The mass distributions of Fe, Al, and Si in $M_{oxalate}$ are in the range of 64%-76%, 20%-35% and 1%-5%, respectively. The corresponding molar distributions of Fe, Al and Si in $M_{oxalate}$ in the range of 46%-62%, 32%-52% and 1-8%, respectively confirm the main contribution of Fe in the amorphous form of metal oxide. However, in comparison with $M_{DCB\text{-}CB}$ results, a much higher contribution of Al can be measured. Indeed, ratios of $M_{oxalate}$ / M_{DCB} in the range 73%-95%, 26%-54% and 14%-54% are calculated for Al, Fe and Si respectively, which indicate that Al is predominantly present in metal oxide particles as amorphous crystalline forms or complexes. It must be also remarked that the distribution of amorphous form of Fe ($Fe_{oxalate}$ /Fe_{DCB}) is obviously higher (~50%) in the forest soil of Wüstebach in comparison with other topsoils. It must be noted that $Fe_{oxalate}$ /Fe_{DCB} of 27-94% have been reported for a large series of agriculture topsoils (Hiemstra et al., 2010b).

Table 4.2.4-2 Distribution of oxalate-extracted metal oxides in the soil fractions

Soil	Fraction	M_{blank} mg g^{-1}			M_{oxalate} mg g^{-1}			$M_{\text{oxalate}}/Me_{\text{DCB}}$ %		
		Al	Fe	Si	Al	Fe	Si	Al	Fe	Si
Selh	<2 mm	0.04	0.03	0.12	0.88±0.03	3.36±0.19	0.21±0.01	82.3	28.6	37.7
	2-20 µm	0.08	0.06	0.21	2.00±0.06	6.86±0.25	0.46±0.02	89.4	30.7	38.6
	< 2 µm	0.03	0.02	0.14	3.74±0.01	11.5±0.05	0.85±0.01	95.1	29.1	51.7
Roll	<2 mm	0.03	0.01	0.04	2.60±0.02	6.43±0.17	0.11±0.01	78.5	38.5	33.5
	2-20 µm	0.02	0.01	0.03	4.13±0.16	7.58±0.17	0.17±0.01	89.1	35.5	47.9
	< 2 µm	0.02	0.03	0.07	8.11±0.05	14.6±0.12	0.33±0.01	69.2	25.7	43.7
Wüst	<2 mm	0.08	0.05	0.04	4.17±0.28	11.9±0.84	0.11±0.01	72.9	45.3	13.9
	2-20 µm	0.07	0.05	0.07	5.25±0.07	15.2±0.08	0.2±0.02	83.6	51.9	37.1
	< 2 µm	0.22	0.17	0.26	8.77±0.14	24.3±0.58	0.36±0.01	93.6	53.9	53.6

4.2.2.2 The effect of metal oxides on SSA in particle fractions and bulk soils

An interesting aspect is the determination of the SSA variations, which accompany the removal of metal oxide particles from particle size fractions and bulk soils samples (Kiem and Kögel-Knabner, 2002b; Kretzschmar et al., 1993; Pronk et al., 2011; Séquaris et al., 2013). In Table 4.2.5, the effects of the two extraction methods (DCB and oxalate) on the mineral SSA of the different soil samples are compared. SSA of different samples, before and after treatments, are compared after OC removal by thermal oxidation. After the extraction of metal oxides with the two methods, lower values of SSA_{DCB} and SSA_{oxalate} confirm the large contributions of metal oxide forms to the mineral surface properties (Eusterhues et al., 2005; Pronk et al., 2011; Trolard et al., 1995).

Table 4.2.5 Contribution of extracted metal oxides to the specific surface area of the soil fractions

Soil	Fraction	Metal oxide$_{\text{DCB400}}$			Metal oxide$_{\text{oxalate400}}$		
		SSA_{CB} m^2 g^{-1}	SSA_{DCB} m^2 g^{-1}	$SSA_{\text{(CB-DCB)/CB}}$ %	SSA_{blank} m^2 g^{-1}	SSA_{oxalate} m^2 g^{-1}	$SSA_{\text{(blank-oxalate)/blank}}$ %
Selh	<2 mm	10.38	6.15	41	18.8	15.81	16
	2-20 µm	35.37	24.94	29	41.58	40.51	3
	< 2 µm	87.67	64.32	27	87.36	83.15	5
Roll	<2 mm	15.84	9.02	43	23.12	15.19	34
	2-20 µm	22.23	11.1	51	30.78	28.42	8
	< 2 µm	49.24	32.12	35	69.7	59.84	14
Wüst	<2 mm	17.05	9.46	45	29.6	19.25	35
	2-20 µm	23.93	13.48	44	37.1	28.55	23
	< 2 µm	66.5	37.24	44	87.34	67.77	22

To specify this contribution in different particle size fractions, the differences ($SSA_{CB\ 400}$- $SSA_{DCB\ 400}$) were used to estimate the contribution of metal oxide content to the total mineral SSA of particle size fractions and bulk soil samples according to the Eq. (4.2.3),

$$SSA_{total\ metal\ oxide}\ contribution(\%) = \frac{(SSA_{CB400} - SSA_{DCB400})}{SSA_{CB400}} \qquad \text{Eq. (4.2.3)}$$

In Table 4.2.5, the ratios of about 41%-44%, in the case of bulk soil samples, indicate a rather constant contribution of metal oxide SSA to the total SSA. In the case of particle size fractions < 2 µm (WDC), an increase of metal oxide SSA contribution was measured along the series Selhausen (27%) < Rollesbroich (35%) < Wüstebach (44%). In Fig. 4.2.5, $SSA_{CB-DCB\ 400}$ of particle size fractions (<2 µm, 2-20µm and bulk soil samples) are plotted against the corresponding content of major iron Fe_{DCB-CB} in metal oxide fraction. A satisfactory linear correlation ($R^2 \geq 0.92$) of the type $SSA_{CB-DCB400} = A + B^* Fe_{DCB-CB}$ exits.

In the same way, the differences $SSA_{blank400}$- $SSA_{oxalate400}$ were used to estimate the contribution of amorphous metal oxide content to the total mineral SSA of particle size fractions and bulk soil samples according to the Eq. (4.2.4),

$$SSA_{amorphous\ metal\ oxide}\ contribution(\%) = \frac{(SSA_{blank400} - SSA_{oxalate400})}{SSA_{blank400}} \qquad \text{Eq. (4.2.4)}$$

In the case of bulk soils, an increase of amorphous metal oxide SSA contribution was measured along the series Selhausen (16%) < Rollesbroich (34%) < Wüstebach (35%). In the case of particle size fractions < 2 µm (WDC), lower SSA contributions are measured which also increase along the series Selhausen (5%) < Rollesbroich (14%) < Wüstebach (22%).

It must be noted that a similar clay fraction content of about 20% with illite as dominant clay mineral characterizes the three investigated topsoils (Table 3.1.1 and Table 3.2.1). It allows discussing the metal oxide effects in the topsoils under comparable clay fractions conditions. Taking the content of major extractable Fe_{DCB-CB} or $Fe_{oxalate}$ of WDC for scaling the metal oxides in the clay fraction, it can be simply calculated that the measured content of metal oxide in the bulk topsoils is larger of a factor 1.6, 1.9 and 2.3 in Selhausen, Rollesbroich and Wüstebach bulk topsoils, respectively. This confirms a large distribution of metal oxide outside the clay fraction which also explains the higher SSA contribution of metal oxide in bulk soil than in WDC. It must be remarked that in the case of large surface contacts between amorphous metal oxide-clay minerals, some underestimation of the SSA contribution of metal oxide can be made by using a simple additive law (Pronk et al., 2011). In the case of particle size fractions < 2 µm (WDC), the OM adsorption as organo-mineral complexes is mainly due to a direct interaction with amorphous and crystalline metal oxide surfaces (Mikutta et al., 2006). This can be evidenced in Tables 4.2.5 and Table 3.2.1 by the parallel increases of the metal oxide SSA contribution along the series Selhausen (27%) < Rollesbroich (35%) < Wüstebach (44%) and the TOC content in WDC which also increases along the series Selhausen (21 g kg^{-1}) < Rollesbroich (67 g kg^{-1}) < Wüstebach (71 g kg^{-1}).

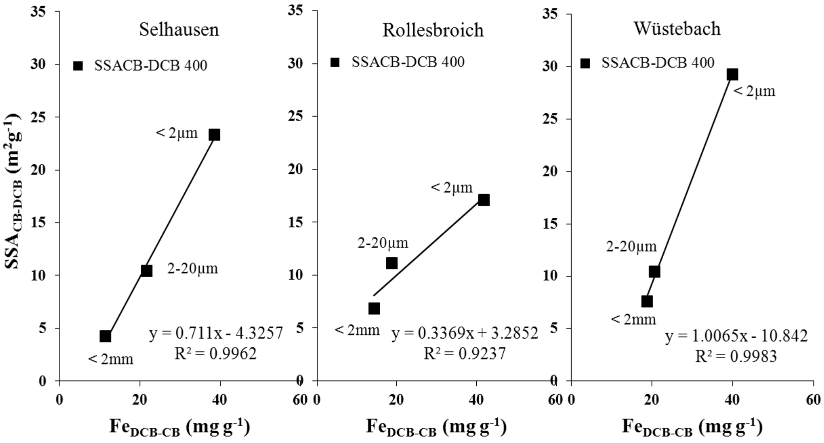

Fig. 4.2.5 The correlation between SSA$_{CB-DCB\ 400}$ (increased mineral SSA) and Fe$_{DCB-CB}$ (iron oxide content) in different particle size fractions in different soils. ■, increased SSA due to metal oxides.

4.2.2.3 Estimation of SSA and particle size of extracted metal oxide from WDC samples

In the case of the particle size fraction < 2 µm (WDC), the SSA of extracted metal oxide by considering a simple additive law for the SSA contributions of metal oxide particles and WDC residues after dithionite dissolution (SSA_{DCB400}) to the mineral surface of WDC (SSA_{CB400}) was estimated as in Eq. (4.2.5),

$$SSA_{CB-DCB} = \frac{SSA_{CB}-(1-W)SSA_{DCB}}{W} \tag*{Eq. (4.2.5)}$$

where SSA_{DCB} is assigned to the aluminosilicate content of WDC and w is the weight fraction of released metal oxide particles from WDC.

Table 4.2.6 Characterization of metal oxides nanoparticles in soil WDCs

	pH	mass $_{(DCB-CB)}$ /%	w /g g^{-1}	SSA$_{\text{metal oxide}}$ /m^2 g^{-1}	d$_p$ /nm
Selh	7.4	8.42±0.97	0.084±0.009	342	5
Roll	6.6	9.28±0.51	0.093±0.005	217	8
Wüst	4.5	7.64±1.61	0.076±0.016	420	4

In Table 4.2.6, specific surface area values between 217-420 m^{2}g^{-1} are found which are typical for iron oxide nanoparticles such as ferrihydrite (Cornell and Schwertmann, 2003). SSA_{DCB} values in the range of 32-64 m^{2}g^{-1} (Table 4.2.5) are also typical for illite (Kaiser and Guggenberger, 2003), the major aluminosilicate in topsoils. In the case of particles with a spherical shape, the specific surface area per particle mass (SSA) is given by

$$SSA = \frac{4\pi r_p^2}{\frac{4}{3}\pi r_p^3 \sigma} = \frac{3}{r_p \sigma} \qquad \text{Eq. (4.2.6)}$$

where r_p is the particle radius and σ the particle density. It follows that the average mean diameter (d_p) of metal oxide particles (nm) is given by

$$d_p = \frac{6000}{SSA\sigma} \qquad \text{Eq. (4.2.7)}$$

with SSA (m^2 g^{-1}) and density σ (g cm^{-3}). An average σ of about 3.6 g cm^{-3} was chosen for the extracted metal oxide particles mixture. d_{np} values between 4-8 nm were calculated for the metal oxide nanoparticles (Table 4.2.6). Similar particle sizes of metal oxides in the range from 1 nm to 10 nm have been reported after DCB extraction of agricultural topsoils by Tjisee et al (Hiemstra et al., 2010b) and of haplic podzol soils by (Eusterhues et al., 2005).

In the case of the deposition of isolated nanoparticles on aluminosilicate particles in WDC, the surface loading due to nanoparticles can be also estimated if considering the projected circular surface area from spherical nanoparticles (πR^2_{np}). Thus, the surface loading ratio (θ) is given by

$$\theta = \frac{N_{np}\pi R_{np}^2}{SSA_{DCB}} \qquad \text{Eq. (4.2.8)}$$

where N_{np} is the number of released nanoparticles per g of WDC and SSA_{DCB} is the specific surface area of aluminosilicate component (m^{2}g^{-1}). N_{np} can be calculated from

$$N_{np} = \frac{w}{\frac{4}{3}\pi R_{np}^{3}\sigma} \qquad \text{Eq. (4.2.9)}$$

where w is the mass (g) of released metal oxide per g of WDC. It follows from Eq. (4.2.8) and Eq. (4.2.9) that

$$\theta = \frac{3w}{4R_{np}\sigma SSA_{DCB}} \qquad \text{Eq. (4.2.10)}$$

θ in percent (%) can be calculated by

$$\theta_{(\%)} = \frac{3*10^{5}w}{4R_{np}\sigma SSA_{DCB}} \qquad \text{Eq. (4.2.11)}$$

with SSA_{DCB} ($\mathrm{m}^2\ \mathrm{g}^{-1}$), w ($\mathrm{g}\ \mathrm{g}^{-1}$), R_{np} (nm) and (σ) of about 3.6 $\mathrm{g\ cm}^{-3}$ for the extracted metal oxide particles mixture. In the case of deposited single metal oxide nanoparticles, an increase along a series Selhausen (11%) < Rollesbroich (16%) < Wüstebach (22%) was estimated for an optimal surface loading. At low pH, the WDC in acidic forest soil has thus the largest surface loading of metal oxide which is favored by the precipitation of metal oxides carrying sufficient positive charge at negatively charged clay surface.

4.2.3 Substructural study on the effect of metal oxide in particle size fraction < 2 µm (WDC)

The major sequestration of OM in particle size fraction < 2 µm (WDC) is controlled by the accessibility to the mineral porous matrix forming by metal oxide and aluminosilicate particles. In the case of WDC, the combination of the two independent SAXS and N_2 gas sorption methods has been used to establish relationships between the both methods and getting complementary information on the porous structure.

4.2.3.1 Application of SAXS and N_2 gas sorption method for the pore size investigation of WDC (Effect of metal oxide particles and OC contents)

After the removal of OM, the effects of metal oxide nanoparticles in the pore structure of WDC have been investigated with SAXS. In Fig. 4.2.6, SAXS results of WDC samples from Wüstebach topsoil before (CB400) and after (DCB400) extractions of metal oxides are compared. The SAXS data are plotted as the scattered intensity I (q) versus the scattering vector ($q = (4\ \pi/\lambda)\ \sin\theta$).

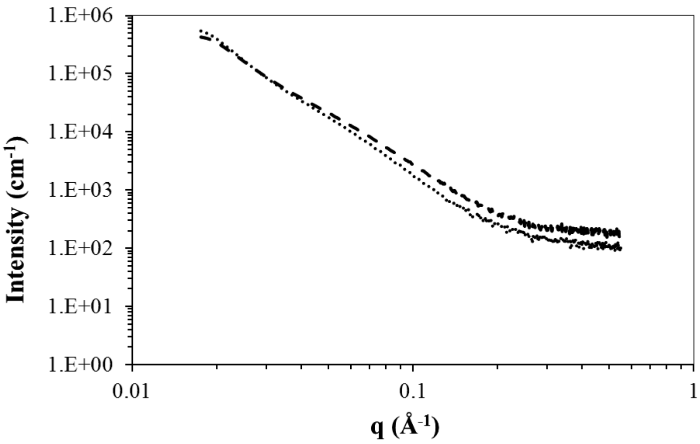

Fig. 4.2.6 SAXS scattering curves of WDC samples from Wüstebach topsoil after CB and DCB treatments following by the thermal oxidation of OM. ······,Wüst WDC_{DCB400}; ----, Wüst WDC_{CB400}.

In Fig. 4.2.7, the Guinier plot was applied when q is small in the range of q: 0.017-0.027 $Å^{-1}$ *i.e* in limited interval range of distance d =2*π/q of 369 -233 Å. The linear fitting of ln I_q against q^2 ($r^2 < 0.999$) gives the gyration radius R_g according to Eq. (2.3.5). In the case of solid sample, R_g can be associated to surface heterogeneities such pore and holes cavities (Glatter and Kratky, 1982) and have been thus used to analyse pore structures (Dubinin et al., 1964; Fukuyama et al., 2001).

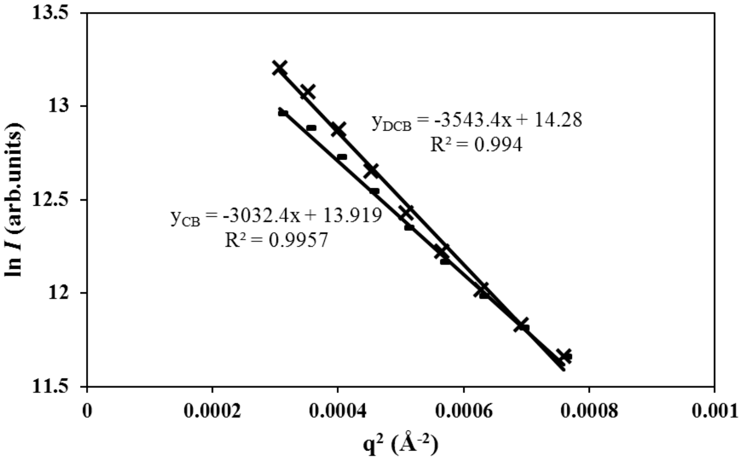

Fig. 4.2.7 Guinier plots of the SAXS data for WDC samples from Wüstebach topsoil. See other conditions in Fig. 4.2.6. □, WDC_{DCB400}; ×, WDC_{CB400}.

R_g results of WDC_{CB400} and WDC_{DCB400} from the three topsoils are shown in Table 4.2.7. R_g values of about 100 Å (10 nm) were calculated in a Guinier region $1 < qR_g < 3$. Systematic higher values of R_g of WDC_{DCB400} accompany the dissolution of metal oxide content with DCB.

Table 4.2.7 Pore structure characteristics (total pore volume, R_g, k) and colloidal properties (d_z , ζ-potential) of WDC samples measured with N_2 gas sorption, SAXS and DLS methods

Sample name	N_2 adsorption Total pore volume (cm^3g^{-1})	SAXS				DLS		
		R_g (Å)	r^2 for Rg	k	r^2 for k	pH	d_z (nm)	ζ (mV)
Selh WDC_{CB400}	3.08E-01	92.9±1.3	0.9945	2.57±0.02	0.9852	7.13	542±11	-28.9±0.4
Selh WDC_{DCB400}	2.72E-01	96.2±1.2	0.9956	2.92±0.03	0.9861	6.91	639±1	-29.6±0.4
Roll WDC_{CB400}	3.28E-01	101.0±1.3	0.9951	2.82±0.02	0.9924	7.10	721±30	-26.9±0.7
Roll WDC_{DCB400}	3.65E-01	106.7±1.5	0.9945	3.08±0.02	0.9923	6.89	769±19	-28.1±0.1
Wüst WDC_{CB400}	3.08E-01	95.4±1.2	0.9957	2.72±0.02	0.9930	7.26	715±28	-26.9±0.0
Wüst WDC_{DCB400}	2.72E-01	103.1±1.5	0.994	2.87±0.02	0.9857	7.17	802±11	-32.5±0.8

In the case of an aggregate structure for the freeze-dried particle size fraction < 2 µm (WDC), it can be assumed that the $R_{g\ DCB}$ increase supports some enlargement of the porous structure. The validity of the Guinier approximation to $qR_g < 3$ would indicate that an ellipsoidal pore shape is more appropriate than spherical or cylindrical pore shapes (Glatter and May, 2006). The presence of metal oxide nanoparticles would thus induce some aggregation in WDC with a contraction of pores radius. Using SAXS, Dékány et al also found an increase of the porosity in sepiolites after the removal of iron and aluminium by an acidic treatment (Dékány et al., 1999).

Characteristic data, SSA and total pore volume (V_p) obtained with the N_2 sorption isotherms, are reported in Table 4.2.7 for WDC_{DCB400} and $WDC_{CB400.}$ As already discussed, SSA results indicate sensitive variations due to the metal oxide extraction. The total pore volume (V_p) of all pores radius up to 1800 Å, determined at a P/P_0 of 0.995, is also sensitive to the DCB treatment. According to the Gurvich´s rule (Lowell et al., 2004), the N_2 sorption results have been used for calculating average pore radius (R_p) in Table 4.2.7 with the following equation:

$$R_P = 2\ V_p / SSA \qquad \text{Eq. (4.2.12)}$$

In Fig. 4.2.8, calculated R_g (SAXS) (Eq. (2.3.5)) and R_p (N_2 gas sorption method) (Eq. (4.2.12)) are reported for WDC_{CB400} and $WDC_{DCB\ 400}$ samples. Fairly good linear correlations ($r^2 \geq 0.93$) between the results exist for WDC_{CB400} ($r^2 = 0.93$) and WDC_{DCB400} ($r^2 = 0.97$) which support a SAXS detection of the porous structure in the mesopore range (2-50 nm). The r_p decrease in WDC_{CB400} thus confirms with the N_2 sorption method lower pore sizes before the metal oxide extraction. Absolute pore size, r_p and r_g, differences can be related to the detection limit and calculation with SAXS and N_2 sorption methods. However, the pore size ratios between WDC_{DCB400} and $WDC_{CB400,}$ in Table 4.2.8 indicate more large variations in the case of the N_2 sorption than with SAXS method, $R_{gDCB400}/R_{gCB400} < R_{pDCB400}/R_{pCB400}$' which require some explanations. Indeed, closed and open pores or total pores are examined by the SAXS method while the N_2 gas sorption method is restricted to the accessible open pores. This selective detection by N_2 gas sorption is demonstrated when the presence of OC in WDC is considered. In Table 4.2.9 and Fig. 4.2.8, the calculated pore parameters, R_g and R_p for WDC_{CB70} are reported. A linear correlation ($r^2 = 0.99$) between R_g and R_p values is satisfactorily confirmed. In comparison with WDC_{CB400}, after thermal oxidation of OC, SAXS and N_2 gas sorption methods give different results for the OC effect on the R_g and R_p determination. In the case of SAXS results, the presence of OC does not interfere in the R_g determination. The corresponding WDC_{CB70} and WDC_{CB400} values are lying in the range of error deviation as also shown by their ratio values $R_{gCB70}/R_{gCB400} = 1$ in Table 4.2.8.

It also confirms by this way that the thermal oxidation treatment has no sensitive effect on the total porous structure of the mineral matrix (Mayer et al., 2004). Mayer et al also conclude from SAXS results that mesopore sizes are mainly controlled by mineral interparticles contacts. On the contrary, in the case of N_2 gas adsorption method, R_p results indicate large differences between WDC_{CB70} and WDC_{CB400} which are due to the presence of OC. Indeed, the accessibility of N_2 gas to open pores is hindered by a blocking effect of OC. It may result in a shift in the distribution of detected open pores with N_2 gas to largest one in WDC_{CB70} as shown by the ratios $R_{pCB70}/R_{pCB400} > 1$. In the case of WDC_{DCB400} and WDC_{CB400}, it can be also assumed from $R_{gDCB400}/R_{gCB400} < R_{pDCB400}/R_{pCB400}$ (Table 4.2.8) that a preferential presence and removal of metal oxide nanoparticles existed in accessible open mesopores which are mainly formed by the arrangement of much larger phyllosilicate particles due to dominant clay mineral illite in WDC (Table 3.2.1). Linear functions ($r^2 = 0.99$) of the type 1/SSA = A + B (R_g) were found between R_g and SSA^{-1} for WDC_{CB} and WDC_{DCB} samples (Table 4.2.8) from three soils. Środoń et al. (Środoń et al., 1992) have established, using electron microscopic measurements, a direct relationship between the mean particle thickness (*T*) and the inverse of total surface area (*1/SSA*) in the case of illite clay minerals. A simultaneous increase of mesopore structure dimension in the clay microfabric, R_g and mean particle thickness *T*, (*1/SSA*) can thus be probed along the soil series Selhausen < Wüstebach < Rollesbroich.

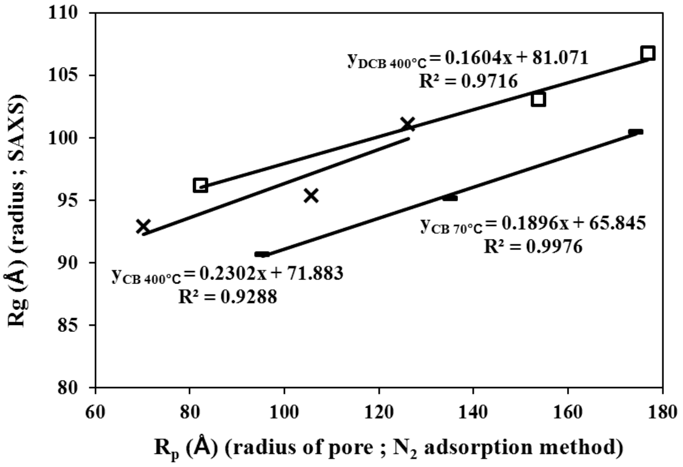

Fig. 4.2.8 Relationship between R_g and R_p for WDC samples from three soils. □, WDC_{DCB400}; ─, WDC_{CB70}; ×, WDC_{CB400}.

Table 4.2.8 R_g and R_p data of WDC_{CB400} and WDC_{DCB400} from topsoils

	Sample	$R_{g\,(SAXS)}$ Å	$R_{gDCB400}/R_{gCB400}$	*SSA* m^2/g	Total V_{pore} cm^3/g	$R_{p\,(N2)}$ Å	$R_{pDCB400}/R_{pCB400}$
Selh	WDC_{CB400}	92.9±1.3	1.03±0.03	87.67	0.31	70.2	1.17
	WDC_{DCB400}	96.2±1.2		64.32	0.27	82.3	
Rolh	WDC_{CB400}	101.0±1.3	1.06±0.03	49.24	0.33	126.2	1.40
	WDC_{DCB400}	106.7±1.5		32.12	0.37	176.8	
Wüst	WDC_{CB400}	95.4±1.2	1.08±0.03	66.50	0.31	105.6	1.46
	WDC_{DCB400}	103.1±1.5		37.24	0.27	153.8	

Table 4.2.9 R_g and R_p data of WDC_{CB70} and WDC_{CB400} from topsoils

	Sample	$R_{g\ (SAXS)}$ Å	R_{gCB70}/R_{gCB400}	*SSA* m^2/g	Total V_{pore} cm^3/g	$R_{p\ (N2)}$ Å	R_{pCB70}/R_{pCB400}
Selh	WDC_{CB}	90.7±1.7	0.98±0.03	58.10	0.23	95.3	1.36
	WDC_{CB}	92.9±1.3		87.67	0.31	70.2	
Rolh	WDC_{CB}	100.5±2.	0.99±0.03	25.09	0.19	174.3	1.38
	WDC_{CB}	101.0±1.		49.24	0.33	126.2	
Wüst	WDC_{CB}	95.2±2.1	1.00±0.03	36.57	0.21	135.1	1.28
	WDC_{CB}	95.4±1.2		66.50	0.31	105.6	

4.2.3.2 Effect of metal oxides on mass fractal of WDC measured with SAXS

The power-law scattering of SAXS results in a large range of q**:** 0.040-0.25 Å^{-1} (d =2*π/q of 25-369 Å) has been considered for determining the effect of metal oxides on the mass fractal of WDC with Eq. (2.3.6)**.** The logarithmic form of the power-law scattering relation gives the exponent k (Fig. 4.2.9)

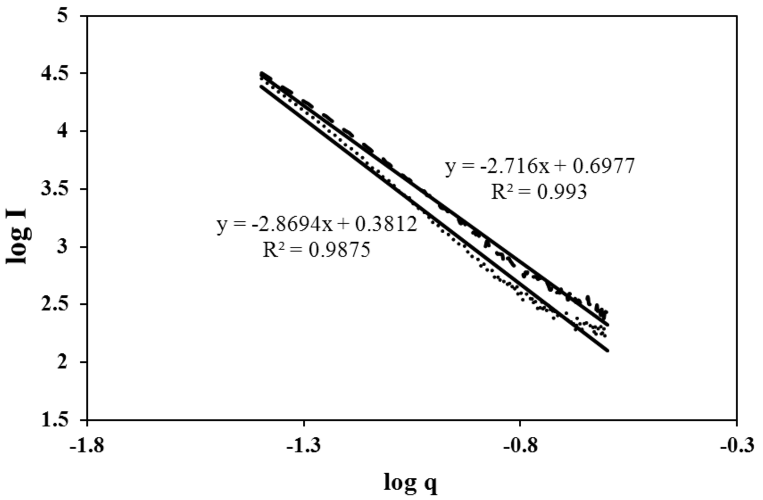

Fig. 4.2.9 The double logarithmic plot between the scattering intensity I(q) and the magnitude of scattering vector q of WDC samples from Wüstebach topsoil after CB and DCB treatments following by the thermal oxidation of OM.······,Wüst WDC_{DCB400}; ---, Wüst WDC_{CB400}.

In Table 4.2.7, k values < 4 are calculated which indicate that conditions for a randomly oriented extended scatterer with uniform electron density and a smooth boundary surface (k = 4 for inhomogeneities with smooth separating surfaces) are not fulfilled with WDC samples. However, in a general way, higher k values or mass fractal dimensions D_m are found with compact structure of aggregates. According to the preceding results which relate *I*(*q*) to the porous structure, the power-law scattering intensity can be interpreted in terms of pore fractal by interchanging the pore space and mass (Schmidt, 1991). The fractal pore system can be considered as the “negative” of the mass fractal from the aggregate solid structure. Higher *k* values in the case of WDC_{DCB400} would thus suppose a fractal contribution of larger pore space due to pore “aggregation” or “fusion” in a more loose aggregate solid structure of WDC samples without nanoparticles. On the contrary, lower *k* values in the case of WDC_{CB400} would indicate a fractal contribution of dispersed small spore space in a more compact aggregate solid structure of WDC samples in the presence of nanoparticles. It can be noted that similar to r_g, *k* values of Rollesbroich soil are higher than Wüstebach and Selhausen soils which will be further discussed. Dékány et al. (Dékány et al., 1999) have found that mass fractal dimension D_m with SAXS can reveal the internal porosities in sepiolite minerals. A decrease of D_m (related to the increasing pore fractal in this study) when extracting Al and Fe ions with acid treatment which resulted in increasing the porosity of the mineral, is in good agreement with the results of this work.

4.2.3.3 Contribution of metal oxide nanoparticles to the colloidal properties of mineral WDC

The colloidal properties of WDC_{CB400} and WDC_{DCB400} have been investigated after dispersion of freeze-dried mineral WDC in water (0.4 g l^{-1}) by dynamic light scattering and microelectrophoresis methods. In Table 4.2.7, respective hydrodynamic diameter *(d_z)* and zeta potential (ζ) values at pH of about 7 ± 0.2 are reported. In the case of WDC_{DCB400} samples, ζ values become more negative after the release of positively charged metal oxide particles. Metal oxide particles containing Fe and Al have generally points of zero charge of about pH 7-9 (Benjamin et al., 1996; Goldberg and Glaubig, 1987; Parks and Bruyn, 1962; Tombácz and Szekeres, 2001). The permanent negative charge of remaining aluminosilicate, as in the case of illite clay minerals (Jiang et al., 2012), determines the microelectrophoretic properties of WDC_{DCB400}. It is interesting to note a parallel increase of d_z values for WDC_{DCB400} samples, which also supports, in comparison to $WDC_{CB400,}$ some expansion of aggregate size due to some electrostatic repulsion between negatively charged aluminosilicate residues. These colloidal results, obtained at a µm scale, can be thus directly related to the R_g (SAXS), *k* (SAXS), R_p (N_2 gas sorption) results which also demonstrate, at a nm scale, a corresponding increase of the porous mineral matrix structure for WDC after the removal of metal oxide nanoparticles. Systematic higher values for D_z, R_g, R_p and *k* (Tables 4.2.7 and 4.2.8) are generally found with Rollesbroich WDC, which can be related to the mineralogical composition of the soil fraction < 2 μm. Indeed, higher kaolinite content (Table 3.2.1) characterizes this soil was also detected by FTIR. The contribution of its typical lower SSA (Manning and Goldberg, 1996) can be also detected in the SSA of Rollesbroich WDC (Table 4.2.5). It can be assumed that the introduction of kaolinite particles of lower aspect ratios (Manning and Goldberg, 1996) creates, in WDC aggregates, large pores in the arrangement of dominant illite particles of higher aspect ratios. It is interesting to note that the calculated d_p (8 nm) for metal oxide particles from Rollesbroich soil (Table 4.2.6) is larger which also supports the low steric hindrance for their formation and deposition in larger accessible mesopore (r_p of 18 nm).

4.2.4 Conclusion

In the investigated topsoils of the three TERENO test sites at Selhausen (arable soil), Rollesbroich (grassland soil) and Wüstebach (forest soil), iron oxide is the major metal oxide in different soil fractions and bulk soil. The mass distributions of Fe_{DCB-CB} are in the range of 88%-91% in the total DCB extracted crystalline and amorphous forms of metal oxides (M_{DCB-CB}). In the case of oxalate extracted metal oxides ($M_{oxalate}$), the predominant amorphous form is found with metal oxide containing aluminum ($Al_{oxalate}$ 70%-95%) in comparison with metal oxide containing iron ($Fe_{oxalate}$ 26%-54%). Considering the total crystalline and amorphous forms of iron oxide, the distribution of amorphous forms of metal oxide expressed by $Fe_{oxalate}$/ Fe_{DCB} is in the range of 14%-54% where the distribution of the amorphous iron oxide form is at the highest (54%) in the forest soil of Wüstebach. The SSA variations expressed in (SSA_{CB400}- SSA_{DCB400})/$SSA_{DCB\ 400}$ are used to estimate the contribution of metal oxide content to the total mineral SSA of particle size fractions and bulk soil samples. In bulk soils the SSA contribution (41%-44%) is rather constant while in the case of WDC, an increase of metal oxide SSA contribution is measured along the series Selhausen (27%) < Rollesbroich (35%) < Wüstebach (44%). There is a good linear correlation between released $SSA_{CB-DCB400}$ and the Fe_{DCB-CB} content. The SSA contribution of amorphous metal oxide forms in bulk soils (16%-35%) is higher than in the case of WDC (5%-22%) which is also an indication for a distribution of metal oxide outside the clay fraction. In the case of WDC, SSA of 217-420 m^2g^{-1} and nanoparticle sizes of 4-8 nm are found for the total extracted metal oxide. The calculated deposition of single metal oxide nanoparticles to the surface of aluminosilicate residues varies along a series of Selhausen (11%) < Rollesbroich (16%) < Wüstebach (22%).

This study shows that the combination of the N_2 gas sorption and SAXS methods enables the characterisation soil porosity in the mesopore range. Fairly good linear correlations (r^2~0.93-0.99) can be firstly established between R_g from Guinier plots (SAXS) and R_p according to the Gurvich´s rule (N_2 gas sorption) A decrease of pore dimensions R_g and R_p ,in the nm range, implies a contraction of the WDC pore structure in the presence of metal oxide nanoparticles. Higher relative R_p variations between WDC_{CB400} and WDC_{DCB400} samples, $R_{pDCB400}/R_{pCB400}$, than in the case of R_g results suppose that only a fraction of total pores, accessible open pores to N_2 gas sorption, are preferentially modified by the presence of metal oxide nanoparticles. This can be exemplified by the WDC_{CB70} results which show that $R_{p,}$ in contrast to R_g, depend on the blocking effect of the OC content in open pores. The double logarithmic plots of the power-law scattering of SAXS $I(q)$ against q can be variously interpreted. A mass fractal contribution of larger pore space in a more loose aggregate structure of WDC samples would characterize WDC samples without nanoparticles. In the presence of nanoparticles, the fractal results can be associated to a contribution of dispersed small spore space in a more compact aggregate structure of WDC sample. The colloidal characterization of WDC from the three topsoils with DLS and microelectrophoretic methods also indicate, in a µm range, that the DCB treatment increases the particle size. An increase of surface negative ζ-potential values may explain some expansion of the aggregate structure by the release of positively charged metal oxide nanoparticles. It can be concluded that the presence of metal oxides (crystalline and amorphous) increases the surface area of the soil and renders the mesopore structure of the mineral matrix more compact. The comparison of R_g, R_p, k, d_z and d_p results between soils indicate some dependence on the clay mineralogy of WDC. It can be assumed that a higher content of kaolinite in the investigated grassland topsoil increases the mesopore size in clay microfabric mainly formed by illite clay minerals.

4.3 Temperature effect on the sedimentation and aggregation behaviour of WDCs

4.3.1 The temperature effect on the soil particle size fractionation

4.3.1.1 The temperature effect on the particle size distributions after the soil particle size fractionation

The effects of temperature on the whole soil particle size fractionation procedure (chapter 3.2.1) were investigated, which thus includes the temperature effects on the WDC release during the shaking and the sedimentation steps.

Table 4.3.1 Soil particle size fraction distribution under different fractionation temperature conditions

Soils	T/ °C	WDC g kg^{-1}	2-20 µm / g kg^{-1}	20-2000 µm/ g kg^{-1}
Selh	7	84.0±1.7	270.5±6.9	635.0±8.4
	15	81.2±1.7	246.1±8.0	666.0±5.4
	23	80.8±2.0	275.6±1.8	631.5±0.4
	35	71.0±1.2	310.5±6.3	601.1±7.0
Roll	7	44.6±1.8	325.0±21.8	592.2±26.6
	15	47.0±0.5	402.7±20.7	517.7±16.5
	23	41.4±1.5	379.0±15.5	543.1±11.2
	35	37.4±1.4	322.9±16.5	592.3±19.7
Wüst	7	47.5±2.4	431.7±54.8	494.5±48.8
	15	40.4±1.2	452.5±28.7	484.1±28.7
	23	40.8±1.3	501.1±11.9	433.2±15.8
	35	33.4±0.5	504.4±84.8	437.6±70.6

Table.4.3.1 shows the WDC distributions in three soils after fractionation under different temperature conditions. The mass of released WDC decreases along the series Selhausen > Rollesbroich ≥ Wüstebach while the clay content of the three soils is about 20% (Table 3.1.1). In the last both soils, it can be assume that high TOC contents (Table 4.2.1) stabilize the soil texture, which avoid small size particles to be easily washed away (Chapter 4.4) from the soil aggregates (Kjaergaard et al., 2004a; Tombácz et al., 2004).

In the Fig. 4.3.1, the cumulative fraction *F* (°C) (Eq. 4.3.1) is plotted in the function of the temperature,

$$F(°C) = \frac{M_T}{M_\infty} \qquad \text{Eq. (4.3.1)}$$

where M_T is the cumulative mass of WDC after the fractionation procedure (6 hours shaking, 12 hours sedimentation) at different temperatures and M_∞ is the total mass of WDC that can be mobilized from clay aggregates or deposits, which has been defined as the total clay (TC) fraction in soil. F(°C) decreased when the temperature increased: linear relationships (R^2_{Selh}= 0.8756; R^2_{Roll}=0.9975; $R^2_{Wüst}$=0.9044) were calculated.

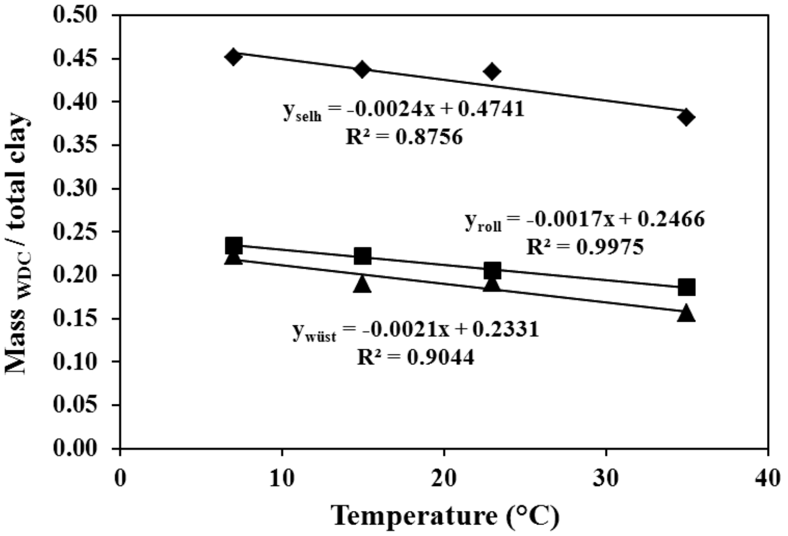

Fig. 4.3.1 Cumulative fraction F(°C) of WDC from soil clay contents in the function of the applied temperature during the whole soil particle size fractionation procedure. ◆, Selhausen; ■, Rollesbroich; ▲, Wüstebach; ─, linear fitting.

The fractionation results indicate a low decrease of the gained WDC mass (stable in the dispersion after sedimentation) when the applied temperature increases, which is apparently in contradiction with an awaited increase of the WDC release from bulk soil samples by increasing the thermal energy. Lavee et al. (Lavee et al., 1996) found that the temperature can affect the soil aggregate stability dynamics and when temperature increases, the aggregate stability decreases in the seasonal scale. Indeed, this temperature effect must be distinguished from the sedimentation process on the WDC mobilization during the shaking process. It follows that a decrease of WDC amount against the temperature can be due to a more rapid sedimentation of WDC at higher temperatures which overshadows the effect of the temperature on the WDC mobilization from soil. These operational conditions for the detection of released WDC have been investigated in the case of Selhausen soil.

4.3.1.2 Temperature effect on the physic-chemical properties of the colloidal soil particle size fraction

Table 4.3.2 The chemical properties of the colloidal phase (WDC and electrolyte phase) after the soil particle size fractionation under different temperature conditions

	T	WDC		Electrolyte phase				
	°C	TOC %	TN %	pH	DOC $mgkg^{-1}$	Ca mM	Mg mM	Na mM
Selh	7	2.15±0.15	0.38±0.03	6.81±0.08	5.53	0.315	0.038	0.048
	15	2.26±0.01	0.37±0.01	6.96±0.02	5.88	0.337	0.038	0.050
	23	2.25±0.05	0.36±0.02	7.33±0.04	5.88	0.366	0.040	0.052
	35	2.09±0.09	0.38±0.03	7.24±0.08	7.93	0.382	0.043	0.054
Roll	7	7.03±0.29	0.86±0.02	6.14±0.03	26.47	0.062	0.031	0.073
	15	6.95±0.40	0.88±0.02	6.61±0.05	23.33	0.064	0.031	0.074
	23	6.92±0.11	0.66±0.02	6.53±0.05	23.06	0.065	0.031	0.078
	35	7.35±0.13	0.62±0.00	7.00±0.06	36.36	0.090	0.042	0.088
Wüst	7	7.11±0.17	0.79±0.00	4.84±0.65	30.74	0.011	0.029	0.030
	15	7.23±0.25	0.8±0.02	4.48±0.04	28.10	0.010	0.027	0.031
	23	7.29±0.20	0.8±0.01	4.48±0.04	27.08	0.015	0.025	0.033
	35	7.74±0.06	0.83±0.01	4.49±0.04	32.38	0.008	0.018	0.033

The chemical properties in Table 4.3.2 concern the chemical properties of the separated WDC from the soil particle size fractionation and the remaining electrolyte phase after 90 minutes of centrifugation. The TOC and TN contents of gained freeze-dried WDC after soil particle size fractionation at the different temperatures were rather constant. However, some increases of DOC, Ca^{2+}, Mg^{2+} and Na^{+} concentrations were observed along the temperature. A solubility increase of corresponding salts in soil water at higher temperature can be evoked which is also related to a pH increase in the case of Selhausen and Rollesbroich electrolyte phases. In comparison, the effects of temperature on the chemical properties of the electrolyte phase are rather weak in the case of acidic Wüstebach soils.

4.3.1.3 Characterization of WDC hydrodynamic particle size and zeta potential in the colloidal phase after the soil particle size fractionation at different temperatures

The measured hydrodynamic particle sizes with PCS of WDC in the colloidal phase after soil particle size fractionation at different temperatures were plotted in Fig.4.3.2. For all soil WDC particles, a size decrease with the increase of the fractionation temperature. This can be correlated to the effect of temperature on the sedimentation velocity and the distribution of particle size during the sedimentation step.

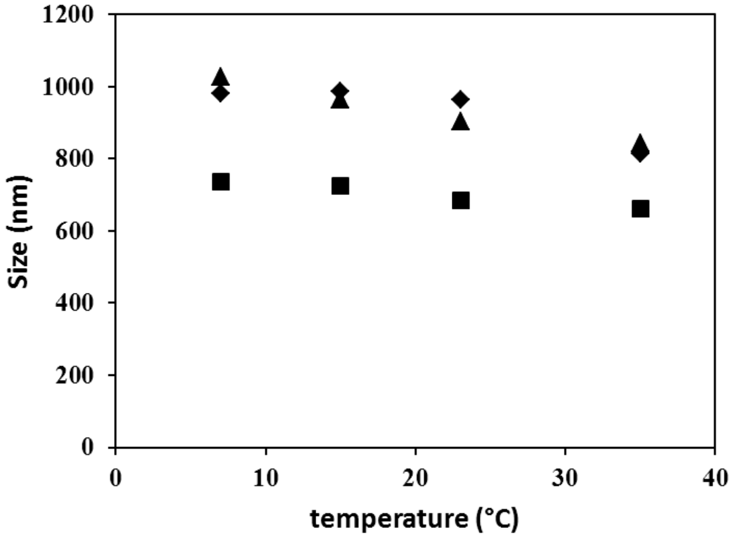

Fig. 4.3.2 Temperature effect on the WDC size after fraction. ◆, Roll; ■, Selh;▲,Wüst.

Indeed, it can generally assume that large WDC particles are quickly removed from the suspension by gravity force. This can be accelerated by a decrease of the water viscosity at higher temperatures. It follows that a shift takes place in the distribution of particle size to small particle sizes after sedimentation at higher temperatures. This can be confirmed by the specific surface area (SSA) of the mineral WDC particles after the removal of OC at 400 °C. An increase of SSA when the fractionation temperature increases, also indicates a decrease of the WDC particles size.

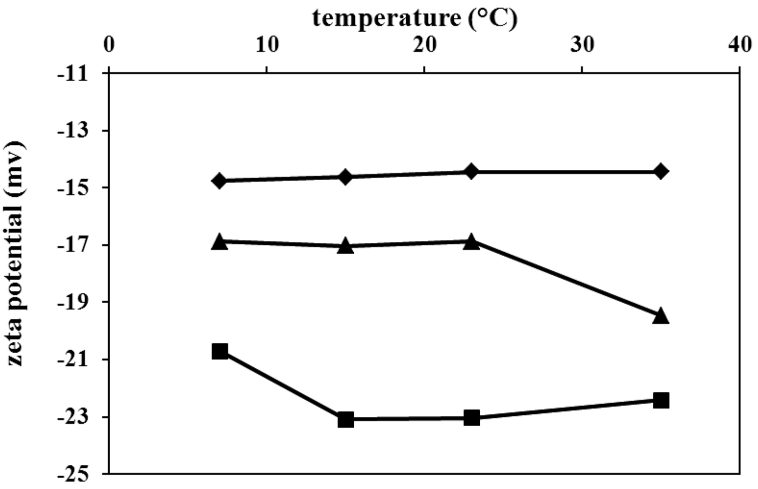

Fig. 4.3.3 Temperature effect on the WDC zeta potential. ◆, Selh; ■, Roll;▲,Wüst.

The temperature effect on the zeta potential of WDC in the colloidal phase was recorded in Fig. 4.3.3. The results indicate that there is no sensitive effect on the zeta potential values (standard error, ± 5 mV) of the colloid dispersion after fractionation at the different temperatures. Negative zeta potential values in the range of from -24 mV to -12 mV for the three soils are typical (Kim et al., 2009) of negatively charged soil particles under the soil electrolyte conditions in Table 4.3.2 .

4.3.2 Effect of the temperature on the WDC velocity during the sedimentation step

The sedimentation of WDC dispersion (stable WDC dispersion gaining at room temperature after 16 hours of sedimentation) were conducted along the increasing time (1-12 h) at two temperatures 7°C and 35°C, in order to detect the temperature effect on the colloid dispersion stability. The sedimented WDC mass was calculated from the loss of the initial concentration in the aqueous phase (concentration, 8.26 mg mL^{-1}; volume, 25 ml) at different times. The results in Fig. 4.3.4 thus show an increase of the WDC sedimented mass against the sedimentation time.

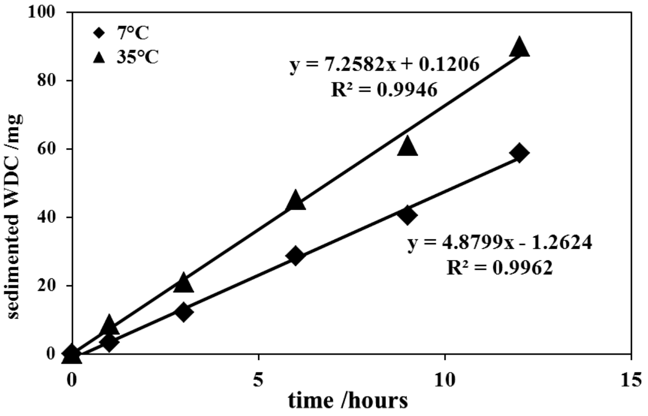

Fig. 4.3.4 Temperature effect on the WDC sedimented mass with the Selhausen soil. ◆, 7°C; ▲,35°C; ─, linear fitting.

A linear increase can be measured with fitting correlation parameters close to 1 at the two temperatures, ($R^2_{7\,°C}$ = 0, 9962; $R^2_{35\,°C}$ = 0, 9946). There is a large difference in the slopes between the two temperature ($\text{slope}_{7\,°C}$, 4.88; $\text{slope}_{35\,°C}$, 7.26).

According to (Eq. (2.1.3) and Eq. (2.1.4)), in the case of similar WDC particles (*d* and *ρ* are constant), it follows that $WDC_{sed,T}$ only depends on the viscosity, η, which sensitively varies in the case of water at different temperatures. Thus, a decrease of the water viscosity at high temperature would result in an increase of the sedimentation velocity or $WDC_{sed,T}$, which can be observed in Fig. 4.3.4.

Under the same sedimentation conditions, a rapid sedimentation of particle at a high temperature can thus apparently decrease the real efficiency of the release or mobilization kinetics, which is measured at the end of the first fractionation (shaking) step. A correction due to viscosity changes must be thus introduced in the sedimentation step in order to scale under the same experimental conditions, the effect of the temperature on the mobilization step of WDC from soils. This has been operationally performed in the next chapter part (4.4) by comparing the mobilization efficiency after a sedimentation step under the same time and temperature conditions.

The effect of the viscosity on the sedimentation step has been tested with the results from Fig. 4.3.4. The experimental conditions at 7°C can be chosen as a reference for measuring a relative variation of the sedimentation along the experimental temperature range T from 7°C to 35°C at different times.

$$WDC_7 \frac{\eta_7}{c_7} = WDC_T \frac{\eta_T}{c_T} \qquad \text{Eq. (4.3.2)}$$

It follows that

$$\frac{\eta_T}{\eta_7} = \frac{WDC_7}{WDC_T} \frac{C_T}{C_7} \qquad \text{Eq. (4.3.3)}$$

In the case of T = 35°C, experimental results of Table 4.3.3 have been used to calculate the ratio of water viscosity at 35°C and 7°C with data according to Eq. 4.3.2 and Eq.4.3.3.

Table 4.3.3 The calculated ratio of water viscosity under different temperature (7°C, 35°C)

time	Sedimented mass		Concentration-WDC		Cal- $\eta_{35°C}/\eta_{7°C}$
hour	7°C (mg)	35°C (mg)	7°C (g/L)	35°C (g/L)	
1	3.358	8.679	8.083	7.803	0.374
3	12.248	21.031	7.615	7.153	0.547
6	28.702	45.046	6.749	5.889	0.556
9	40.575	60.999	6.125	5.050	0.548
12	58.818	89.973	5.164	3.525	0.446

The average ratio of water viscosity at 35°C and 7°C was 0.494 ± 0.08 (Table 4.3.3). This value is supported by the results from Experimental Data taken from Dortmund Data Bank (DDBST, GmbH, 2011) where a $\eta_{35°C}/\eta_{7°C} = 0.508$ is reported. These results (7°C and 35°C) satisfactorily indicate that a temperature effect on the viscosity must be considered in the sedimentation results for the measurement of WDC release kinetics.

4.3.3 Temperature effect on the aggregation kinetics of Selhausen WDC

According to the DLVO theory (Chapter 2.1.2 and Chapter 4.1), charged particles are stabilised by electrostatic repulsion between the diffuse electrical double layers surrounding the particles.

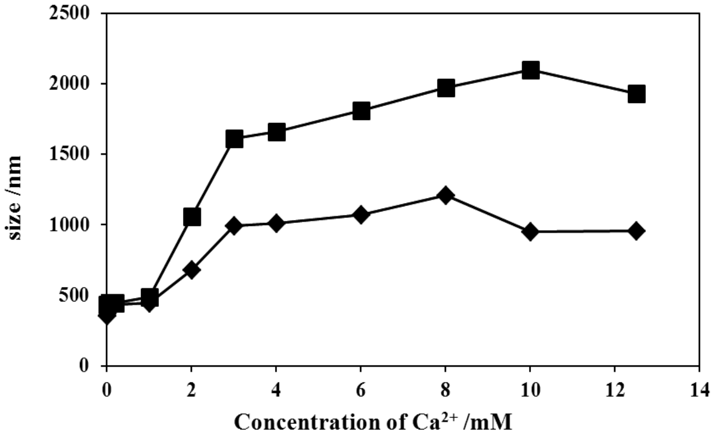

Fig. 4.3.5 The temperature effect on particle size of WDC (time of equilibrium, 1000 sec) in the presence of $CaCl_2$. ◆, 7°C; ■, 35°C.

PCS measurements at different temperature were performed to study the temperature effect on the aggregation kinetic of WDC particles (Chapter 4.1) in the presence of varying $CaCl_2$ concentrations under soil pH conditions. A representative plot depicting the temperature dependence of particles size at 1000 seconds is given in Fig. 4.3.5. The particle size in the presence of increasing concentrations of Ca^{2+} becomes larger at high temperatures. According to Stokes-Einstein equation Eq.(2.1.2), the increase of temperature decreases the viscosity of the dispersion (Teutenberg et al., 2009) and increases the diffusion coefficient of the Selhausen WDC, which affects the rate of WDC aggregation. In the case of amidine latex colloids (García-García et al., 2006), it has been shown that an increase of the temperature will decrease the surface potential and shifts the total potential energy (DLVO theory) to more attractive interaction which reduces the stability of colloids. G. Tarì (Tarì et al., 2000) found increasing temperature leads to a gradual diminution of alumina surface ionization, dielectric constant, and a total energy barrier which with the DLVO theory will enhance the colloid coagulation. In the present case with WDC, the determined size of WDC at Ca^{2+} solution reported in Fig. 4.3.5 increases when the temperature increases $\text{size}_{7°C} < \text{size}_{35°C}$, which demonstrates that the aggregation of WDC to large particles also affects the particle size distribution and velocity of the WDC during the sedimentation process. This explains the favorable distribution of lower WDC particle size in the electrolyte phase after sedimentation at higher temperatures (Fig. 4.3.2).

4.3.4 Conclusion

The temperature effect can variously affect the soil fractionation procedure including the shaking step and the sedimentation step. After shaking and sedimentation at different temperatures, the gained WDC mass in the suspension decreases with the increasing temperature. It supposes a larger effect of temperature on the sedimentation velocity than on the release mechanism. The linear correlation ($R^2_{7\,°C}$ = 0. 9962; $R^2_{35\,°C}$ = 0.9946) of the increased WDC sedimented mass along the time can be detected. The calculated ratios of water viscosity deriving from the sedimentation velocity (Stoke´s law) at 35°C and 7°C at different sedimentation times are very near to the reference value ($\eta_{35°C}/\ \eta_{7°C} = 0.508$), which satisfactorily indicates that a viscosity effect can be used to scale the sedimentation results. A shift of WDC particle size distribution to lower particle size at higher temperatures can be detected. This can be related, with the help of PCS method, to a more rapid growing aggregation of WDC which are more rapidly sedimented. It follows that the temperature during the sedimentation step must be kept constant when measuring the effect of different temperatures on the WDC mobilization (shaking step) which is investigated in Chapter 4.4.

4.4 Diffusion-controlled mobilization of water-dispersible colloids (WDCs) from three topsoils in batch experiments

4.4.1 Effect of electrolyte solution on WDC mobilization

4.4.1.1 Critical coagulation concentration of cations for WDC aggregation

A prerequisite condition for the release of WDC from soil aggregates is the increase of electrostatic repulsion force between mineral surfaces conditioned by a decrease of the ionic strength in the soil electrolyte solution during soil watering. In order to determine the salt concentration range which ensures the rapid dispersion of WDC from aggregates, the aggregation kinetics of WDC under various salt concentrations was studied. The CCCs of Ca^{2+} for three negatively charged WDCs (negative ζ-potential) samples at the original soil electrolyte pH (Selhausen 7.6, Rollesbroich, 6.2 and Wüstbebach 4.8) and the CCC of Ca^{2+} and Na^{+} (Czigány et al., 2005; Jiang et al., 2012; Novich and Ring, 1984; Séquaris, 2010) for WDC at adjusted pH 5.5 and pH 8.5 condition were investigated using the method described in chapter 3.2.4 and are reported in Table 4.4.1.

Table 4.4.1 Critical coagulation concentrations of Na^{+} and Ca^{2+} for soil WDCs and illite

Soil materials	salt	pH	CCC / mM
Selhausen	NaCl	5.5	498 ± 67
		8.5	592 ± 61
	$CaCl_2$	5.5	3.4 ± 0.2
		7.6	4.6 ± 0.5
		8.5	5.3 ± 0.3
Rollesbroich	NaCl	5.5	417 ± 90
		8.5	916 ± 81
	$CaCl_2$	5.5	5.4 ± 0.6
		6.2	6.5 ± 0.1
		8.5	10.2 ± 2.3
Wüstebach	NaCl	5.5	464 ± 53
		8.5	1023 ± 68
	$CaCl_2$	4.8	3.0 ± 0.3
		5.5	4.2 ± 0.2
		8.5	7.8 ± 0.7
Illite	NaCl	5.5	34 ± 3
		8.5	261 ± 22
	$CaCl_2$	5.5	1.3 ± 0.2
		8.5	2.8 ± 0.2

In the case of the powerful coagulating divalent cation, diffusion-controlled coagulation kinetics of WDC are found at concentrations ≥ 3 mM Ca^{2+}. The CCC_{Ca} results at adjusted pHs 5.5 and 8.5 are also included in Table 4.4.1 and Fig. 4.4.1.

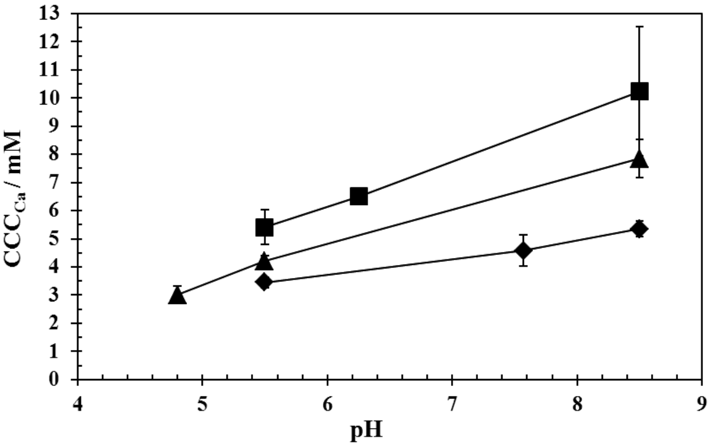

Fig. 4.4.1 Variations of the critical coagulation concentration of Ca^{2+} for WDC soil samples as a function of pH. ◆, Selhausen ; ■, Rollesbroich; ▲, Wüstebach.

An increase of CCC_{Ca} with increasing pH can be observed, which is related to an increase of the colloidal electrostatic stabilization due to a negative ionization of organic and inorganic WDC components, (Jiang et al., 2012; Kjaergaard et al., 2004a; Tombácz et al., 2004). For comparison, CCC values of Na^+ (CCC_{Na}) are also reported at adjusted pHs 5.5 and 8.5. Higher CCC_{Na} values, > 400 mM Na^+, due to a lower charge screening effect of monovalent cation with the negatively charged mineral surfaces have frequently been reported (Grolimund et al., 2001; Jiang et al., 2012). The much lower corresponding CCC values for the dominant illite clay mineral in WDC (Table 3.2.1) must be noted thus confirming the importance of the OC content in the steric stabilization (Heil and Sposito, 1993; Kjaergaard et al., 2004a; Kretzschmar et al., 1993; Séquaris, 2010) of pristine WDC by shifting the CCC to higher values. The lowest CCC for WDC from Selhausen (Fig. 4.4.1 and Table 4.4.1) in comparison to the WDC from the two other soils can thus be related to its lowest TOC content (Table 3.2.1). Ratios of CCC_{Na} to CCC_{Ca} of a factor 100 clearly indicate the relative importance of divalent cations in the stability of the released WDC dispersion from soil. According to the Schulze – Hardy rule, a dependence of CCC on the inverse sixth power of the cation valence ($CCC_M^+/CCC_M^{2+} = 64$) can be supported fairly well (Overbeeck, 1980;

Jiang *et al.*, 2012). Unfavorable attachment conditions prevail in soils because most colloids and grain surfaces are negatively charged.

4.4.1.2 Electrolyte conditions for WDC detachment

Modelling the interactions of WDC in the homoaggregation and heteroaggregation processes during the contact of large sand-quartz grains allows us to precisely define the energy conditions for the stability of soil aggregates by varying the Ca^{2+} concentration. The modelling is based on the DLVO theory, which allows potential-energy diagrams to be calculated along the distance (*H*) between interacting particles (Fig. 4.4.2). The total interaction energy between soil minerals was modelled from DLVO theory (Chapter 2.1.2). The Hogg, Healy and Fuerstenau (HHF) relation between two charged spheres when the surface potentials of each remain constant during the interaction was used for modelling the repulsive electrostatic double-layer interaction energy (Chapter 2.1.2.4).

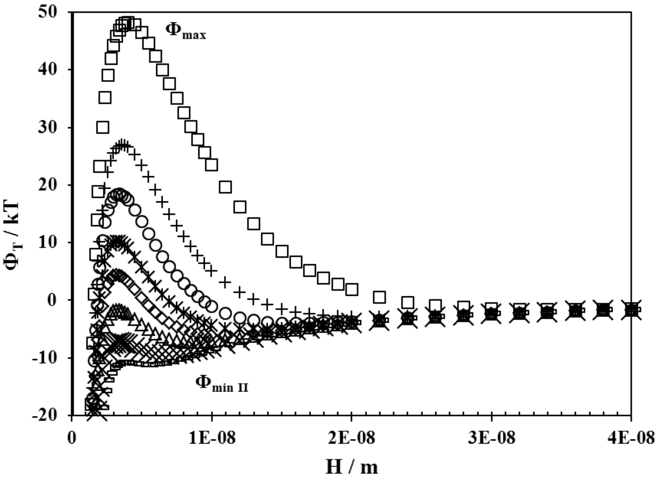

Fig. 4.4.2 Calculated DLVO interaction potential-energy (Φ_T) diagrams as a function of separation distance (H) of topsoil colloids (Selhausen and sand) for different Ca^{2+} concentrations □, 0.001 M Ca^{2+}; +, 0.002 M Ca^{2+};○, 0.003 M Ca^{2+};★, 0.004 M Ca^{2+}; ◇, 0.05 M Ca^{2+}; △, 0.06 M Ca^{2+}; ×, 0.08 M Ca^{2+} ; –, 0.01 M Ca^{2+}.

The potential-energy diagrams are characterized by the presence of an energy maximum (Φ_{max}), which acts as a repulsive energy barrier (Fig. 4.4.2). The height of Φ_{max} controls the coagulation of particles in close contact in a deep energy primary minimum (not shown) at a short separation distance (< 3 nm). A secondary energy minimum (Φ_{minII}) at some distance (H >10 nm) controls a more reversible coagulation.

The DLVO model was used in order to compare the effectiveness of the van der Waals attractive forces, expressed in the Hamaker constant (A), during the coagulation process. Thus, a scaling of A (A_{scaled}) was made under *CCC* solution conditions with $\mathrm{CaCl_2}$ where the attraction and repulsion energies are equal. Regarding the low Ψ_{d} or ζ_{CCC} values, the Eiler and Korff (Eilers and Korff, 1940; Overbeek, 1980) relation Eq. (2.2.8) was used where κ_{CCC} is calculated from the ionic strength (I_{ccc}) at the *CCC* (Séquaris, 2010). The scaling results A_{scaled} of topsoil colloids and soil clay materials are shown in Table 4.4.2. Using the A_{scaled} values, an estimation of the effective A of the investigated soil WDC across water can be made by taking a Hamaker constant value of 1.75 10^{-20} J in water for the sand (quartz) particle as a reference (Hough and White, 1980; Tan et al., 2005), an estimate of A can be thus made from A_{scaled} with

$$\mathrm{A}_{estimated} = \frac{\mathrm{A}_{scaled}\ soil\ material}{\mathrm{A}_{scaled}\ sand\ (quartz)}(1.75\times10^{-20}\ J) \qquad \text{Eq. (4.4.1)}$$

The estimated A values of WDC from soil samples are reported in Table 4.4.2.

Table 4.4.2 Comparison of aggregation kinetics parameters of three soil WDCs in $\mathrm{Ca^{2+}}$ system at natural pH

Soils	pH	$\mathrm{CCC_{Ca}}$ mM	Zeta potential mV	K $\mathrm{m^{-1}}$	$\mathrm{A_{scaled}}$	$\mathrm{A_{estimated}}$ J
Selh	7.6	4.6	-12.5	3.8E+08	4.1E-13	8.6E-21
Roll	6.3	6.5	-10.1	4.6E+08	2.2E-13	4.1E-21
Wüst	4.8	3.0	-10.9	3.1E+08	3.8E-13	6.1E-21

In Table 4.4.3, the calculated A values and particle radius were reported which are used in the calculation of the total interaction energy Φ_{T} , Eq.(2.1.8).

Table 4.4.3 Comparison of the Hamaker constants (A) between WDC and WDC with sand colloid

Soils	pH	r / m	A (WDC / WDC) / J	Ap / J	A (WDC / sand) / J
Selh	7.57	2.2E-07	8.6E-21	8.1E-20	1.2E-20
Roll	6.25	2.6E-07	4.1E-21	6.6E-20	8.5E-21
Wüst	4.8	2.7E-07	6.1E-21	7.3E-20	1.0E-20
sand	-	1.0E-04	1.75E-20	1.1E-19	-
water	-	-	-	3.7E-20	-

In the case of unfavorable interactions, it has been generally assumed (Franchi and O'Melia, 2003; Hahn and O'Melia, 2003; McDowell-Boyer et al., 1986) that the depth of a shallow energy secondary minimum (Φ_{minII}) characterizes a reversible character of the WDC mobility in soil aggregates. In the case where ϕ_{minII} is sufficiently well developed <-1.5 kT, WDC aggregation or deposition can take place *i.e.*, under solution conditions where Φ_{minII} is deeper than the average thermal energy of particles, 1.5 kT, (6 x 10^{-21} J) (Israelachvili, 1992). In Fig. 4.4.3, calculated Φ_{minII} were reported in the case of the three soils (Selhausen, Rollesbroich and Wüstebach) for WDC homoaggregation and WDC interacting with the surface of large sand-quartz grains (*r*, 100 µm).

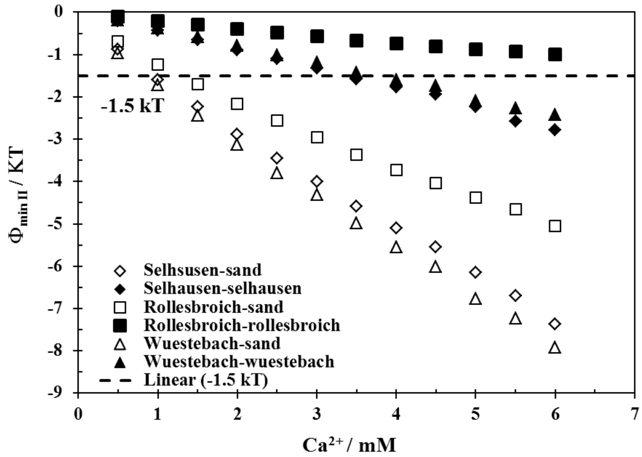

Fig. 4.4.3 Variations of the secondary energy minimum (ϕ_{minII}) as a function of the Ca^{2+} concentration (DLVO calculation) for WDC/WDC and WDC/sand grain interactions. WDC/WDC: ◆, Selhausen ;■, Rollesbroich; ▲, Wüstebach. WDC/sand grain: ◇, Selhausen ;□, Rollesbroich ; △, Wüstebach.

The results indicate that WDC aggregates are only kinetically stabilized at Ca^{2+} concentrations much higher than 3.5 mM and 1 mM, respectively, *i.e.* in a Ca^{2+} concentration range exceeding the concentration in the electrolyte phase of the batch experiments (Table 4.4.4) with deionized water.

Table 4.4.4 Colloidal properties salt concentrations of water dispersible colloid dispersion at 23°C

Soil samples	pH [a]	Ca^{2+} / mM	Na^{+} / mM	d_Z / nm	Zeta potential / mV
Selhausen	7.4	1.44	0.20	684 ± 18	-(14 ± 5)
Rollesbroich	6.5	0.24	0.32	962 ± 24	-(23 ± 5)
Wüstebach	4.5	0.08	0.12	903 ± 54	-(17 ± 5)

[a] soil / water = ½

Under low Na^{+} and Ca^{2+} concentration conditions in the electrolyte phase, ≤ 0.32 mM and ≤ 1.44 mM, respectively, a rapid disappearance of the interaction between WDC/WDC or WDC/grain follows in the secondary minimum of soil aggregates by thermal energy (Fig. 4.4.3). This soil electrolyte chemistry effect can explain a rapid detachment of WDC from the aggregates as a non-limiting rate in the first step of the WDC mobilization process.

4.4.2 Diffusion-limited mobilization of WDC

In order to study the time effect on WDC release with batch experiments at 23°C, shaking times were fixed at 5 min, 30 min, 1 h, 2 h, 4 h and 8 h. WDC fractions of the three soils for individual experiments at each shaking time were collected after sedimentation at 23°C. An estimation of corresponding applied energy was made from the rotation energy in comparison with other work (Raine and So, 1997) using end-over shaking and ultrasonic methods. In the case of an end-over shaking time of 60 min, kinetic and equivalent ultrasonic energy of about 40-60 Jg^{-1} was used to disperse about 30% of the < 2 μm particle-size content (F(t) ~ 0.30) in different soils.

4.4.2.1 Effects of time and temperature on WDC release from topsoil samples in batch experiments

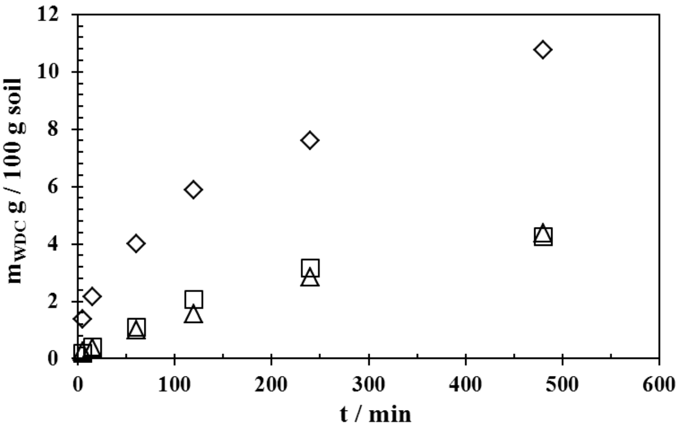

Fig. 4.4.4 Release of WDC mass (m_{WDC}) from the three TERENO topsoils as a function of shaking time at 23°C in batch experiments. ◇,Selhausen ; □, Rollesbroich; △, Wüstebach.

In Fig. 4.4.4, the released WDC mass (m_{WDC}) is plotted against the shaking time for the three topsoils at 23°C. This first-order equation is failed to describe the WDC release from bulk soil and a nonlinear increase of m_{WDC} was generally observed. The best fitting by plotting the cumulative fraction $F(t)$, (Eq. (4.3.1)) against the square root of shaking time ($t^{0.5}$) (Table 3.1.1). A linear relationship was obtained in Fig. 4.4.5, which indicates a diffusion-controlled transport of WDC (Eq. (4.4.2)) from topsoils (Jacobsen et al., 1998; Jacobsen et al., 1997; Lægdsmand et al., 1999):

$$F(t) \propto D^{0.5} t^{0.5} \qquad \text{Eq. (4.4.2)}$$

where D is an effective particle diffusion coefficient. The slopes of the linear relationship in Table 4.4.5, $F(t)\ t^{-0.5} \propto D^{0.5}$, thus allow the potential mobilization of WDC to be compared between the three topsoils.

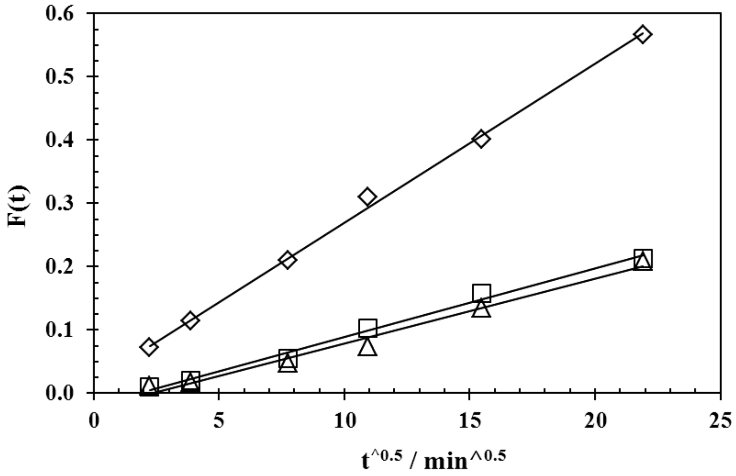

Fig. 4.4.5 Cumulative fraction *F(t)* of WDC from soil clay contents as a function of the square root of shaking time . ◇, Selhausen ; □, Rollesbroich; △, Wüstebach; ——, linear fitting. See other conditions in Fig. 4.4.4.

A higher *F*(*t*) $t^{-0.5}$ slope is observed in the case of Selhausen soil, which characterizes a much higher WDC release than in the case of Rollesbroich and Wüstebach soils (Table 4.4.5).

Table 4.4.5 WDC diffusion parameters at 23°C

Soil samples	F(t) $t^{-0.5}$/ min$^{0.5}$	D_w / m^2 min^{-1} [a]	l_t / m [b]	V_{water}ml g^{-1}
Selhausen	0.0251 ± 0.0005 (r^2 = 0.99)	(4.0 ± 0.2)10^{-11}	(5.7 ± 0.2)10^{-4}	0.642
Rollesbroich	0.0108 ± 0.0005 (r^2 = 0.99)	(2.9 ± 0.2)10^{-11}	(1.1 ± 0.1)10^{-3}	0.957
Wüstebach	0.0102 ± 0.0007 (r^2 = 0.98)	(3.1 ± 0.1)10^{-11}	(1.2 ± 0.1)10^{-3}	1.139

[a] averaged D_z with PCS method ; [b] calculated l_t with Eq. (4.4.5)

Although the soil clay fraction contents of about 20% in the three soils are more or less equivalent (Table 3.1.1), it can be assumed that any variation in soil parameters (Table 3.1.1 and Table 4.2.4) such as TOC, soil pH and polyvalent cations with their metal oxide forms would affect the release kinetics. Indeed, a sensitive decrease of *F*(*t*) $t^{-0.5}$ can be apparently correlated to TOC content increase or pH decrease, as will be discussed later.

In order to evaluate the soil parameters conditioning WDC release kinetics, the effect of temperature in the batch experiments was investigated (Fig. 4.4.6).

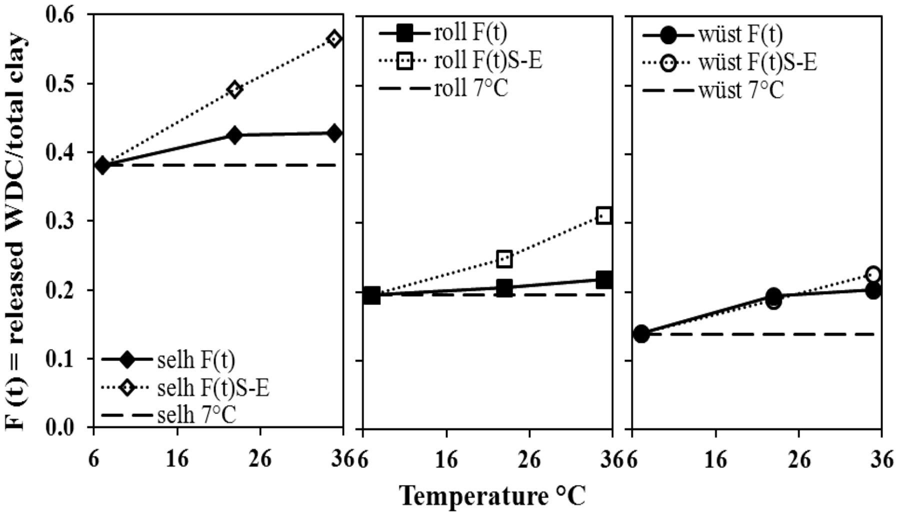

Fig. 4.4.6 Effect of temperature on *F(t)* during a shaking time of 360 min.◆, Selhausen ;■, Rollesbroich; ●, Wüstebach ; ·········, calculated *F*(t)$_{\text{S-E}}$ due to temperature effect on *D* using Eq. (4.4.2) and Eq.(4.4.3). See also text. ———, *F (t)* at 7°C, blank.

After a shaking time of 360 min. at 7°C, 23°C and 35°C, respectively, the reported *F*(t) values correspond to the extent of WDC release, measured under similar sedimentation conditions at a reference temperature of 23°C (see Materials and methods). A slight increase of *F*(t) along the temperature can be observed and was further analysed.

4.4.2.2 Modelling WDC cumulative fraction release

Assuming a spontaneous detachment of WDC from bulk soil aggregates in contact with deionized water, the effect of temperature on pure WDC diffusion-controlled transport in water was first modelled. An increase of *F (t)*$_{\text{S-E}}$ was calculated along the temperature according to the Stokes-Einstein equation (Eq.(2.1.2) where a decrease of the water viscosity (η) and an increase of the absolute temperature (T) were taken into account in the particle diffusion in water (D_{w}) under batch experiment conditions (Eq. (2.1.2)). For calculation of the WDC diffusion coefficient (D_w) at batch experiment temperatures, the measured D_{w} values with photon correlation spectroscopy (PCS) at 20°C were used to calculate D_{w} values at batch experiment temperatures (Table 4.4.6) by taking into account the variations of water viscosity (η) and temperature (°K) according to Eq.(4.4.3).

$$D_t = D_{20} \frac{\eta_{20}}{\eta_{20}} \frac{T_t}{T_{20}} \qquad \text{Eq. (4.4.3)}$$

Table 4.4.6 Calculated D_w at different temperatures for three soils

D_w	Selhausen		Rollesbroich		Wüstebach	
T batch	D_w / 20°C	$D_{w\ \text{calculated}}$	D_w / 20°C	D_w calculated	D_w / 20°C	D_w calculated
°C	(PCS)		(PCS)		(PCS)	
7°C	3.5E-11	2.4E-11	2.6E-11	1.8E-11	2.5E-11	1.7E-11
23°C	3.7E-11	4.0E-11	2.7E-11	2.9E-11	2.9E-11	3.1E-11
35°C	3.6E-11	5.3E-11	3.2E-11	4.6E-11	3.1E-11	4.5E-11

F(t)$_{\text{S-E}}$ values at 23°C and 35°C in Fig. 4.4.6 were thus calculated from *F(t)* values at 7°C (280K) for each soil according to Eq. (4.4.4).

$$F(t)_{S-E\,T}/F(t)_{280K} = \left(\frac{D_T}{D_{280K}}\right)^{0.5} \qquad \text{Eq. (4.4.4)}$$

In the case of Wüstebach soil, the variation of *F(t)*$_{\text{S-E}}$ values along the temperature is close to measured *F(t)* values whereas in the case of Selhausen and Rollesbroich soils, the calculated *F(t)*$_{\text{S-E}}$ variations are much higher. In the latter cases, lower experimental *F(t)* values at 23°C and 35°C lead to the assumption that not only η, R variations but also other temperature-sensitive soil parameters must be considered which are counteracting *F(t)*$_{\text{S-E}}$ in the WDC diffusion-controlled transport. It has been shown (Kookana et al., 1992) that desorption phenomena of chemicals in soils depends not only on the diffusion coefficient D_w of chemicals but also on the thickness of an immobile water layer l_t at the soil surface. This can be modelled by Equation Eq. (4.4.5) in the case of a diffusion process from a plane sheet of thickness l_t with uniform initial concentration in the sheet and constant zero surface concentration (Crank, 1975). In the case of WDC escaping from soil aggregates, the cumulative fraction of WDC along time *t* is given by:

$$F(t) = \frac{4}{\pi^{0.5}} \left[\frac{D_W t}{l_t^{\,2}}\right]^{0.5} \qquad \text{Eq. (4.4.5)}$$

Assuming that immobile waters layer reside in macropores (DeNovio et al., 2004; Laegdsmand et al., 2007) of soil aggregates, it seems evident that soil texture variations due to soil parameter variations would also affect the WDC transport. In Table 4.4.5, the thickness l_t was calculated at 23°C from *F*(*t*) $t^{-0.5}$ slope using Equation (4.4.5), after the introduction of D_w, from the PCS analysis in the case of the three topsoils. Calculated l_t values, from 500 µm to 1000 µm, support a macropore range in soil aggregates where WDC (< 2 µm) are diffusing from clay aggregates (cluster) or deposited layers at the surface of large soil particles. The holding linear relationships $F(t)$ $t^{-0.5}$, up to $F(t\,)$~ 0.6 in Fig. 4.4.5, independent of remaining clay content variations during WDC release, also support a WDC diffusion mechanism from large and stable macro-pore structures formed by silt and sand particles. In order to correlate l_t values to soil texture variations, an estimation of the bulk soil aggregate structure in the water phase was made by measuring the sedimentation volume of saturated soil samples under the same experimental conditions as for the WDC release kinetics. Three grams of air-dried bulk soil and 6 g of deionized water were placed into a 0.01-l centrifugation tube with straight wall and mixed by gently shaking by hand. After the temperature of the sample reached the required incubation treatment temperature, the bulk soil samples were re-homogenized before sedimentation. The height of the soil sedimentation volume in the each centrifugation tube was measured. The measured sedimentation volume (V_{sed}) in test tubes allows a distribution of mineral (V_{min}), OC (V_{OC}) and water (V_{water}) volume phases to be calculated. Thus, a simple additive relation was assumed where specific volumes (v) of 0.385 cm^3 g^{-1} and 0.71 cm^3 g^{-1} were chosen for the mineral (v_{min}) and organic matter (v_{OC}) phases, respectively. The contents of the two mineral (m_{min}.) and OC (m_{OC}) phases are given by the corresponding mass (m) where the total m refers to 1 g of dried soil sample containing about 80% of (silt + sand) particles.

Using Eq. (4.4.6), the water volume (V_{water}) in V_{sed} can thus be calculated:

$$V_{sed} = V_{OC} + V_{min} + V_{water} = m_{oc}v_{oc} + m_{min}v_{min} + V_{water} \qquad \text{Eq. (4.4.6)}$$

Table 4.4.7 Calculated SSA of dried soil samples

Soils	OM	Mineral	V OM	V mineral	Vsedi (soil + water)			V water		
	%	%	ml g^{-1}	ml g^{-1}	7°C	23°C	35°C	7°C	23°C	35°C
Selh	2.01	97.994	0.014	0.377	1.000	1.033	1.133	0.608	0.642	0.742
Roll	7.52	92.48	0.053	0.356	1.350	1.367	1.417	0.941	0.957	1.007
Wüst	20.8	79.2	0.148	0.305	1.600	1.592	1.700	1.147	1.139	1.247

In Table 4.4.7, the V_{water} values at 23°C are reported for the three soils. Obviously, a similar variation can be observed with l_t and V_{water} values, which supports a decrease of the WDC release kinetics, $F(t)$ $t^{-0.5}$ slope, between Selhausen and Rollesbroich or Wüstebach soils when the soil texture parameter, V_{water}, increases. In order to support this observation, the temperature effect on V_{water} was also compared at 7°C, 23°C and 35°C in Table 4.4.7 and were compared to the corresponding thickness l_t which was also calculated with Equation (4.4.5) and D_w values (Table 4.4.6).

A satisfactory linear correlation between the variations of V_{water} and l_t at different temperatures can be established (for all the soils, n=9, R^2=0.89), which supports the contribution of the temperature to a soil macropore expansion measured by V_{water} and the associated l_t. Thus, the relative increase of l_t against the temperature counteracts, in Fig.4.4.6, the calculated $F(t)_{\text{S-E}}$ increase due to the temperature dependence of D_w in the Stokes-Einstein relation, Eq.2.1.2. The results thus support a mobilization of WDC in the soil aggregate structure where diffusion through a boundary stagnant water phase in macropore to the mobile phase would be a limiting step in the low mechanical energy range of the batch experiments. For comparison, in the case of column experiments, a diffusion–limited mobilization of colloids has been proposed at irrigation intensities in the range of 1.6 mm h^{-1} – 30 mm h^{-1} corresponding to natural rainstorm events (Jacobsen et al., 1998; Jacobsen et al., 1997). It is worth noting that an increase of mechanical forces accelerates the mobilization of WDC by reducing the stagnant water layer and more generally favors WDC detachment by a direct physical perturbation (Ryan and Elimelech, 1996; Torkzaban et al., 2007).

The V_{water} is thus a scaling parameter, which can be useful for estimating the relative extent of WDC mobilization between the three TERENO soils with a similar soil clay fraction. As already noted, there is evidence that variations of release kinetics can be related to other soil parameters as TOC, pH and multivalent cations and their metal oxide forms measuring with Fe_d, Al_d, Fe_o and $Al_{o.}$ They are known for conditioning the soil texture. Indeed, large soil aggregate structures (Tisdall and Oades, 1982) are stabilized by the presence of POC and multivalent cations and their metal oxide forms. In the case of Rollesbroich and Wüstebach topsoils, these soil parameters are sensitively more elevated than in Selhausen topsoil (Table 3.1.1 and Table 4.2.4). They support, at more acidic pH, a stabilization of greater stagnant water contents in soil macropores and a slowing down of WDC transport by increasing the corresponding l_t. It is of interest that there is no significant WDC mobilization difference between forest (Wüstebach) and grassland (Rollesbroich) soils whereas major differences occur between these soils and the arable soil (Selhausen).

4.4.3 Conclusions

Under soil electrolyte conditions, WDC mobilization from saturated bulk soil is a diffusion-controlled mobilization of WDC from topsoils which can be demonstrated in batch experiments after a rapid detachment step of WDC from soil aggregates. Modelling the temperature effect on the release kinetics shows that the thickness of the immobile water layer, l_t, in the soil aggregates limits the extent of WDC mobilization. This was experimentally demonstrated at three different temperatures from variations in the water volume of the sediment of soaked soil (V_{water}) among the three TERENO soils, where a linear correlation between l_t and V_{water} was found (n = 9, $R^2 = 0.89$). Results show that an increase in the soil structure parameter V_{water} with increasing temperature weakens WDC mobilization from bulk soil, and counteracts the estimated temperature effect according to the Stokes-Einstein relation on particle diffusion in bulk water. It was demonstrated that there is no significant difference in WDC mobilization between forest (Wüstebach) and grassland (Rollesbroich) soils, whereas major differences occurred between these two soils and the arable soil (Selhausen) despite all three having similar clay contents. This can be related to greater immobile water contents (larger l_t and V_{water}) in the soil macro-pores of forest and grassland soils, where at more acidic soil pH, POC and polyvalent cations with their metal oxide forms will contribute to water immobilization. The results show that the temperature-sensitive soil structure parameters l_t and V_{water} play key roles in WDC mobilization kinetics and thus to the understanding of soil erosion processes.

Chapter 5

Conclusions

Firstly, the combination of PCS and zeta-potential methods allow following the aggregation kinetics of potential water dispersible colloids (WDC), illite and quartz particles, under various chemical conditions. The importance of the pH, nature and concentration of electrolyte ions on the stability of colloidal dispersions can be analysed by measuring the *CCC*. The main role played by the cation valence in decreasing the stability of the colloidal particles at lower concentrations of Ca^{2+} is confirmed. A higher stability of the dispersion of colloidal quartz particles than for illite particles was related to lower van der Waals interaction forces, which were scaled by the Eilers and Korff relation, $\zeta_{\mathrm{CCC}}^2 / K$ and the fast aggregation rate with $\Phi k_{\mathrm{a,\ fast}}$. The variations of *CCC* with the pH and the anion nature demonstrate the sensitivity of the edge site to illite particles in the aggregate formation. A high dispersibility of WDC particles was detected in the Na-system after interaction with oxalate anions. This is related to the capacity of bifunctional carboxylic acid to interact through inner-sphere complexes with surface Al and Si. In the Ca-system, the strong coagulation power of calcium prevails over the surface effects of anions, which supports attractive ion-ion correlation forces between equally highly charged illite colloids. However, the distribution of its coagulating free Ca^{2+} species in suspension can be limited by the complexation capacity of the anion as in the case of oxalate. The results in mixed Na-Ca systems are of great interest for the interpretation of coagulation/deposition processes under soil chemical conditions. It was shown that the CCCs of mixed Na-Ca systems can be calculated using the *CCCs* for colloidal illite and quartz particles in pure Na and Ca systems. Dispersion effects due to adsorbed oxalate as a representative of ubiquitous polyvalent low molecular weight organic acids in NOM could be here analysed as a function of the molar ratios of calcium to sodium in solution.

Secondly, the OC effect on surface and pores structure of soil fractions and bulk soil can be probed by different gas sorption methods. In the case of N_2, strongly bound OC to mineral µpore impedes the accessibility of N_2 to the mineral surface. In contrast, no decrease of the CO_2 sorption in the presence of OC shows an additional adsorption of CO_2 at mineral surface due to organic matter where CO_2 is preferentially bound to non-associated OC as the POM fraction. A blocking effect of micropore to N_2 sorption due to an OC sorption or sequestration up to 40 g OC kg^{-1} at mineral surface of the clay content (~ 20% in the three bulk soil samples) can be hypothesized. In the three studied soils, iron oxide is the major metal oxide in different soil fractions and bulk soils. The variations of ($SSA_{CB\ 400}$- $SSA_{DCB\ 400}$)/ $SSA_{DCB\ 400}$ were used to estimate the contribution of metal oxide content to the total mineral SSA of particle size fractions and bulk soil samples. In bulk soil, the contribution is rather constant and in the case of WDC, an increase of metal oxide SSA contribution were measured along the series Selhausen (27%) < Rollesbroich (35%) < Wüstebach (44%). There is good linear correlation of released $SSA_{CB\text{-}DCB\ 400}$ against the $Fe_{DCB\text{-}CB}$ content. Predominant amorphous structure ($M_{oxalate}$) was found in for the aluminum oxide (70%-95%) content in comparison with iron oxides (26%-54%). The distribution of amorphous iron oxide form is at the highest (~ 50%) in the forest soil of Wüstebach in comparison with other soils. The surface contribution of amorphous metal oxide in bulk soils SSA is higher than in the case of WDC which also indicates a distribution of metal oxide outside the clay fraction. A simultaneous increase of pore structure dimension, R_g and mean particle thickness T (1/SSA) were calculated from Guinier plot. A decrease of ellipsoidal pore dimensions R_g (SAXS) and R_p (N_2 gas adsorption) implies a contraction of the WDC pore structure in the presence of metal oxide nanoparticles. Higher relative variations for N_2 adsorption results than SAXS results may suppose that only a fraction of total pores, measured by SAXS method, the open pores are preferentially modified by the presence of metal oxide nanoparticles. The fractal results from the Porod plots can be variously interpreted. A fractal contribution of larger pore space in a more loose aggregate structure of WDC samples would characterize WDC samples without nanoparticles. In the presence of nanoparticles, the fractal results can be associated to a contribution of dispersed small spore space in a more compact aggregate structure of WDC sample.

Thirdly, the temperature effect can variously affect the soil fractionation procedure including the shaking step and the sedimentation step. After shaking and sediment at different temperature, the gained WDC mass in the suspension decrease with the increasing temperature which is due to the larger effect of temperature on the acceleration for sedimentation velocity than for release mechanism. The measured size of the WDC decreases and SSA value increases with the increasing temperature respect. A linear increase of sedimentation along the time were observed ($R^2_{7\ °C} = 0.9962$; $R^2_{35\ °C} = 0.9946$). The calculated ratios of water viscosity according to the sedimentation velocity at 35°C and 7°C at different sedimentation time are very near to the results from reference value (η 35°C/ η 7°C=0.508), which satisfactorily indicates that a viscosity effect can be used to scale the sedimentation results. It follows that the temperature during the sedimentation step must be kept constant for measuring the effect of different temperature on the shaking step. The aggregation kinetics of WDC at 7°Cand 35°C indicate different aggregation kinetics with the WDC in the electrolyte condition under different temperature which may also a fact in affecting the velocity of WDC sedimentation.

Finally, a diffusion-controlled transport of WDC from topsoils can be evidenced in batch experiments under soil electrolyte conditions after a rapid detachment of WDC from soil aggregates. Modelling the temperature effect on the release kinetics shows that immobile water layer thickness at the soil aggregate surface limits the extent of WDC mobilization. The importance of the soil aggregate structure in the diffusion- controlled step can be experimentally demonstrated from variations of V_{water} associated with *SSA* between the three TERENO soils where TOC and pH soil parameters affect the soil texture. At acidic soil pH, a low mobilization of WDC in forest (Wüstebach) and grassland (Rollesbroich) topsoils, can be thus related to greater stagnant water contents in soil macropores where POC and polyvalent cations with their metal oxide forms contribute to their immobilizations.

References

Axe, K. and Persson, P. 2001. Time-dependent surface speciation of oxalate at the water-boehmite (gamma-AlOOH) interface: implications for dissolution. Geochimica et Cosmochimica Acta 65:4481-4492.

Baldock, J., and Skjemstad, J. 2000. Role of the soil matrix and minerals in protecting natural organic materials against biological attack. Organic Geochemistry 31:697-710.

Bale, H.D. and Schmidt, P.W. 1984. Small-Angle X-Ray-Scattering Investigation of Submicroscopic Porosity with Fractal Properties. Physical Review Letters 53:596-599.

Barberis, E., Marsan, F.A., Boero, V. and Arduino, E. 1991. Aggregation of soil particles by iron oxides in various size fractions of soil B horizons. Journal of Soil Science 42:535-542.

Benjamin, M.M., Sletten, R.S., Bailey, R.P. and Bennett, T. 1996. Sorption and filtration of metals using iron-oxide-coated sand. Water Research 30:2609-2620.

Bennett, P.C. 1991. Quartz dissolution in organic-rich aqueous systems. Geochimica et Cosmochimica Acta 55:1781-1797.

Bin, G., Cao, X., Dong, Y., Luo, Y. and Ma, L.Q. 2011. Colloid Deposition and Release in Soils and Their Association With Heavy Metals. Critical Reviews in Environmental Science and Technology 41:336-372.

Binnemans, K., Van Deun, R., Thijs, B. Vanwelkenhuysen, I. and Geuens, I. 2004. Structure and mesomorphism of silver alkanoates. Chemistry of materials 16:2021-2027.

Bissonnais, Y.L. 1996. Aggregate stability and assessment of soil crustability and erodibility: I. Theory and methodology. European Journal of Soil Science 47:425-437.

Borkovec, M., Wu, Q., Degovics, G., Laggner, P. and Sticher, H. 1993. Surface area and size distributions of soil particles. Colloids and Surfaces A: Physicochemical and Engineering Aspects 73:65-76.

Bornemann, L., Herbst, M., Welp, G., Vereecken, H. and Amelung, W. 2011. Rock fragments control size and saturation of organic carbon pools in agricultural topsoil. Soil Science Society of America Journal 75:1898-1907.

Bronick, C.J. and Lal, R. 2005. Soil structure and management: a review. Geoderma 124:3-22.

Brubaker, S.C., Holzhey, C.S. and Brasher, B.R. 1992. Estimating the water-dispersible clay content of soils. Soil Science Society of America Journal 56:1226-1232.

Burke, I.C., Yonker, C.M., Parton, W.J., Cole, C.V., Schimel, D.S. and Flach, K. 1989. Texture, Climate, and Cultivation Effects on Soil Organic Matter Content in U.S. Grassland Soils. Soil Sci Soc Am J 53:800-805.

Cambardella, C.A. and Elliott, E.T. 1992. Particulate soil organic-matter changes across a grassland cultivation sequence. Soil Science Society of America journal 56:777-783.

Chevallier, T., Woignier, T., Toucet, J. and Blanchart, E. 2010. Organic carbon stabilization in the fractal pore structure of Andosols. Geoderma 159:182-188.

References

Childs, C.W. 1992. Ferrihydrite: A review of structure, properties and occurrence in relation to soils. Zeitschrift für Pflanzenernährung und Bodenkunde 155:441-448.

Chorom, M. and Rengasamy, P. 1995. Dispersion and zeta potential of pure clays as related to net particle charge under varying pH, electrolyte concentration and cation type. European Journal of Soil Science 46:657-665.

Christensen, B.T. 2001. Physical fractionation of soil and structural and functional complexity in organic matter turnover. European Journal of Soil Science 52:345-353.

Cohaut, N., Blanche, C., Dumas, D., Guet, J.M., and Rouzaud, J.N. 2000. A small angle X-ray scattering study on the porosity of anthracites. Carbon 38:1391-1400.

Cornell, R.M. and Schwertmann, U. 1996. The Iron Oxides Wiley-VCH Verlag GmbH, Germany

Cornell, R.M. and Schwertmann, U. 2003. The iron oxides: structure, properties, reactions, occurrences and uses Wiley-vch.

Crank, J. 1975. The Mathematics of Diffusion 2nd edn Oxford University Press.

Czigány, S., Flury, M. and Harsh, J.B. 2005. Colloid stability in vadose zone Hanford sediments. Environmental Science & Technology 39:1506-1512.

Dalal, R.C. and Bridge, B.J. 1996. Aggregation and organic matter storage in sub-humid and semi-arid soils, p. 263–307, *In* M. R. Carter and B. A. Stewart, (eds.) Structure and Organic Matter Storage in Agricultural Soils. ed. CRC Press, Boca Raton, Florida.

DDBST. GmbH, 2011. Dortmund Data Bank, www.ddbst.com.

de Jonge, H. and Mittelmeijer-Hazeleger, M.C. 1996. Adsorption of CO2 and N2 on Soil Organic Matter: Nature of Porosity, Surface Area, and Diffusion Mechanisms. Environmental Science & Technology 30:408-413.

Dékány, I., Turi, L., Fonseca, A. and Nagy, J.B. 1999. The structure of acid treated sepiolites: small-angle X-ray scattering and multi MAS-NMR investigations. Applied Clay Science 14:141-160.

Delhorme, M., Labbez, C., Caillet, C.l. and Thomas, F. 2010. Acid−Base Properties of 2:1 Clays. I. Modeling the Role of Electrostatics. Langmuir 26:9240-9249.

DeNovio, N.M., Saiers, J.E. and Ryan , J.N. 2004. Colloid movement in unsaturated porous media: Recent advances and future directions. Vadose Zone Journal 3:338-351.

Dubinin, M.M., Plavnik, G.M. and Zaverina, E.D. 1964. Integrated study of the porous structure of active carbons from carbonized sucrose. Carbon 2:261-268.

Duiker, S.W., Rhoton, F.E., Torrent, J., Smeck, N.E. and Lal, R. 2003. Iron (Hydr)Oxide Crystallinity Effects on Soil Aggregation. Soil Sci Soc Am J 67:606-611.

Eilers, H. and Korff, J. 1940. The significance of the phenomenon of the electrical charge on the stability of hydrophobic dispersions. Transactions of the Faraday Society 35:229-241.

Eusterhues, K., Rumpel, C. and Kögel-Knabner, I. 2005. Organo-mineral associations in sandy acid forest soils: importance of specific surface area, iron oxides and micropores. European Journal of Soil Science 56:753-763.

References

Feng, X., Simpson, A.J. and Simpson, M.J. 2005. Chemical and mineralogical controls on humic acid sorption to clay mineral surfaces. Organic Geochemistry 36:1553-1566.

Filimonova, S.V., Knicker, H. and Kögel-Knabner, I. 2006. Soil micro- and mesopores studied by N2 adsorption and 129Xe NMR of adsorbed xenon. Geoderma 130:218-228.

Fox, T.R. and Comerford, N.B. 1990. Low-Molecular-Weight Organic Acids in Selected Forest Soils of the Southeastern USA. Soil Sci Soc Am J 54:1139-1144.

Franchi, A. and O'Melia, C.R. 2003. Effects of natural organic matter and solution chemistry on the deposition and reentrainment of colloids in porous media. Environmental Science & Technology 37:1122-1129.

Frenkel, H., Goertzen, J.O. and Rhoades , J.D. 1978. Effects of clay type and content, exchangeable sodium percentage, and electrolyte concentration on clay dispersion and soil hydraulic conductivity. Soil Science Society of America Journal 42:32-39.

Frenkel, H., Levy, G.J. and Fey, M.V. 1992. Clay dispersion and hydraulic conductivity of clay-sand mixtures as affected by the addition of various anions. Clays and clay minerals 40:515-521.

Fuerstenau, D.W. 1970. Interfacial processes in mineral/water systems. Pure and Applied Chemistry 24:135-164.

Fukuyama, K., Kasahara, Y., Kasahara, N., Oya, A. and Nishikawa, K. 2001. Small-angle X-ray scattering study of the pore structure of carbon fibers prepared from a polymer blend of phenolic resin and polystyrene. Carbon 39:287-290.

Furrer, G. and Stumm, W. 1986. The coordination chemistry of weathering: I. Dissolution kinetics of δ-Al2O3 and BeO. Geochimica et Cosmochimica Acta 50:1847-1860.

Gaboriaud, F. and Ehrhardt , J.-J. 2003. Effects of different crystal faces on the surface charge of colloidal goethite (α-FeOOH) particles: an experimental and modeling study. Geochimica et Cosmochimica Acta 67:967-983.

García-García, S., Jonsson, M. and Wold, S. 2006. Temperature effect on the stability of bentonite colloids in water. Journal of Colloid and Interface Science 298:694-705.

Gilkes, R., Scholz, G. and Dimmock, G. 2006. Lateritic deep weathering of granite. Journal of Soil Science 24:523-536.

Glatter, O. and Kratky, O. 1982. Small angle X-ray Scattering Academic Press, London.

Glatter, O. and May, R. 2006. Small-angle techniques p. 110, *In* E. Prince, (ed.) International Tables for Crystallography Volume C: mathematical,physical and chemical tables. ed. Kluwer Academic Publishers, Netherlands.

Goldberg, S. and Glaubig, R.A. 1987. Effect of saturating cation, pH, and aluminum and iron oxide on the flocculation of kaolinite and montmorillonite. Clays and Clay Minerals 35:220-227.

Gregory, .J. 2006. Particles in Water: Properties and Processes, CRC Press, Taylor & Francis Group, Boca Raton, FL

Gregory, J. 2005. Particles in water: properties and processes CRC.

References

Grolimund, D. and Borkovec, M. 2005. Colloid-Facilitated Transport of Strongly Sorbing Contaminants in Natural Porous Media: Mathematical Modeling and Laboratory Column Experiments†. Environmental Science & Technology 39:6378-6386.

Grolimund, D. and Borkovec, M. 2006. Release of colloidal particles in natural porous media by monovalent and divalent cations. Journal of Contaminant Hydrology 87:155-175.

Grolimund, D., Elimelech, M. and Borkovec, M. 2001. Aggregation and deposition kinetics of mobile colloidal particles in natural porous media. Colloids and Surfaces A: Physicochemical and Engineering Aspects 191:179-188.

Grolimund, D., Borkovec, M., Barmettler, K. and Sticher, H. 1996. Colloid-Facilitated Transport of Strongly Sorbing Contaminants in Natural Porous Media: A Laboratory Column Study. Environmental Science & Technology 30:3118-3123.

Grolimund, D., Elimelech, M., Borkovec, M., Barmettler, K., Kretzschmar, R. and Sticher, H. 1998. Transport of in Situ Mobilized Colloidal Particles in Packed Soil Columns. Environmental Science & Technology 32:3562-3569.

Grolimund, D., Barmettler, K., Borkovec, M. 2007. Colloid facilitated transport in natural porous media: fundamental phenomena and modelling Springer-Verlag, Berlin Heidelberg, Germany.

Gu, B. and Doner, H.E. 1992. The microstructure of dilute clay and humic acid suspensions revealed by freeze-fracture electron microscopy. Clays and clay minerals 40:246-250.

Guinier, A. and Fournet, G. 1955. Small Angle Scattering of X-rays J. Wiley & Sons, New York.

Gustafsson, J.P. 2011. Visual MINTEQ.ver. 3.0, 3.0 ed, Dept. of Land and Water Resources Engineering.Stockholm, Sweden.

Hahn, M.W. and C.R. O'Melia. 2003. Deposition and reentrainment of brownian particles in porous media under unfavorable chemical conditions: Some concepts and applications. Environmental Science & Technology 38:210-220.

Hancock, G.R., Murphy, D. and Evans, K.G. 2010. Hillslope and catchment scale soil organic carbon concentration: An assessment of the role of geomorphology and soil erosion in an undisturbed environment. Geoderma 155:36-45.

Heil, D. and Sposito, G. 1993. Organic matter role in illitic soil colloids flocculation: I. Counter ions and pH. Soil Science Society of America Journal 57:1241-1246.

Hesterberg, D. and Page, A.L. 1990. Flocculation Series Test Yielding Time-Invariant Critical Coagulation Concentrations of Sodium Illite. Soil Sci Soc Am J 54:729-735.

Hiemenz, P.C. 1986. Principles of Colloid and Surface Chemistry, 2nd CRC, New York.

Hiemstra, T., Antelo, J. van Rotterdam, A.M.D. and van Riemsdijk, W.H. 2010a. Nanoparticles in natural systems II: The natural oxide fraction at interaction with natural organic matter and phosphate. Geochimica et Cosmochimica Acta 74:59-69.

Hiemstra, T., Antelo, J., Rahnemaie, R. and Riemsdijk, W.H.V. 2010b. Nanoparticles in natural systems I: The effective reactive surface area of the natural oxide fraction in field samples. Geochimica et Cosmochimica Acta 74:41-58.

Hogg, R., Healy, T.W. and Fuerstenau, D.W. 1966. Mutual coagulation of colloidal dispersions. Transactions of the Faraday Society 62:1638-1651.

References

Höhr, A., Neumann, H.-B., Schmidt, P.W., Pfeifer, P. and Avnir, D. 1988. Fractal surface and cluster structure of controlled-pore glasses and Vycor porous glass as revealed by small-angle x-ray and neutron scattering. Physical Review B 38:1462-1467.

Holthoff, H., Egelhaaf, S.U., Borkovec, M., Schurtenberger, P. and H. Sticher. 1996. Coagulation Rate Measurements of Colloidal Particles by Simultaneous Static and Dynamic Light Scattering. Langmuir 12:5541-5549.

Hough, D.B. and White, L.R. 1980. The calculation of hamaker constants from liftshitz theory with applications to wetting phenomena. Advances in Colloid and Interface Science 14:3-41.

Igwe, C.A., Akamigbo, F.O.R. and Mbagwu, J.S.C. 1995. Physical Properties of Soils of Southeastern Nigeria and the Role of Some Aggregating Agents in Their Stability. Soil Science 160:431-441.

Igwe, C.A., Zarei, M. and Stahr, K. 2009. Colloidal stability in some tropical soils of southeastern Nigeria as affected by iron and aluminium oxides. CATENA 77:232-237.

Israelachvili, J. 1992. Intermolecular and surface forces, second edition: With applications to colloidal and biological systems (Colloid Science) Academic Press.

Jacobsen, O.H., Moldrup, P., de Jonge, H. and de Jonge, L.W. 1998. Mobilization and transport of natural colloids in a macroporous soil. Physics and Chemistry of The Earth 23:159-162.

Jacobsen, O.H., Moldrup, P., Larsen, C., Konnerup, L. and Petersen, L.W. 1997. Particle transport in macropores of undisturbed soil columns. Journal of Hydrology 196:185-203.

Jarvis, N.J., Villholth, K.G. and Ulén, B. 1999. Modelling particle mobilization and leaching in macroporous soil. European Journal of Soil Science 50:621-632.

Jiang, C.-L., Séquaris, J.-M., Vereecken, H. and Klumpp, E. 2012. Effects of inorganic and organic anions on the stability of illite and quartz soil colloids in Na-, Ca- and mixed Na–Ca systems. Colloids and Surfaces A: Physicochemical and Engineering Aspects 415:134-141.

Johnson, S.B., Yoon, T.H., Slowey, A.J. and Brown, G.E. 2004. Adsorption of Organic Matter at Mineral/Water Interfaces: 3. Implications of Surface Dissolution for Adsorption of Oxalate. Langmuir 20:11480-11492.

Johnson, S.B., Brown, G.E., Healy, T.W. and Scales, P.J. 2005. Adsorption of Organic Matter at Mineral/Water Interfaces. 6. Effect of Inner-Sphere versus Outer-Sphere Adsorption on Colloidal Stability. Langmuir 21:6356-6365.

Jones, D.L. 1998. Organic acids in the rhizosphere – a critical review. Plant and Soil 205:25-44.

Jones, D.L. and Edwards, A.C. 1998. Influence of sorption on the biological utilization of two simple carbon substrates. Soil Biology and Biochemistry 30:1895-1902.

Kaiser, K. and Guggenberger, G. 2000. The role of DOM sorption to mineral surfaces in the preservation of organic matter in soils. Organic Geochemistry 31:711-725.

Kaiser, K. and Guggenberger, G. 2003. Mineral surfaces and soil organic matter. European Journal of Soil Science 54:219-236.

Kalbitz, K., Schwesig, D., Rethemeyer, J. and Matzner, E. 2005. Stabilization of dissolved organic matter by sorption to the mineral soil. Soil Biology and Biochemistry 37:1319-1331.

References

Kaplan, D.I., Bertsch, P.M. and Adriano, D.C. 1997. Mineralogical and Physicochemical Differences between Mobile and Nonmobile Colloidal Phases in Reconstructed Pedons. Soil Sci Soc Am J 61:641-649.

Kaplan, D.I., Bertsch, P.M. Adriano, D.C. and Miller, W.P. 1993. Soil-borne mobile colloids as influenced by water flow and organic carbon. Environmental Science & Technology 27:1193-1200.

Kaplan, D.I., Sumner, M.E., Bertsch, P.M. and Adriano, D.C. 1996. Chemical conditions conducive to the release of mobile colloids from ultisol profiles. Soil Science Society of America Journal 60:269-274.

Kiem, R. and Kögel-Knabner, I. 2002a. Refractory organic carbon in particle-size fractions of arable soils II: organic carbon in relation to mineral surface area and iron oxides in fractions <6 µm. Organic Geochemistry 33:1699-1713.

Kiem, R. and Kögel-Knabner, I. 2002b. Refractory organic carbon in particle-size fractions of arable soils II: organic carbon in relation to mineral surface area and iron oxides in fractions < 6 µm. Organic Geochemistry 33:1699-1713.

Kim, D.-H., Ryu, B.-G., Park, S.-W., Seo, C.-I. and Baek, K. 2009. Electrokinetic remediation of Zn and Ni-contaminated soil. Journal of Hazardous Materials 165:501-505.

Kjaergaard, C., Hansen, H.C.B., Koch, C.B. and Villholth, K.G. 2004a. Properties of water-dispersible colloids from macropore deposits and bulk horizons of an agrudalf. Soil Science Society of America Journal 68:1844-1852.

Kjaergaard, C., de Jonge, L.W., Moldrup, P. and Schjonning, P. 2004b. Water-dispersible colloids: effects of measurement method, clay content, initial soil matric potential, and wetting rate. Vadose Zone Journal 3:403-412.

Kjaergaard, C., Moldrup, P., de Jonge, L.W. and Jacobsen, O.H. 2004c. Colloid Mobilization and Transport in Undisturbed Soil Columns. II. The Role of Colloid Dispersibility and Preferential Flow. Vadose Zone Journal 3:424-433.

Kjellander, R., Marcelja, S., Pashley, R.M. and Quirk, J.P. 1988. Double-layer ion correlation forces restrict calcium-clay swelling. The Journal of Physical Chemistry 92:6489-6492.

Kleber, M., Mikutta, R., Torn, M.S. and Jahn, R. 2005. Poorly crystalline mineral phases protect organic matter in acid subsoil horizons. European Journal of Soil Science 56:717-725.

Kögel-Knabner, I., Guggenberger, G., Kleber, M., Kandeler, E., Kalbitz, K., Scheu, S., Eusterhues, K. and Leinweber, P. 2008. Organo-mineral associations in temperate soils: Integrating biology, mineralogy, and organic matter chemistry. Journal of Plant Nutrition and Soil Science 171:61-82.

Kookana, R.S., Aylmore, L.A.G. and Gerritse, R.G. 1992. Time-Dependent Sorption of Pesticides During Transport in Soils. Soil Science 154:214-225.

Kretzschmar, R., Robarge, W.P. and Weed, S.B. 1993. Flocculation of kaolinitic soil clays: effects of humic substances and iron oxides. Soil Science Society of America Journal 57:1277-1283.

Kretzschmar, R., Borkovec, M., Grolimund, D., Elimelech, M. and Donald, L.S. 1999. Mobile Subsurface Colloids and Their Role in Contaminant Transport. Advances in Agronomy Volume 66:121-193.

References

Kubicki, J.D., Schroeter, L.M., Itoh, M.J., Nguyen, B.N. and Apitz, S.E. 1999. Attenuated total reflectance Fourier-transform infrared spectroscopy of carboxylic acids adsorbed onto mineral surfaces. Geochimica et Cosmochimica Acta 63:2709-2725.

Lægdsmand, M., Villholth, K.G., Ullum, M. and Jensen, K.H. 1999. Processes of colloid mobilization and transport in macroporous soil monoliths. Geoderma 93:33-59.

Laegdsmand, M., Moldrup, P. and De Jonge, L.W. 2007. Modelling of colloid leaching from unsaturated, aggregated soil. European Journal of Soil Science 58:692-703.

Lagaly, G. 2006. Chapter 5. Colloid Clay Science, p. 141-245, *In* B. K. G. T. Faïza Bergaya and L. Gerhard, (eds.) Developments in Clay Science. ed. Elsevier.

Lavee, H., Sarah, P. and Imeson, A.C. 1996. Aggregate stability dynamics as affected by soil temperature and moisture regimes. Geografiska annaler Series A Physical geography 78:73-82.

Lowell, S., Shields, J., Thomas, M. and Thommes, M. 2004. Mesopore Analysis, p. 101-128 Characterization of Porous Solids and Powders: Surface Area, Pore Size and Density. ed. Particle Technology Series. Springer Netherlands.

Majzik, A. and Tombácz, E. 2007a. Interaction between humic acid and montmorillonite in the presence of calcium ions II. Colloidal interactions: Charge state, dispersing and/or aggregation of particles in suspension. Organic Geochemistry 38:1330-1340.

Majzik, A. and Tombácz, E. 2007b. Interaction between humic acid and montmorillonite in the presence of calcium ions I. Interfacial and aqueous phase equilibria: Adsorption and complexation. Organic Geochemistry 38:1319-1329.

Manning, B.A. and Goldberg, S. 1996. Modeling arsenate competitive adsorption on kaolinite, montmorillonite and illite. Clays and Clay Minerals 44:609-623.

Martinez, C.E., Kleinschmidt, A.W. and Tabatabai, M.A. 1998. Sulfate adsorption by variable charge soils: Effect of low-molecular-weight organic acids. Biology and Fertility of Soils 26:157-163.

Masiello, C.A., Chadwick, O.A., Southon, J., Torn, M.S. and Harden, J.W. 2004. Weathering controls on mechanisms of carbon storage in grassland soils. Global Biogeochem Cycles 18:GB4023.

Mayer, L.M. and Xing, B. 2001. Organic Matter–Surface Area Relationships in Acid Soils. Soil Sci Soc Am J 65:250-258.

Mayer, L.M., Schick, L.L., Hardy, K.R., Wagai, R. and McCarthy, J. 2004. Organic matter in small mesopores in sediments and soils. Geochimica et Cosmochimica Acta 68:3863-3872.

Mbagwu, J.S.C. and Schwertmann, U. 2006. Some factors affecting clay dispersion and aggregate stability in selected soils of Nigeria. International agrophysics.

McDowell-Boyer, L.M., Hunt, J.R. and Sitar, N. 1986. Particle transport through porous media. Water Resources Research 22:1901-1921.

McGechan, M.B. and Lewis, D.R. 2002. SW—Soil and Water: Transport of Particulate and Colloid-sorbed Contaminants through Soil, Part 1: General Principles. Biosystems Engineering 83:255-273.

References

Mehra, O.P. and Jackson, M.L. 1960. Iron oxide removal from soils and clays by dithionite-citrate system bufferd with sodium bicarbonate. p. 317–327 Proc. Clays and Clay Minerals Proceedings of the 7th National Conference1960.

Mikutta, R., Kleber, M. and Jahn, R. 2005. Poorly crystalline minerals protect organic carbon in clay subfractions from acid subsoil horizons. Geoderma 128:106-115.

Mikutta, R., Kleber, M., Torn, M.S. and Jahn, R. 2006. Stabilization of soil organic matter: association with minerals or chemical recalcitrance? Biogeochemistry 77:25-56.

Mikutta, R., Mikutta, C., Kalbitz, K., Scheel, T., Kaiser, K. and Jahn, R. 2007. Biodegradation of forest floor organic matter bound to minerals via different binding mechanisms. Geochimica et Cosmochimica Acta 71:2569-2590.

Miller, W.P. and Baharuddin, M.K. 1986. Relationship of soil dispersibility to infiltration and erosion of southeastern soils. Soil Science 142:235-240.

Mittelbach, P. 1964. Zur Röntgenkleinwinkelstreuung verdünnter kolloider systeme:VIII Diskussion des Streuverhaltens regelmäÿiger Körper und Methoden zur Bestimmung von Gröÿe und Form kolloider Teilchen. Acta Phys Anstriaca 19:53-102.

Nearing, M., Pruski, F.F. and O'Neal, M.R. 2004. Expected climate change impacts on soil erosion rates: A review. Journal of Soil and Water Conservation 59:43-50.

Nearing, M.A., Jetten, V., Baffaut, C., Cerdan, O., Couturier, A., Hernandez, M. , Le Bissonnais, Y., Nichols, M.H., Nunes, J.P., Renschler, C.S., Souchère, V. and van Oost, K. 2005. Modeling response of soil erosion and runoff to changes in precipitation and cover. CATENA 61:131-154.

Nickel, E. 1979. Geochemistry of colloid systems. For earth scientists. Earth-Science Reviews 15:296-297.

Norrish, K. 1954. The swelling of montmorillonite. Discussions of the Faraday Society 18:120-134.

Novich, B.E. and T.A. Ring. 1984. Colloid stability of clays using photon correlation spectroscopy. Clays and clay minerals 32:400-406.

O'brien, N.R. 1971. Fabric of kaolinite and illite floccules. Clays and clay minerals 19:353-359.

Oades, J. 1984. Soil organic matter and structural stability: mechanisms and implications for management. Plant and Soil 76:319-337.

Oster, J.D., Shainberg, I. and Wood, J.D. 1980. Flocculation Value and Gel Structure of Sodium/Calcium Montmorillonite and Illite Suspensions. Soil Sci Soc Am J 44:955-959.

Overbeek, J.T.G. 1980. The rule of Schulze and Hardy. Pure and Applied Chemistry 52

1151-1161.

Parfitt, R.L., Theng, B.K.G., Whitton, J.S. and Shepherd, T.G. 1997. Effects of clay minerals and land use on organic matter pools. Geoderma 75:1-12.

Parks, G.A. and Bruyn, P.L.d. 1962. The zero point of charge of oxides. The Journal of Physical Chemistry 66:967-973.

References

Pernyeszi, T. and Dékány, I. 2003. Surface fractal and structural properties of layered clay minerals monitored by small-angle X-ray scattering and low-temperature nitrogen adsorption experiments. (in English) Colloid Polym Sci 281:73-78.

Pierotti, R. and Rouquerol, J. 1985. Reporting physisorption data for gas/solid systems with special reference to the determination of surface area and porosity. Pure Appl Chem 57:603-619.

Pimentel, D., Harvey, C., Resosudarmo, P., Sinclair, K., Kurz, D., McNair, M., Crist,S., Shpritz, L., Fitton, L., Saffouri, R. and Blair, R. 1995. Environmental and economic costs of soil erosion and conservation benefits. Science 267:1117-1123.

Pinheiro-Dick, D. and Schwertmann, U. 1996. Microaggregates from Oxisols and Inceptisols: dispersion through selective dissolutions and physicochemical treatments. Geoderma 74:49-63.

Polubesova, T. and Nir, S. 1999. Modeling of organic and inorganic cation sorption by illite. Clays and clay minerals 47:366-374.

Polyakov, V. and Lal, R. 2004. Modeling soil organic matter dynamics as affected by soil water erosion. Environment International 30:547-556.

Pronk, G.J., Heister, K. and Kögel-Knabner, I. 2011. Iron Oxides as Major Available Interface Component in Loamy Arable Topsoils. Soil Sci Soc Am J 75:2158-2168.

Quirk, J.P. 1994. Interparticle Forces: A Basis for the Interpretation of Soil Physical Behavior. Advances in Agronomy Volume 53:121-183.

Radlinski, A.P., Mastalerz, M., Hinde, A.L., Hainbuchner, M., Rauch, H., Baron, M., Lin, J.S., Fan, L. and Thiyagarajan, P. 2004. Application of SAXS and SANS in evaluation of porosity, pore size distribution and surface area of coal. International Journal of Coal Geology 59:245-271.

Raine, S.R. and So, H.B. 1997. An investigation of the relationships between dispersion, power, and mechanical energy using the end-over-end shaking and ultrasonic methods of aggregate stability assessment. Soil Research 35:41-54.

Roden, E.E. and Zachara, J.M. 1996. Microbial reduction of crystalline iron (III) oxides: Influence of oxide surface area and potential for cell growth. Environmental Science & Technology 30:1618-1628.

Rosenqvist, J., Axe, K., Sjöberg, S. and Persson, P. 2003. Adsorption of dicarboxylates on nano-sized gibbsite particles: effects of ligand structure on bonding mechanisms. Colloids and Surfaces A: Physicochemical and Engineering Aspects 220:91-104.

Ryan, J.N. and Gschwend, P.M. 1994. Effects of ionic strength and flow rate on colloid release: relating kinetics to intersurface potential energy. Journal of Colloid and Interface Science 164:21-34.

Ryan, J.N. and Elimelech, M. 1996. Colloid mobilization and transport in groundwater. Colloids and Surfaces A: Physicochemical and Engineering Aspects 107:1-56.

Saggar, S., Parshotam, A., Sparling, G.P., Feltham, C.W. and Hart, P.B.S. 1996. 14C-labelled ryegrass turnover and residence times in soils varying in clay content and mineralogy. Soil Biology and Biochemistry 28:1677-1686.

Sarig, S. and Steinberger, Y. 1993. Immediate effect of wetting event on microbial biomass and carbohydrate production-mediated aggregation in desert soil. Geoderma 56:599-607.

References

Schahabi, S. and Schwertmann, U. 1970. Der Einfluß von synthetischen Eisenoxiden auf die Aggregation zweier Lößbodenhorizonte. Zeitschrift für Pflanzenernährung und Bodenkunde 125:193-204.

Schlautman, M.A. and Morgan, J.J. 1994. Adsorption of aquatic humic substances on colloidal-size aluminum oxide particles: Influence of solution chemistry. Geochimica et Cosmochimica Acta 58:4293-4303.

Schlesinger, W.H. 1995. Soil respiration and changes in soil carbon stocks, p. 159–168, *In* Woodwell GM and M. GM, (eds.) Biotic feedbacks in the global climatic system: will the warming feed the warming. ed. Oxford Univ. Press, New York.

Schmidt, P. 1991. Small-angle scattering studies of disordered, porous and fractal systems. Journal of Applied Crystallography 24:414-435.

Schmidt, P.W., Avnir, D., Levy, D., Höhr, A., Steiner, M. and Röll, A. 1991. Small-angle x-ray scattering from the surfaces of reversed-phase silicas: Power-law scattering exponents of magnitudes greater than four. The Journal of chemical physics 94:1474.

Schwertmann, V.U. 1964. The differentiation of iron oxide in soils by a photochemical extraction with acid ammonium oxalate. Zeitschrift für Pflanzenernährung und Bodenkunde 105:194-201.

Sen, T.K., Shanbhag, S. and Khilar, K.C. 2004. Subsurface colloids in groundwater contamination: a mathematical model. Colloids and Surfaces A: Physicochemical and Engineering Aspects 232:29-38.

Séquaris, J.-M. 2010. Modeling the effects of Ca^{2+} and clay-associated organic carbon on the stability of colloids from topsoils. Journal of Colloid and Interface Science 343:408-414.

Séquaris, J.-M., Klumpp, E. and Vereecken, H. 2013. Colloidal properties and potential release of water-dispersible colloids in an agricultural soil depth profile. Geoderma:94-101.

Séquaris, J.-M., Guisado, G., Magarinos, M., Moreno,C., Burauel, P., Narres, H.-D. and Vereecken, H. 2010. Organic-carbon fractions in an agricultural topsoil assessed by the determination of the soil mineral surface area. Journal of Plant Nutrition and Soil Science 173:699-705.

Séquaris, J.-M. and Lewandowski, H. 2003. Physicochemical characterization of potential colloids from agricultural topsoils. Colloids and Surfaces A: Physicochemical and Engineering Aspects 217:93-99.

Seta, A.K. and Karathanasis, A.D. 1996. Water dispersible colloids and factors influencing their dispersibility from soil aggregates. Geoderma 74:255-266.

Shainberg, I., Levy, G.J., Rengasamy, P. and Frenkel, H. 1992. Aggregate stability and seal formation as affected by drops' impact energy and soil amendments. Soil Science 154:113-119.

Shang, C., Rice, J.A. and Lin, J.-S. 2001. Thickness and surface characteristics of colloidal 2:1 aluminosilicates using an indirect fourier transform of small-angle X-ray scattering data. Clays and Clay Minerals 49:277-285.

Six, J., Elliott, E.T. and Paustian, K. 2000a. Soil macroaggregate turnover and microaggregate formation: a mechanism for C sequestration under no-tillage agriculture. Soil Biology and Biochemistry 32:2099-2103.

Six, J., Elliott, E.T. and Paustian, K. 2000b. Soil Structure and Soil Organic Matter II. A Normalized Stability Index and the Effect of Mineralogy. Soil Sci Soc Am J 64:1042-1049.

References

Sollins, P., Swanston, C. and Kramer, M. 2007. Stabilization and destabilization of soil organic matter—a new focus. Biogeochemistry 85:1-7.

Środoń, J., Elsass, F., Mchardy, W.J. and Morgan, D.J. 1992. Chemistry of illite-smectite inferred from tem measurement of fundamental particles. Clay minerals 27:137-158.

Strobel, B.W. 2001. Influence of vegetation on low-molecular-weight carboxylic acids in soil solution—a review. Geoderma 99:169-198.

Tan, G.L., Lemon, M.F., Jones, D.J. and French, R.H. 2005. Optical properties and London dispersion interaction of amorphous and crystalline SiO_2 determined by vacuum ultraviolet spectroscopy and spectroscopic ellipsometry. Physical Review B 72:205117.

Tarì, G., Olhero, S.M. and Ferreira, J.M.F. 2000. Influence of Temperature on Stability of Electrostatically Stabilized Alumina Suspensions. Journal of Colloid and Interface Science 231:221-227.

Teutenberg, T., Wiese, S., Wagner, P. and Gmehling, J. 2009. High-temperature liquid chromatography. Part II: Determination of the viscosities of binary solvent mixtures—Implications for liquid chromatographic separations. Journal of Chromatography A 1216:8470-8479.

Thomsen, I.K., Schjønning, P., Jensen, B., Kristensen, K. and Christensen, B.T. 1999. Turnover of organic matter in differently textured soils: II. Microbial activity as influenced by soil water regimes. Geoderma 89:199-218.

Tipping, E., Chamberlain, P.M., Fröberg, M., Hanson, P.J. and Jardine, P.M. 2012. Simulation of carbon cycling, including dissolved organic carbon transport, in forest soil locally enriched with 14C. (in English) Biogeochemistry 108:91-107.

Tisdall, J.M. and Oades, J.M. 1982. Organic matter and water-stable aggregates in soils. Journal of Soil Science 33:141-163.

Tombácz, E. and Szekeres, M. 2001. Interfacial Acid−Base Reactions of Aluminum Oxide Dispersed in Aqueous Electrolyte Solutions. 1. Potentiometric Study on the Effect of Impurity and Dissolution of Solid Phase. Langmuir 17:1411-1419.

Tombácz, E., Libor, Z., Illés, E., Majzik, A. and Klumpp, E. 2004. The role of reactive surface sites and complexation by humic acids in the interaction of clay mineral and iron oxide particles. Organic Geochemistry 35:257-267.

Torkzaban, S., Bradford, S.A. and Walker, S.L. 2007. Resolving the coupled effects of hydrodynamics and DLVO forces on colloid attachment in porous media. Langmuir 23:9652-9660.

Trolard, F., Bourrie, G., Jeanroy, E., Herbillon, A.J. and Martin, H. 1995. Trace metals in natural iron oxides from laterites: A study using selective kinetic extraction. Geochimica et Cosmochimica Acta 59:1285-1297.

Van Oost, K., Govers, G., Quine, T.A., Heckrath, G., Olesen, J.E., De Gryze, S. and Merckx, R. 2005. Landscape-scale modeling of carbon cycling under the impact of soil redistribution: The role of tillage erosion. Global Biogeochem Cycles 19:GB4014.

Violante, A. and Pigna, M. 2002. Competitive Sorption of Arsenate and Phosphate on Different Clay Minerals and Soils. Soil Sci Soc Am J 66:1788-1796.

References

Wagai, R. and Mayer, L.M. 2007. Sorptive stabilization of organic matter in soils by hydrous iron oxides. Geochimica et Cosmochimica Acta 71:25-35.

Wijnja, H. and Schulthess, C.P. 2000. Vibrational Spectroscopy Study of Selenate and Sulfate Adsorption Mechanisms on Fe and Al (Hydr)oxide Surfaces. Journal of Colloid and Interface Science 229:286-297.

Yan, L., Englert, A.H., Masliyah, J.H. and Xu, Z. 2011. Determination of Anisotropic Surface Characteristics of Different Phyllosilicates by Direct Force Measurements. Langmuir 27:12996-13007.

Zhou, J., Ralston, J., Sedev, R. and Beattie, D.A. 2009. Functionalized gold nanoparticles: Synthesis, structure and colloid stability. Journal of Colloid and Interface Science 331:251-262.

Zhuang, J., McCarthy, J.F., Perfect, E., Mayer, L.M. and Jastrow, J.D. 2008. Soil Water Hysteresis in Water-Stable Microaggregates as Affected by Organic Matter. Soil Sci Soc Am J 72:212-220.

Curriculum Vitae

Personal Data

Family name: Jiang
First name: Canlan
Data of birth: 12th, October 1984
Place of birth: Changsha, China
Nationality: Chinese

Educations

2009.10 ~ 2013.6	**Institut für Bio- und Geowissenschaften IBG-3: Agrosphäre** **Forschungszentrum Jülich, Germany** **RWTH, Aachen University, Germany** PhD student in natural science Supervisors: Prof. Dr. Erwin Klumpp, Direct supervisor: Dr. Jean-Marie Séquaris, Adviser in RWTH: Prof. Dr. Andreas Schäffer
2006.9 ~ 2009.7	**Nanjing Agricultural University, China** **Institute of Soil Science, Chinese Academy of Sciences** Master in soil science Supervisors: Prof. Huixin Li and Prof. Yuanqiu He
2002.9 ~ 2006.7	**Hunan Agricultural University, China** Bachelor in agriculture resource and environmental science

Band / Volume 167
Coupled modeling of water, vapor and heat in unsaturated soils - Field applications and numerical studies
C. Steenpaß (2013), X, 123 pp
ISBN: 978-3-89336-854-9

Band / Volume 168
An analysis of the global atmospheric methane budget under different climates
A. Basu (2013), v, 110 pp
ISBN: 978-3-89336-859-4

Band / Volume 169
Experimental determination of the partitioning coefficient of nopinone as a marker substance in organic aerosol
B. Steitz (2013), 132 pp
ISBN: 978-3-89336-862-4

Band / Volume 170
Ion Beam Treatment of Functional Layers in Thin-Film Silicon Solar Cells
W. Zhang (2013), xi, 191 pp
ISBN: 978-3-89336-864-8

Band / Volume 171
Pulvermetallurgische Herstellung von porösem Titan und von NiTi-Legierungen für biomedizinische Anwendungen
M. Bram (2013), X, 238 pp
ISBN: 978-3-89336-866-2

Band / Volume 172
IEK-3 Report 2013. Langlebige Elektrochemische Verfahrenstechnik
(2013), ca. 185 pp
ISBN: 978-3-89336-868-6

Band / Volume 173
Combined Steady State and High Cycle Transient Heat Load Simulation with the Electron Beam Facility JUDITH 2
Th. Loewenhoff (2013), XVI, 108 pp
ISBN: 978-3-89336-869-3

Band / Volume 174
High-Quality Thorium TRISO Fuel Performance in HTGRs
K. Verfondern, H. Nabielek, M.J. Kania, H.-J. Allelein (2013), viii, 109 pp
ISBN: 978-3-89336-873-0

Band / Volume 175
Characterization of effective hydraulic properties of unsaturated porous media using spectral induced polarization (SIP)
K. Breede (2013), xiv, 72 pp
ISBN: 978-3-89336-875-4

Band / Volume 176
Zur Mikrostruktur siliziumbasierter Dünnschichten für die Photovoltaik
F. Köhler (2013), i, 100 pp
ISBN: 978-3-89336-876-1

Band / Volume 177
Grundlagen für die Transformation von Energiesystemen
Texte und Ergebnisse der Cadenabbia-Tagung 2012
der Konrad-Adenauer-Stiftung und des Forschungszentrum Jülich GmbH
L. Gruber, J.-F. Hake (Eds.) (2013), VI, 114 pp
ISBN: 978-3-89336-877-8

Band / Volume 178
Thermo - mechanical investigations and predictions
for oxygen transport membrane materials
G. Pećanac (2013), 143 pp
ISBN: 978-3-89336-878-5

Band / Volume 179
Thermomechanische Charakterisierung neu entwickelter Feuerfestwerkstoffe
E. Skiera (2013), III, 133 pp
ISBN: 978-3-89336-885-3

Band / Volume 180
Entwicklung und Herstellung von metallgestützten Festelektrolyt-Brennstoffzellen mit Hilfe des Hohlkathoden-Gasflusssputterns
M. Haydn (2013), XVI, 174 pp
ISBN: 978-3-89336-886-0

Band / Volume 181
Characterization and stability investigation of water dispersible colloids (WDCs) in natural soils
C. Jiang (2013), X, 102 pp
ISBN: 978-3-89336-887-7

Weitere ***Schriften des Verlags im Forschungszentrum Jülich*** unter
http://wwwzb1.fz-juelich.de/verlagextern1/index.asp

Energie & Umwelt / Energy & Environment
Band / Volume 181
ISBN 978-3-89336-887-7

JÜLICH
FORSCHUNGSZENTRUM